CHARLES UNIVERSITY IN PRAGUE
Faculty of Science
Department of Experimental Plant Biology

ACADEMY OF SCIENCES OF THE CZECH REPUBLIC
Institute of Experimental Botany
Laboratory of Cell Biology

Dissertation

Functional studies of selected members of the *Arabidopsis* formin family

Denisa Oulehlová

Prague 2010

Supervisor:
doc. RNDr. Fatima Cvrčková, Dr. rer. nat.

Consultant:
RNDr. Viktor Žárský, CSc.

Following people contributed by direct experimental work to the results included in this thesis:

Martin Potocký (Institute of Experimental Botany) designed PLDδ- and Exo70A1-derived oligopeptides in chapter 4.1 and further designed a set of antisense oligonucleotides in chapter 5.2.1
Fatima Cvrčková (Faculty of Sciences, Charles university) did design of formin-derived oligopeptides in chapter 4.2 and contributed to the selection and characterization of insertional mutants in chapter 5.2
Michal Hála (Institute of Experimental Botany) prepared protein fractions using size exclusion chromatography in chapter 4.3
Mieke Wolters-Arts (Radboud University, Nijmegen, Netherlands) did sectioning of the samples for microscopy in chapter 5.2.1
Jan Derksen (Radboud University, Nijmegen, Netherlands) did cryo-fixation and scanning electron microscopy of pollen samples in chapter 5.2.1
Matyáš Fendrych (Institute of Experimental Botany) did cloning and localization analysis of the subfragment GFP:AtFH16Δ1 in chapter 5.3.4
Tamara Pečenková (Institute of Experimental Botany) started preliminary experiments with split-YFP mentioned in chapter 6.2.5

Fatima Cvrčková

Declaration

I hereby declare that I have developed the thesis independently and that I informed all co-authors about the presentation of their results in this thesis. This dissertation has not been submitted for another qualification to this or any other university.

Prague, May 2010

Denisa Oulehlová

Summary

Formins are multidomain proteins containing a conserved formin-homology 2 (FH2) domain, which catalyzes *de novo* nucleation of actin filaments. In yeast and animal cells, both mechanisms and regulation of formin function have been extensively studied, yet much less is known about action of plant formins, which considerably differ from yeast and animal ones in the domain composition. In higher plants, formins are classified into two groups, Class I and Class II, and so far, experimental data are available only for the first group members. Here I present results of experimental study of several members of the large formin family in *Arabidopsis*, including the characterization of a Class II formin AtFH16.

Arabidopsis genome contains 21 formin-encoding genes, and though they greatly differ in their expression levels and pattern, all of them are transcriptionally active. We selected 17 homozygous T-DNA insertional mutants in 14 formin genes. Under standard cultivation conditions, no obvious phenotypic discrepancies between wild type and mutant plants were found. To impair two dominant pollen formins, an *atfh3atfh5* double-mutant was prepared and even in this case, both microspore development and pollen tube growth remained unaffected. Consistently, polarized growth of tobacco pollen tubes was not altered after the targeting of Class I formins by antisense oligonucleotides (ODNs). I also cloned cDNA of *AtFH3* and revised existing gene predictions (Cvrčková et al., 2004; Appendix 1).

To study *in situ* localization of pollen-specific AtFH3 together with other formins and cell polarity regulators, a set of rat polyclonal antibodies against synthetic KLH-conjugated oligopeptides was prepared and tested. However, most rat antisera recognized the same background KLH-related plant antigen (KRAP) in *Arabidopsis* and tobacco. We characterized KRAP with respect to size and cellular localization and examined possible antigen-specific reasons for the failure of most immunizations (Oulehlová et al., 2009; Appendix 2).

A Class II formin AtFH16 with an unusual domain composition was closely characterized. Under specific conditions (hard tilted agar or continuous darkness), an *atfh16* null mutant exhibited moderate phenotypical changes, especially shortening and waving of etiolated hypocotyls that was further emphasized after treatments with cytoskeletal drugs. Our results indicate involvement of AtFH16 in some aspects of cell expansion in *Arabidopsis* seedlings. Furthermore, we cloned full-lenght cDNA of *AtFH16* and characterized subcellular localization of AtFH16-derived variants *in vivo*. Co-localization studies revealed that AtFH16 can associate with filamentous cytoskeletar structures; in some cases, it labels stabilized actin cables via its N-terminal part, but mostly, AtFH16 decorates microtubules. We identified that a presence of the conserved FH2 domain is required for AtFH16 localization on microtubules.

Our results suggest that *Arabidopsis* Class I formins might not be essential for microspore development and for subsequent polarized growth of pollen tubes. Further, Class II formin AtFH16 is capable of microtubule association and could be a potential cytoskeletar cross-linker.

Acknowledgements

In this place, I would like to express my gratitude to my supervisors, Fatima Cvrčková and Viktor Žárský, who gave me a solid portion of inspiration. Many thanks to all the colleagues and friends in the Laboratory of cell biology (Institute of Experimental Botany) and the Laboratory of plant cell morphogenesis (Charles University) for all their help and brilliant atmosphere. Special thanks go to Martin Potocký and Michal Hála, my main advisors in experimental work.

For the longstanding support and patience, I would like to thank my family, especially my husband Filip. Finally, my deepest thanks go to my son Vojtěch, who had no choice than to support me.

The work on this thesis was supported by the Czech Ministry of Education project MSM LC06004 together with the grants GAAV KJB600380601 and GACR 204/05/0268.

Contents

Chapter 1

AIMS OF THE THESIS

- Obtain a collection of homozygous insertion mutants in multiple members of the *Arabidopsis* formin gene family.

- Taking into account both phylogenetic information and publicly available expression data for the *Arabidopsis* formin family, select representative genes for further characterization of mutant phenotypes, as well as for characterization of the encoded proteins.

- Characterize mutants in selected Class I and Class II formin genes with emphasis on their possible role in polarized cell growth.

- Clone a selected Class II formin gene and characterize the subcellular localization of the corresponding protein using either immunohistological methods (including preparation of antibodies) or tagged protein expression.

Chapter 2

CURRENT STATE OF KNOWLEDGE

2.1. Introduction

Formins are members of multigene family characterized by the presence of a conserved formin homology 2 (FH2 domain). These proteins are present in all eukaryots studied, with many species possesing multiple isoforms. The first member identified 20 years ago, mouse Formin-1, gave the name to the whole family, as its disruption was thought to be responsible for the limb and kidney deformity defects in mice (Mass et al., 1990). Though the later experiments revealed that impairment of another gene (gremlin) was in fact the cause of the limb deformity phenotype (Zuniga et al., 2004), the name for formins remained unchanged and actually turned out to truly characterize function of FH2 proteins, actin nucleators and regulators of cytoskeletar dynamics. When bioinformatic analyses of *Arabidopsis* genome sequence uncovered the presence of plant-specific formin families (Cvrčková, 2000; Deeks et al., 2002; Cvrčková et al., 2004), another decade of extensive research of formin functions, including studies on plant family members, brought exciting information about regulation of crucial cellular processes.

Formins are generally multidomain proteins with C-terminally located highly conserved FH2 domain accompanied with a variable N-terminus. Based on their effects on cytokinesis and development that coincidentally corresponded to the proposed Formin-1 disruption phenotype in mice, additional formins from various organisms were identified. *Drosophila* gene *diaphanous* was identified as a crucial factor required for cytokinesis during development of germline and eggs leading to sterility or even lethality in case of females (Castrillon and Wasserman, 1994). According to its sequence similarity, another eukaryotic protein essential for proper cytokinesis and cell polarity estabilishment, Bni1p from *Saccharomyces cerevisiae*, turned out to share the conserved FH2 domain thus belonging to the formin family. The *BNI1* gene was originally isolated as a gene whose mutation was synthetically lethal with the *cdc12* mutation of yeast septin (Zahner et al., 1996). At the same time, Bni1p interaction with a small GTPase Rho1p and its implication in regulation of cytoskeletar reorganization were discovered (Kohno et al., 1996), roughly indicating action and regulation of proteins which later became known as diaphanous-related formins (DRFs). Most DRFs act as direct effectors of Rho-family GTPases sharing besides FH2 domain also a C-terminally located polyprolin-rich region called the FH1 domain, the diaphanous autoregulatory domain (DAD) and a N-terminally located domains serving for Rho GTPase binding and FH2 domain dimerization, the processes essential for formin activation and function.

DRFs probably represent the most studied, and also evolutionarily oldest, group of FH2 proteins (Rivero et al., 2005; Chalkia et al., 2008), They were the first formins shown to direct actin filament assembly by a mechanism independent of other nucleation factors such as the Arp2/3 complex and later described Spire (Evangelista et al., 2002; Puryne et al., 2002; Sagot et al., 2002; Sagot and Klee et al., 2002). Although the increasing number

of formins identified in various organisms uncovered a huge variability within N-terminal gene regions suggesting other regulatory interactions involved besides small GTPases, with some examples even lacking the FH1 domain (Rivero et al. 2005, Grunt et al. 2008, Chalkia et al. 2008), recent studies indicate that formins including plant family members act as universal nucleators of actin assembly, can mediate cytoskeletar crosstalk and participate in the control of cell shape, morphogenesis and cytokinesis (for review, see e.g. Faix and Grosse, 2006; Goode and Eck, 2007; Chesarone et al., 2010).

2.2. Structure and domain composition of formins

2.2.1. FH2 domain, the only connecting link of a multigene family

As an ancient protein family with extensive domain rearrangements occurring during evolution, formins utilized and incorporated various regulatory domains. However, two features are mostly shared within the family: the well-conserved FH2 domain typical for all formins, representing a „functional core“ of the protein capable of *de novo* nucleation of actin filaments by a unique mechanism referred to as processive capping, and a poorly conserved poly-proline region named the FH1 domain, which contributes to actin assembly by interaction with profilin. Whereas few representatives of metazoan formins lack the FH1 domain, and the presence of all other domains varies distinctively, the FH2 domain represents the connecting link of the whole diverse formin family.

The FH2 domain usually consists of ~ 400-500 amino acids. As such, it is sufficient in some cases for association with barbed ends of growing actin filaments (Kovar et al., 2006) and also for actin filament nucleation (Puryne et al., 2002; Sagot et al., 2002, Michelot et al., 2005). However, the presence of the FH1 domain turned out to be essential for function of several proteins studied, where its cooperation with the FH2 domain enables or significantly increases the elongation rates of formin bound filaments. (Kovar and Pollard, 2004; Romero et al., 2004; Ingouff et al., 2005). Furthermore, recombinant FH2 or FH1FH2 domains can compete with capping proteins and thus prevent growing actin filaments from their inhibitory activities (Zigmond et al., 2003; Schirenbeck et al., 2005; Ye and Zheng et al., 2009).

2.2.2. Diaphanous-related formins

Apart of consensual organization of FH1 and FH2 domains, other regions of miscellaneous roles are located mostly in the N-termini of formin proteins (Fig. 2.1). In case of the well examined diaphanous-related group, proteins can switch between active or inactive state through an autoinhibition process, which is regulated by Rho GTPases. While Rho-dependent action of DRFs together with definition of GTPase binding domain (GBD or also RBD as Rho-binding domain) had been estabilished using yeast model (Kohno et al., 1996; Evangelista et al., 1997; Fujiwara et al., 1998), the molecular nature of DRF autoinhibition was elucidated later using mouse formins mDia1 and mDia2, where a short C-terminally located diaphanous autoregulatory domain (DAD) was identified and proved to inactivate formin molecule by binding to GBD (Fig. 2.2). This inactivation was revealed

by activated GTP-bound Rho that interacted with GBD and released GBD-DAD linkage (Watanabe at al., 1999; Alberts, 2001). Within GBD, previously defined by sequence analysis, a C-terminal segment participating in autoinhibitory process required for binding to DAD was identified and termed the diaphanous-related formin inhibitory domain (DID) (Wallar et al., 2006). Further downstream of GBD, another formin homology domain FH3 was postulated to direct protein localization based on experiments with fission yeast formin Fus1 (Petersen et al., 1998). Nevertheless, FH3 domain of mDia1 was shown to form a stable dimer (Rose et al., 2005) and even in other DRFs it is strongly divergent and actually corresponds to the part of DID plus dimerization domain (DD). DD is sometimes followed by a coiled-coil region (CC) and together, they mediate dimerization of DRFs via N-terminal parts of the proteins (Lammers et al., 2005).

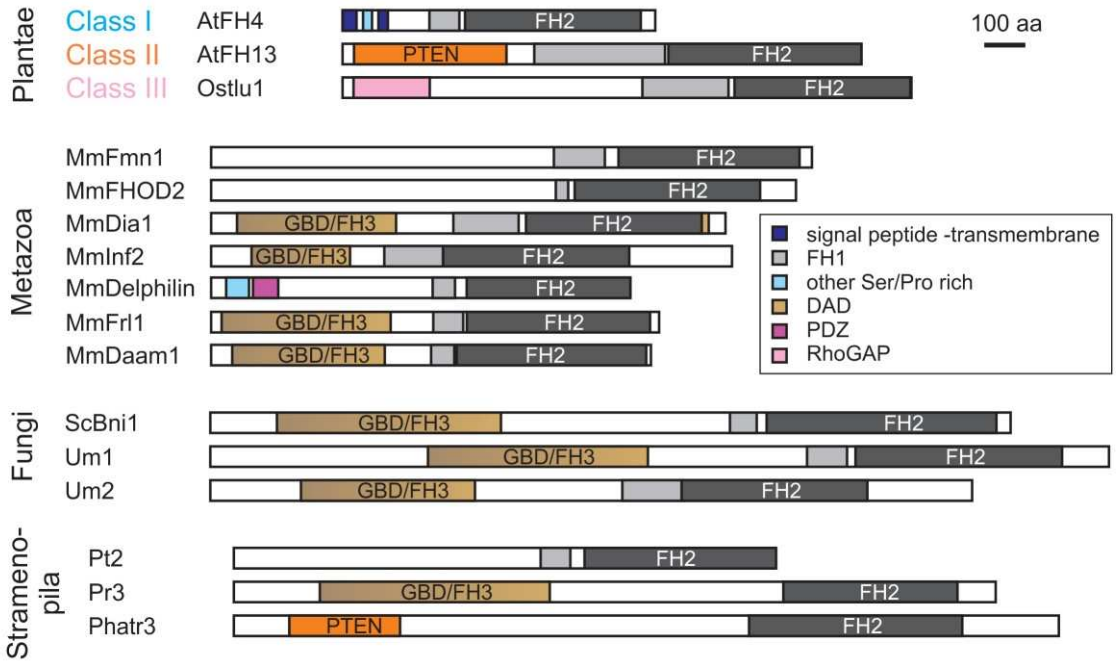

Fig 2.1 Primary organization of structural and functional elements in formins. Most formins of metazoans as well as formins of Dictyostelium and fungi can be classified as conventional formins, with a GBD/FH3-FH1-FH2-DAD structure, although in particular members or alternatively spliced variants a domain (but never the FH2) might be absent. GBD/FH3 is further composed of dimerization and autoinhibitory domains. Plant formins are the only evolutional lineage lacking GBD/FH3 and can be grouped into one of three classes. Drawn to scale. (Grunt et al., 2008).

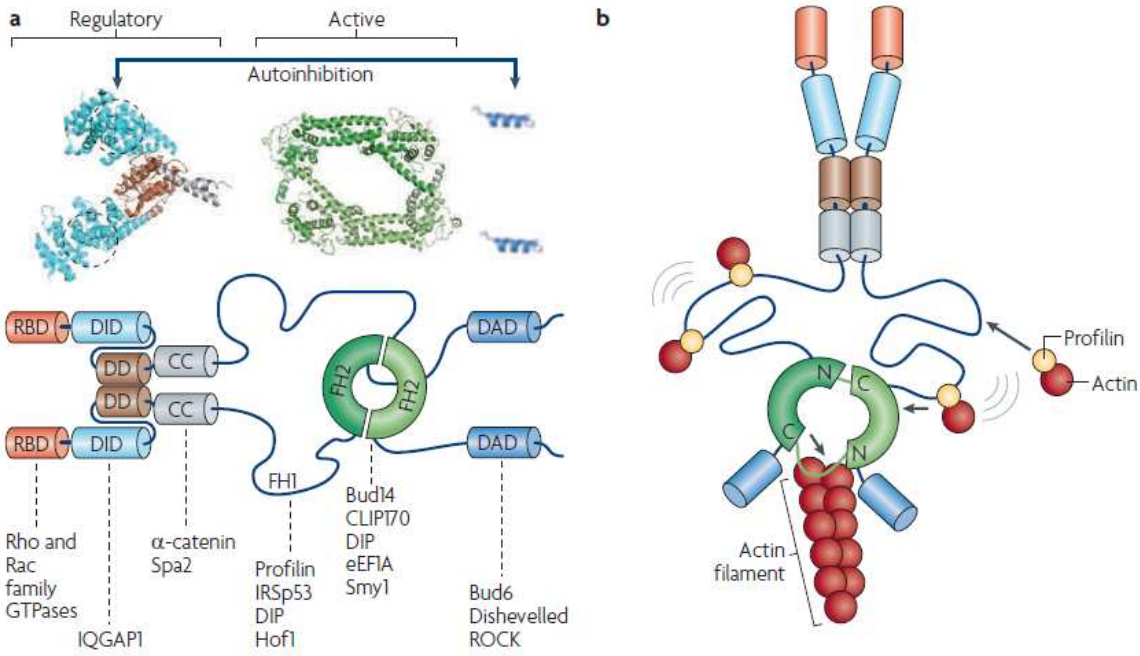

Fig 2.2 Domain organization of autoinhibited formins. a) The crystal structures and a schematic of formin domains, showing the proteins that bind them (with corresponding colours). The amino-terminal crystal spans the diaphanous inhibitory domain (DID) and the coiled-coil (CC) domain of mouse diaphanous 1 (mDia1). The formin homology 2 (FH2) crystal corresponds to the FH2 dimer of Bni1 (Xu et al., 2004). The carboxy-terminal crystal corresponds to the Dia autoregulatory domain (DAD) of mDia1 (Nezami et al., 2006). FH2 dimerizes in an anti-parallel manner to form a doughnut-shaped structure, whereas FH1 (located between the CC and FH2 domains) lacks a predicted structure but might be rope-like. In the crystal structure of the regulatory N-terminal half, the circled areas on the DID indicate the DAD binding sites that mediate autoinhibition. Note that Rho binding to the Rho-binding domain (RBD) may relieve autoinhibitory interactions. Profilin binds FH1 of all formins examined, other binding proteins identified for particular formins are depicted under their interaction domains and are described in more detail in text of chapter 2.5. **b)** Schematic of a formin dimer in action. The dimeric FH2 'rides' the growing barbed end of actin through dynamic motions of its two functional halves, alternating contacts with actin subunits exposed at the filament end. The adjacent rope-like FH1 domains recruit profilin–actin complexes and deliver actin subunits to the growing barbed end (arrows). The grey curved lines emphasis the dynamic motion of the formin on the barbed end (reproduced and adapted from Chesarone et al., 2010).

A number of other fungal and animal formins copy the consensual structure of DRFs described above, although their N-terminal parts are highly variable, especially in case of GBD (Rivero et al. 2005). Besides DRFs, there are six other subfamilies of mammalian formins classified based on their domain structure. One of them is represented by neuronal-specific delphilin that posesses completely different domain composition, where all dimerization and inhibitory domains together with the GBD are replaced by one or two PDZ domains that mediate delphilin association with the δ2 subunit of glutamate receptor (Miyagi et al., 2002; Yamashita et al., 2005; Matsuda et al., 2006). Also *Caenorhabditis* posseses a very unusual FH2 protein called Fozi-1, N-terminal part of which is composed of zinc finger and Q motifs characteristic for transcription factors (Amon et al., 2007).

2.2.3. Structure of plant FH2 proteins

Interestingly, the only evolutional lineage absolutely lacking GBD/FH3 domain layout within the N-terminus is represented by plants (Grunt et al., 2008). Instead, plant formins incorporated structural elements that, together with hallmark features in the FH2 domain, classify plant members into three classes (Fig. 2.1). Members of Class I are characterized by the presence of a signal peptide followed by a transmembrane domain, which was experimentally confirmed to anchor *Arabidopsis* formins AtFH4, AtFH6 and AtFH8 into the plasmatic membrane (Favery et al. 2004; Deeks and Cvrčková et al., 2005; Yi et al., 2005). In Class II formins, regions outside FH2 exhibit much greater variability, with members containing either various repetitive sequences or coiled-coil segments between FH1 and FH2 domains. Moreover, some Class II formins even lack the FH1 domain. However, at least some of the formins possesing such an unusual domain composition are suspected to be pseudogenes and no experimental studies have been done yet to reveal their biological role. Besides, a majority of Class II formins bear a N-terminally located phosphatase and tensin-related domain (PTEN) known from human PTEN antioncogene or metazoan auxilins and other proteins containing auxilin-related domains. Based on a sequence analysis, PTEN-like domains of Class II formins were predicted to be involved in protein localization rather than catalytic processes (Cvrčková et al., 2004). Recent study by Luis Vidali and coleagues confirmed this presumption in case of the PTEN-like domain containing For2 proteins from the moss *Physcomitrella patens*, where the PTEN-like domain itself was sufficient for apical membrane localization *in vivo* (Vidali et al., 2009). Finally, some algal, moss and lycophyte FH2 genes form a specific branch, Class III that is defined by the presence of a novel RhoGAP-related domain. Similarly to PTEN-like domain of Class II formins, certain alteration of conserved residues within the domain compared to known Rho GAPs might abolish catalytic activity of the RhoGAP-related domain, so that its role remains unclear (Grunt et al., 2008).

Dispite the great variability of regions outside the FH2 domain, most of the formins retain functional structures that can mediate their recruitment to the sites of action, usually on membranes. Localization of FH2 proteins can be achieved either directly (transmembrane domains of plant Class I formins, PTEN-like domains of plant Class II members) or via interactors, of which Rho GTPases seem to be the most common (GBD of DRFs, RhoGAP-related domain of plant Class III formins, PDZ interacting with membrane receptor). On the other hand, processes regulating activation of formins remain much more enigmatic, as the autoinhibition and subsequent activation of DRFs by Rho GTPases, for a long time presented as a universal regulatory scheme, turned out to be specific for some formins only, while other FH2 proteins are activated by distinct mechanisms (Matheos et al., 2004; Liu et al., 2008; Takeya et al., 2008) as described later in Chapter 2.5. Nothing is known so far about formin inhibition or activation in case of plants.

2.3. Implication of formins in cellular processes

Simply talking, wherever rearrangements of cytoskeletar network occur, implication of FH2 proteins can be expected. Essential role of formins was proved mainly in dynamic processes such as cell division, polarization and migration, apical growth, vesicle

trafficking or organelle biogenesis and movements, where the rapid and directed turnover of cytoskeletar components is required (Pollard and Borisy, 2003; Faix and Groose, 2006).

2.3.1. Cell polarity and apical growth

Polar development is initiated within a cell by either endogenous or exogenous polarizing signal, which regulates polar distribution of signaling molecules leading to polarity establishment and maintenance through the cytoskeleton and vesicular trafficking. A clear evidence of formin contribution to establishing and maintaining polarized cell patterns originally arose from studies on yeast mutants. Formin For3p localizes at the cell tip and at the cell division site in fission yeast and the loss of its activity results in restricted growth with affected polarity, though the mutant cells still exhibit some degree of polarized growth. As a part of the polarisome complex that is recruited at the cell tip by microtubules, For3p directs a formation of new actin assembly sites (Feierbach and Chang, 2001; Nakano et al., 2002; Martin and Chang, 2006). Bud formation in budding yeast also requires polarized growth and both endogenous formins Bni1p and Bnr1p cooperate during this process. Bni1p localizes at the tip of emerging bud, whereas Bnr1p resides at the bud neck, where it facilitates a rapid formation of short actin filaments. The functions of the two budding yeast formins are partially redundant, as the single mutants, despite exhibiting defects in polarized morphogenesis, are still viable, but the loss of both formins is lethal (Evangelista et al., 1997; Evangelista et al., 2002; Sagot and Klee et al., 2002; Puryne et al., 2004). Similarly, mammalian formins play a crucial role in polarity estabilishment that can be achieved by formin-mediated cooperation between microtubules and actin (Yamana and Arakawa, 2006; Goulimari et al., 2007).

In elongating cells of moss *Physcomitrella pattens* exhibiting apical growth, silencing of Class II formins leads to the loss of polarized layout and instead, spherical cells with disrupted actin cytoskeleton are formed. A full restoration of polarized cell morphology can be achieved by the expression of For2 formins, which localize at the cell tip and generate apical actin structures that promote polarized growth (Vidali et al., 2009). In angiosperms, apically growing cells are represented foremost by elongating root hairs and pollen tubes (Fig. 2.3). In both cell types, overexpression or downregulation of Class I formins causes growth arrest and perturbances within the apical region, as shown in the studies with *Arabidopsis* proteins. Transiently expressed full-lenght or FH1FH2 containing versions of AtFH1 caused excessive formation of actin cables, that extended to the apex (Cheung and Wu, 2004), which is normally formed by so called clear zone. As the name suggests, organells and filamentous cytoskeletar structures are excluded from this area (therefore, it appeares as „clear“ in the microscope), which is characterized by the accumulation of secretory vesicles and fine actin meshwork (Geitmann and Emons, 2000). Similar phenotype was observed as well in case of AtFH3 overexpression, while its downregulation led to the elimination of actin cables followed by swelling of pollen tubes tips and disruption of normal cytoplasmic streaming (Ye and Zheng et al., 2009). Quite a different effect was observed after the stable overexpression of AtFH8 in *Arabidopsis* plants, where the root hair tip growth became affected, resulting in a formation of wavy, swollen or branched hairs. Unlike AtFH1 and AtFH3, visualization of actin cytoskeleton revealed disappearance of organized longitudial filaments in root hairs exhibiting the strong phenotype, possibly related to AtFH8 actin severing activity (Yi et al., 2005). Consistently with these observations, overexpression of an inactive variant of AtFH8 (a

GFP-tagged truncated protein lacking the FH2 domain) inhibited both emergence and elongation of root hairs (Deeks and Cvrčková et al., 2005).

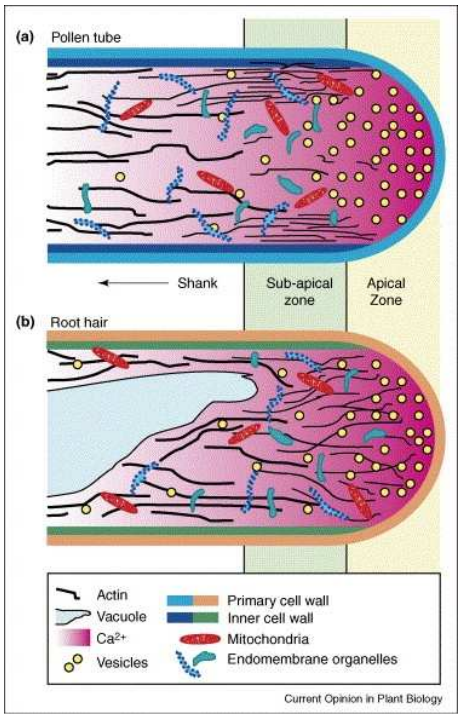

Fig 2.3 Schematic representation of the tip of a growing pollen tube and a root hair. Both growing pollen tubes and growing root hairs are conventionally described as having an apical zone, a sub-apical zone, and a shank. **a)** In pollen tubes, the apical zone (sometimes called the clear zone) has an abundance of vesicles, an absence of organelles and, at its extreme apical tip, only sparse actin filaments. The sub-apical zone contains a dense fringe of cortical actin filaments, that are sometimes described as extending into the central cytoplasm as a meshwork. Thick microfilament bundles (actin cables) are present in the shank, and probably act as 'tracks' for organelle movement. **b)** Root hairs demonstrate the same polarized characteristics as pollen tubes, with a few notable differences. The apical cytoplasm is primarily full of transport vesicles, but a few organelles are also observed. The sub-apical region microfilaments appear as diffuse fine actin bundles, which are generally reported to extend further into the apical zone than those of pollen tubes. Reproduced and adapted from Cole and Fowler (2006).

2.3.2. Cell division

During cell division, FH2 proteins regulate the positioning of the mitotic spindle and further the final stages of the process, when cytokinesis occurs. In eukaryotic cells, the spindle apparatus is the structure that separates the chromosomes into the daughter cells during cell division; correct positioning of the spindle is essential for proper progression of mitosis (Segal and Bloom, 2001). In budding yeast, cells lacking the formin Bni1p are defective in the initial movement of the spindle pole body toward the emerging bud. As mitosis continues, also preanaphase spindles exhibit weird movements in mutant cells

between the mother cell and the bud (Lee et al., 1999). In mammalian cells, the formin mDia1 localizes to the mitotic spindle independent of Rho GTPase activity (Kato et al., 2001). Furthermore, mDia1 co-localizes at the mitotic spindles with a cation channel PKD2, where it is necessary for PKD2 movement. By this mechanism, the formin positively influences intracellular Ca^{2+} release during mitosis (Rundle et al., 2004).

In most cell types, by the end of cell division, the site of subsequent cell separation is labeled by a contractile actomyosin ring (also referred to as the cytokinetic actin ring), that is typical by the presence of short linear filaments undergoing rapid turnover including *de novo* actin assembly. The position, at which the contractile ring assembles, is dictated by the mitotic spindle (Maupin and Pollard, 1986; Pelham and Chang, 2002). In fission yeast, formins For3p and Cdc12p contrubite to the cell division process. For3p localizes at the cell division site; when impaired, cells divide in an asymmetric manner (Feierbach and Chang, 2001), however, mitotic formation and maintanance of actin ring remain unaffected. On the contrary, cells with loss of Cdc12p activity fail to form the actin ring, as Cdc12p directs actin assembly and polymerization of the ring structures. Like the formins, Arp2/3 complex exhibits the same activity during actin ring formation, though it is not clear whether both nucleators function together or independently (Pelham and Chang, 2002). In contrast to the fission yeast, impairment of the Arp2/3 complex in budding yeast and others does not block actin ring formation and subsequent cytokinesis. In budding yeast, assembly of the actin ring requires the formins Bni1p and Bnr1p together with profilin and their activity is directed by Rho1 GTPase in this process (Tolliday et al., 2002). Formin and profilin-dependent ingression of the contractile ring was observed also during cytokinesis in the early embryo of *Caenorhabditis elegans* (Swan et al., 1998; Severson et al., 2002). In mammalian cells, the formin protein, mDia2 directs mitotic spindle migration, while chromosome congression or segregation is formin-independent. Furthermore, mDia2 is essential for proper final contraction of dividing cells, thus governing both early mitosis and late cytokinesis (Dumont et al., 2007; Watanabe et al., 2008).

In plant cells, cytokinesis beggins by emergence of a cell plate, that is composed mainly of Golgi- and endosome- derived vesicles delivering components for membrane and the cell wall formation. Formation and growth of the cell plate is dependent upon the phragmoplast, composed of opposing bundles of microtubules that face one another with their positive ends at the center (Field et al., 1999). The only plant formin so far known to regulate cell division is AtFH5 from *Arabidopsis thalinana*, which is required for an accurate timing of cytokinesis completion in endosperm. Furthermore, a fusion protein AtFH5–GFP localizes to the incipient and expanding cell plate in *Arabidopsis* roots, suggesting its role in cell-plate maturation (Ingouff et al., 2005).

2.3.3. Cell migration, adhesion and filopodium formation

In migrating animal cells, dramatic rearangements of both actin and microtubular cytoskeleton occur, governing adhesion formation and subsequent release, formation of cell protrusions such as filopodia or lamelipodia, and cell contraction. Mammalian formins have been shown to play a crucial role in formation of adhesions, both with or independently of Rho GTPases. Plasma membrane areas that provide anchorage link in many mammalian cell types are called focal adhesions. Towards these points, bundles of actin fibers extend and their assembly was shown to be regulated by RhoA (Ridley and

Hall, 1992) and its effector mDia1 in fibroblasts. In some cases, mDia1 action independent of RhoA is sufficient to induce formation of dynamic adhesions (Riveline et al., 2001), while in other cell types as human osteosarcoma cells, mDia1 depletion does not inhibit focal adhesions formation, suggesting other formins or regulators such as the Arp2/3 complex to be involved in dynamic actin assembly during this process (Hotulainen and Lappalainen, 2006). In epithelilal cells, formation of radial actin cables necessary for cell to cell adhesion is catalyzed by the formin Fmn1, that is recruited to the adhesion site by α-catenin (Kobielak et al., 2004), whereas hDia1 and mDia1 control the formation of cell-cell junctions via E-cadherin and associated proteins in a RhoA-dependent manner. Though the mechanism of Dia action is not known, it was shown to be mostly microtubule-independent; suggestions have been made about Dia either indirectly regulating lateral mobility of cadherin receptors or protecting cadherin from endocytosis by modulation of submembranous actin network (Carramusa et al., 2007).

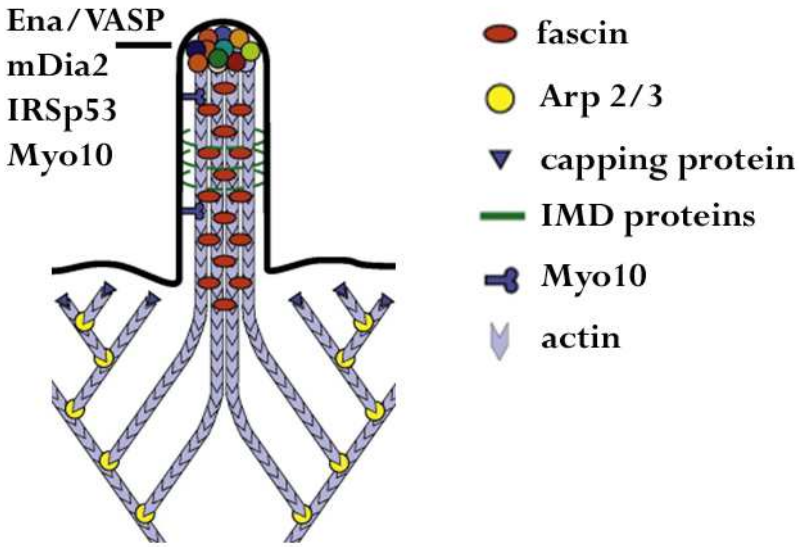

Fig 2.4 Schematic diagram of the structure of a filopodium. The central core is composed of a parallel bundle of actin filaments orientated with their plus or barbed ends towards the tip. The tip region contains a cluster of proteins including mDia2, Myo10, Ena/VASP proteins and IRSp53. The filaments in the stem are held together by the actin cross-linking protein fascin, and by links to the plasma membrane mediated by ERM proteins. IMD proteins line the interface between the actin bundle and the plasma membrane and help stabilise membrane curvature. At the base of the filopodium, the actin filaments splay out and are integrated into the dendritic network of actin below the plasma membrane. Reproduced from Mellor (2010).

Membrane protrusions capable of dynamic extension and retraction called filopodia contain parallel actin filament bundles, which are actively polymerized at the filopodial tips (Fig 2.4). The process of filopodia formation was shown to be Arp2/3 independent, whereas it requires activity of two actin elongation factors, formins and Ena/VASP. Both elongators reside at the tips of filopodia, where the growing barbed ends of actin filaments are located (Bear et al., 2002; Pellegrin and Mellor, 2005; Schirenbeck et al., 2005; reviewed by Mellor, 2010).

Another cytoskeletar structure implicated in cell adhesion and migration are the stress fibres, structured by short actin filaments together with myosin II. In contrast to the actin bundles in filopodia, stress fibres filaments overlap, exhibiting alternating polarity (Cramer et al., 1997). They can be generated by two distinct mechanisms. Dorsal stress

fibers, which are connected to the substrate via a focal adhesion at one end, are assembled through formin-driven polymerization at focal adhesions, while transverse arcs, which are not directly anchored to substrate, consist of Arp2/3-nucleated actin bundles annealed with myosin bundles. Interestingly, in Arp2/3 knockdown cells, two dorsal stress fibers growing from opposite sides of the lamella can fuse with each other to form a ventral stress fiber, which emphasizes the role of formins in the stress fibres formation (Watanabe et al., 1999; Hotulainen and Lappalainen, 2006).

2.3.4. Organelle and vesicle trafficking

The cytoskeleton participates in organelle and vesicle movement generally by three mechanisms. Long-distance transport occurs with the help of motor proteins along cytoskeleton „rails“, whereas local mesh of fine cytoskeletar structures can function as a barrier for vesicle transport. The third mechanism is represented by dynamically polymerized actin comets that can actively push the vesicles. The two later mechanisms act independently on motor proteins (reviewed in Ridley, 2006; Žárský et al., 2009).

In ophistokonts, formins regulate dynamics of both organelles and vesicles. During bud formation in yeast, Bni1 and the GTPase Rho1 control nuclear migration on microtubules (Fujiwara et al., 1999). In mammals, the diaphanous family (DRF) formin mDia1 specifically controls anchoring of mitochondria at the cell periphery as the effector of the GTPase RhoA. Constitutively active forms of mDia1 capture mitochondria on actin filaments and dramatically inhibit their motility. Interestingly, increased F-actin concentration itself generated by jasplakinolide does not have the similar inhibitory effect. Such a pathway was shown to be conserved in *Drosophila* and mammals (Minin and Kulik et al., 2006). Though nothing has been reported yet about formin-mediated control of organelle dynamics in plants, motility and redistribution of mitochondria and other membrane organelles in plant cells is known to be also actin-dependent (Sheanan et al., 2004a; Semenova et al., 2008), so that formin activity could be expected. However, for example stabilization of actin filaments on its own by jasplakinolide is able to markedly slow down mitochondrial velocity in the cortical cytoplasm of pollen tubes. Formins, if implicated, could function indirectly through remodelling actin network and density (Zheng et al., 2009).

All three mammalian DRFs formins mDia1, mDia2 and mDia3 are also found on various endosomal compartments. In mouse and human cells, mDia1 is recruited to endosomes by activated GTPase RhoB, where it is required for the formation of the actin coat around endosomes, which aligns them along subcortical actin fibres (Fernandez-Borja et al., 2005). Similarly, the same GTPase RhoB activates another formin, mDia2, also necessary for vesicle trafficking through the regulation of actin dynamics (Wallar et al., 2007). The last member of the mammalian DRFs subgroup mDia3 associates on early endosomes together with GTPase RhoD; its enhanced activity promotes the alignment of endosomes along actin filaments and reduces endosome motility. Furthermore, mDia2 and RhoD stimulate a function of a signalling protein Src tyrosine kinase when localized on early endosomes/Rab5-positive vesicles (Gasman et al., 2003).

Since Rho GTPase-induced remodelling of cytoskeleton is known to regulate also the secretory pathway in both opisthokonts and plants (Ridley, 2006), one would expect at least some FH2 proteins to directly participate in this process. So far, only one report about possible formin implication in exocytosis has been published. Yeast GTPase Rho3, known

to regulate the exocytotic pathway and actin cytoskeleton, was shown to bind the Exo70 subunit of the exocyst complex, and also to associate with the formin Bni1p in yeast two-hybrid system (Robinson et al., 1999). Nevertheless, taking into acount the importance of both secretion and formin function for the cell polarization, additional roles of FH2 proteins in this process could emerge.

2.3.5. Morphogenesis

All the cellular processes described in the previous four chapters have a close connection with developmental processes of multicellular organisms, which have been thoroughly studied, in particular, in meatzoa. Through the regulation of cytokinesis, several formins are essential for fertility. Loss of the formin Diaphanous in *Drosophila* impairs cytokinesis in germline, leading to male sterility. Also trans-heterozygous females are sterile because of cytokinetic defects in eggshels, i.e. the somatically derived follicle cells. Interestingly, null *diaphanous* mutation in females results in several defects during the larval stage such as polyploidy of neuroblasts, subsequently leading to early pupal lethality (Castrillon and Wasserman, 1994).

Vertebrate homologues of *Drosophila Diaphanous* seem to share the same functions, as their impairment mostly leads to the embryonic and fertility deffects as well. During the gastrulation of zebrafish embryo, downregulation of formin zDia2 blocks epiboly and related processes. Rather than cytokinesis, cellular movements based on membrane bleb-like structures and filopodia formation are impaired in zDia2 downregulated lines (Lai et al., 2008). Sterility occurs in humans as a result of a *hDia* mutantion, where spermatogenesis or oogenesis turned out to be impaired due to the cytokinetic deffects (Bione et al., 1998). In rats, mDia1 and mDia2 were found to localize into Sertoli cells, the so calles „nurse“ cells of the testes, suggesting formin regulation of spermatogenesis similarly to the situation in humans (Mironova and Millette, 2008).

Besides DRFs, other formins participate in morphogenetic processes. Mammalian Fmn2 regulates development of oocytes and its loss affects females fertility. On the cellular level, Fmn2 directs metaphase spindle positioning during meiosis, as well as the late phase of cytokinesis, and though the resulting oocytes can be fertilized, embryo development is blocked or severely affected (Leader et al., 2002; Dumont et al., 2007). In *Xenopus*, Daam1 controls gastrulation of embryos, acting as a part of a conserved Wnt/Fz (Frizzled) pathway establishing cell polarity, where it participates together with RhoA and Dishevelled in signal trasduction (Habas et al., 2001). In *Drosophila*, a different function of the Daam formin was uncovered; it determines the cuticle pattern of the respiratory system via actin organization beneath the apical surface of the tracheal cells (Matusek et al., 2006), whereas the control of oocyte development is mediated by the formin Cappuccino (Emmons et al., 1995). Fozi-1 from *Caenorhabditis elegans*, a FH2 protein with an unusual architecture possesing motifs characteristic of transcription factors, controls the asymmetric differentiation of neurons in the embryo (Johnston et al., 2006). During postembryonic stages, it functions redundantly with the myogenic regulatory factor MyoD in striated muscle fate specification (Amin et al., 2007).

Though the amoeba *Dictyostelium discoideum* belongs to unicellular organisms, the cells can aggregate and subsequently undergo programmed cell differentiation and morphogenesis to form multicellular structures (fruiting bodies) under starvation. Formin ForC, that lacks FH1 domain, is specifically involved in multicellular stages, where it

controls cellular movements. Mutants lacking ForC form aberrant fruiting bodies which do not rise above the substrate, while movements during vegetative growth and early aggregate formation under starvation remain unaffected (Kitayama and Uyeda, 2003).

In plants, embryo development depends on the nutrition supply provided by endosperm cells. *Arabidopsis* plants lacking the Class I formin AtFH5 are defective in endosperm posterior pole structures due to the improper cellularization (Ingouff et al., 2005). Expression of *AtFH5* is restricted to the maternal allele in the posterior endosperm by polycomb group-dependent imprinting. When members of endosperm-specific polycomb group complex are impaired, multiple defects occur, including much enlarged posterior structures and the absence of cellularization (Luo et al., 1999; Guitton et al., 2004). Interestingly, in such cases *AtFH5* is ectopically expressed outside the posterior endosperm and its action is responsible for the enlargement of the chalazal cyst and ectopic cyst structures in those polycomb mutants. Double mutats lacking AtFH5 and an endosperm polycomb group member *MEDEA* (MEA) are seed-lethal, as they fail to produce posterior endosperm structures (Fitz Gerald et al., 2009). Silencing of Class II formins in the moss *Physcomitrella* restricts apical growth of protonema cells resulting in the formation of stunted plants composed of spherical cells, whereas silencing of all other formins does not affect plant morphology (Vidali et al., 2009).

2.4. Actions of formins on the cytoskeleton

2.4.1. Formin´it.

As key regulators of the actin cytoskeleton, formins were discovered to direct both *de novo* nucleation of actin subunits and further elongation of actin filaments. Actin monomers are capable of spontaneous self-association, though the intermediates are unstable and mostly dissociate. Nevertheless, a small portion of dynamic intermediates that assemble into the larger precursors is sufficient to trigger spontaneous elongation *in vitro,* so that nucletion in principle may take place without participation of additional proteins (Fig 2.5). However, cytoskeletal processes *in vivo* are known to be tightly orchestrated and impairment of regulatory mechanisms can result in severe defects in cellular processes (Cvrčková et al., 2004b). Therefore, a pool of actin monomers is imobilized by association with monomer-binding proteins such as profilins and thymosins (Tobacman et al., 1983; Pollard and Cooper, 1984) and the process of monomers assembly is governed by specialized nucleators. To date, four groups of actin nucleators utilizing different mechanisms for assembly of actin monomers have been discovered.

The first actin nucleator described, Arp2/3 complex, promotes the formation of branched actin filaments, as the nucleation occurs on a pre-existing (mother) filament. After that, the new (daughter) filament grows at a 70° angle, while the Arp2/3 complex remains attached at its pointed (slower) end (Mullins et al., 1997; Welch et al., 1997). In order to form a nucleation core, Arp 2/3 complex structurally mimics polymerization intermediates (Pollard, 2007). As the Arp2/3 complex itself binds to actin monomers only weakly, the presence of so called nucleation promoting factor (NPF) is required for Arp 2/3 mediating initiation of actin assembly. The family of molecular switches known as Wiskott-Aldrich syndrome proteins (WASPs) were shown to activate Arp2/3 by evoking conformational changes in actin-related subunits Arp2 and Arp3, resulting in a closed

conformational state resembling the actin dimer (Kiselar et al., 2007). In addition, WASPs further recruit 1-2 actin monomers, thus creating the nucleation core.

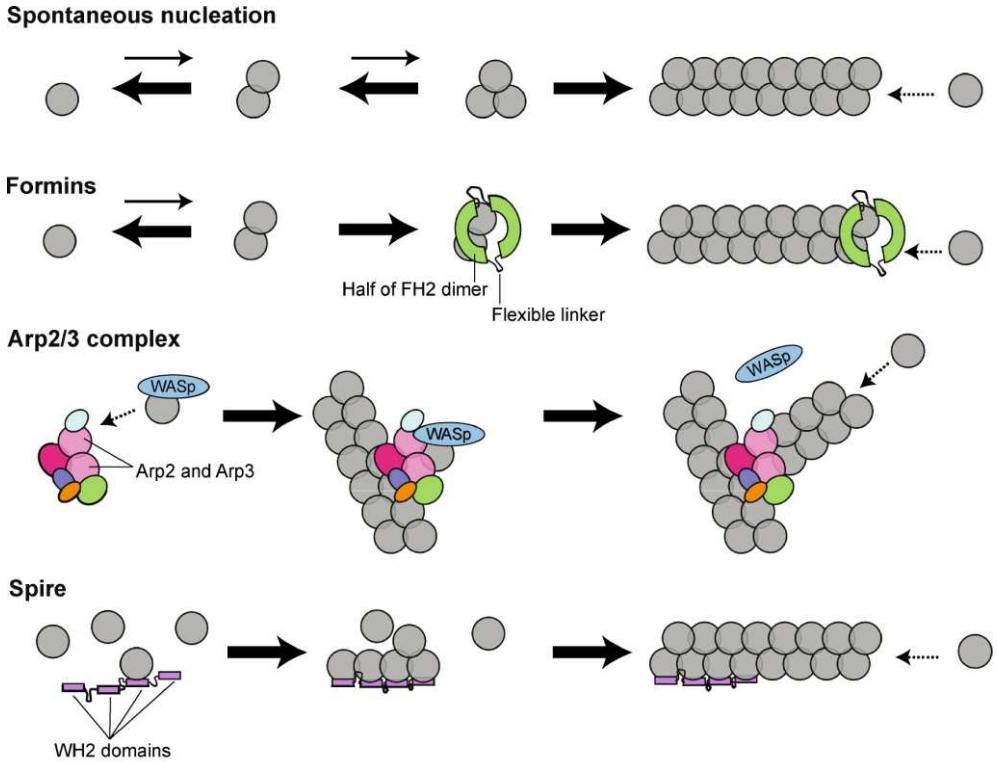

Fig 2.5 Proposed mechanisms of actin assembly factors. Comparison of the mechanisms by which formins, the Arp2/3 complex and Spire, nucleate actin polymerization (top). Spontaneous actin assembly from purified monomers is shown for comparison. Note that actin dimers and trimers are highly unstable species that rapidly dissociate. The three known cellular nucleators of actin assembly each overcome these kinetic barriers by a different mechanism. Formins stabilize actin polymerization intermediates, likely short-pitch dimers. The Arp2/3 complex, associated withWASp actin, is thought to mimic an actin trimer. Spire recruits and organizes up to four actin monomers into a stable prenucleation complex. In each panel, the dotted line (with arrow) points to the barbed end of the polymerized filament. The two halves of the formin FH2 dimer are green, connected by flexible linkers (black). The two actin-like subunits of Arp2/3 complex (Arp2 and Arp3) are pink. The four WH2 domains of Spire (purple) each are capable of binding one actin monomer (reproduced from Goode and Eck, 2007).

Formins, another group of actin nucleators, catalyze a formation of unbranched filaments *de novo*, so that no pre-existing filamentous structures are needed. There are already plenty of biochemical data available describing nucleation processes catalyzed by various FH2 proteins. So far, all experiments were done using recombinant or overexpressed proteins, and though no purified endogenous formins have been tested yet, it seems that FH2 domains almost universally nucleate actin polymerization. Besides the first formin with approved nucleation activity, Bni1p from *S. cerevisiae*, many other yeast and metazoan formins including plant ones were shown to share nucleation abilities, though there are big differences in the efficiency of actin assembly promotion in different formins. For example, Bnr1p from budding yeast is an order of magnitude more potent nucleator and even elongator *in vitro* than Bni1p (Moseley and Goode, 2005). FH2 domain-containing constructs of murine mDia1 further exceed nucleation rates of both yeast

formins Bni1p and Bnr1p. Similarly to other formins tested, the presence of the FH1 domain is necessary for nucleation when actin monomers are profilin bound (Li and Higgs, 2003) and also activity of the FH1FH2 part of Bni1p is stimulated by increasing profilin concentration (Sagot et al., 2001). On the other hand, the FH1FH2 fragment of human Daam1 is 100-fold less potent in nucleation compared to Bni1p (Moseley et al., 2006), and isolated FH2 domain of the *Arabidopsis* formin AtFH5 cannot promote *in vitro* nucleation at all (Ingouff and Gerald et al., 2005).

In vitro experiments proved that the FH2 domain promotes nucleation from the pool of purified actin monomers, which is nearly inhibited by the association of monomeric actin with profilin (Puryne et al., 2002; Sagot et al., 2002; Pring et al., 2003). Interestingly, though the FH2 domain contains two actin-binding sites, it does not bind actin monomers, but can associate with barbed (growing) ends or other parts of existing filamentous actin. This raises the question how do formins catalyze actin assembly *in vivo*, where the majority of actin monomers is buffered by binding to profilin. The FH2 domain forms a dimer of donut-like shape, and the crystal structure of the yeast Bni1p FH2 domain in complex with actin revealed that the same domain conformation could provide nucleation from actin monomers by stabilization of spontaneously formed actin dimers or trimers (Otomo et al., 2005). Such a mechanism has been also suggested based on a time course polymerization assay using the same protein (Pring et al., 2003). This would mean that endogenous formins might relay on the very small amounts of dynamic free actin monomers available within the cell to form a nucleation core, whereas for further filament elongation, they utilize profilin-actin pool, as described below. However, the profilin-interacting FH1 domain may considerably change the nucleation kinetics, as mentioned above.

The third group of actin nucleators is represented by Spire, Cordon bleu (Cobl) and Leiomodin (Lmod) that directly recruit actin monomers to form a nucleation core. Binding of monomeric actin is mediated by WASP-homology 2 (WH2) domains, originally described as actin-binding sites of WASP family proteins necesarry for Arp2/3 activation, though the number of WH2 domains differs (Chesarone and Goode, 2009). The most detailed data are available for Spire (Fig. 2.5), which possesses four WH2 domains and creates a prenucleation complex via stable association of four actin monomers. This structure resembles the single-stranded segment of an actin filament and can be utilized for further elongation (Quinlan et al., 2005; Bosch et al., 2007). The number and layout of WH2 domains is different in both Cordon bleu and Leiomodin compared to Spire, however, the mechanism of organizing actin monomers into a polymerization seed seems to be very similar (Ahuja et al., 2007; Chereau et al., 2008). After nucleation, all the three proteins further catalyze the formation of linear actin filaments, similarly to formins.

A vertebrate protein JMY, first identified as a transcriptional co-activator, shares sequence and functional similarities with both WASP and Spire, so that it assembles filaments directly using a Spire-like mechanism and simultaneously activates Arp2/3 complex. The spatio-temporary regulation of JMY needs to be elucidated yet, but one might suggest that by first nucleating new mother filaments and then activating Arp2/3 to branch off these filaments, JMY could promote rapid formation of a branched actin network (Zuchero et al., 2009).

2.4.2. Actin´it

Once a nucleation seed is completed, actin filament can spontaneously elongate *in vitro* when supplied with free actin monomers. Elongation occurs mainly at their fast-growing (barbed) ends at a rate lineary proportional to the concentration of available actin monomers. However, uncontrolled behaviour of monomeric actin is inhibited *in vivo* by several mechanisms including buffering of monomers by profilin and association of abundant capping proteins with barbed ends of actin filaments. There are several capping proteins described; their name characterizes their function well, as they bind to the growing end of the filament and physically block addition of actin monomers. Furthermore, some of these proteins exhibit also severing activities, so that depolymerization of nascent filament is triggered (reviewed by Wear and Cooper, 2004; Hussey et al., 2006). To overcome this endogenous inhibition, cells express so called „actin elongation factors“ or „actin elongators“ that shield growing barbed ends of filaments from capping proteins and control the rate of elongation process. Only two groups of actin elongators have been discovered so far: formins and enabled/vasodilatator stimulated phosphoprotein (Ena/VASP). Ena/VASP is a family of ubiquitously expressed animal proteins that were reported to move with and protect growing barbed ends of actin filaments. Like formins, they bind the profilin-actin complex and form multimers, though tetramers are assembled rather than dimers (Haffner et al., 1995; Ferron et al., 2007). However, Ena/VASP increased the rate of actin polymerization in the presence of the barbed end cappers only when immobilized on beads, while no actin nucleation or elongation activities could be detected in solution, in a setup routinely used for formins (Bear et al., 2002; Barzik et al., 2005) Thus, formins represent the only regulating factors capable of both actin nucleation and elongation and the only actin elongation factors so far described in plants.

The persistent association of formin with the growing barbed ends, sometimes referred to as „leaky capping“, now as „processive capping“, was firstly described by Pruyne and colleagues, who showed gold-labeled Bni1p molecules to be located near barbed ends of actin filaments on electron micrographs (Pruyne at al., 2002). Later on, formins were proved to compete with capping proteins; they were also able to protect and elongate actin filaments even when the concentrations of capping proteins vastly exceeded formins concentration (Zigmond et al., 2003; Moseley et al., 2004; Harris et al., 2004). The FH2 domain was discovered to dimerise; in case of Bni1p, impairment of dimerisation caused by mutations abolishes actin assembly activity. Although Zigmond and colleagues postulated both dimerisation and tetramerisation of the FH1FH2 fragment from Bni1p, all other structural and biochemical studies confirmed that FH2 and FH1FH2 domains form dimers.

Isolated FH2 domains mostly inhibit elongation rates of actin filaments compared to spontaneous elongation of free barbed ends. Similarly to nucleation efficiency, influence of FH2 domains from different formins on elongation rates varies widely from tight cappers to processive cappers nearly reaching the rates of uncontrolled elongation. For example, the FH2 domain of the mammalian formin FRLα partially inhibits addition of actin monomers at the barbed end, while the same part of mDia1 does not reduce the barbed end elongation rate, though it does block capping protein (Harris et al., 2004). However, activities of FH2 domains are markedly modified by the presence of FH1 domain, so that diffusion-limited growth at free barbed ends can be accelerated up to 19-fold (Paul and Pollard, 2009a). The function of the FH1 domain turned out to be dependent on profilin, which directly associates with FH1. Formin Cdc12p from fission yeast

nucleates purified actin by its FH1FH2 domains, but then restricts barbed end growth by tight capping. Addition of profilin that buffers the pool of actin monomers, inhibits nucleation event, consistent with the nucleation hypothesis described above, while barbed end elongation is accelerated (Kovar et al., 2003). For optimal elongation, only certain concentration range of profilin was found to be supportive, whereas high concentrations inhibited elongation process for all four formins tested in one study, because free profilin competed with profilin-actin for binding FH1 domains (Vavylonis et al., 2006).

Also plant formins were shown to act as potent elongators dependent on FH1 and profilin. The previously mentioned FH2 domain of AtFH5, ineffective of any actin-related activities, nucleates actin filaments that grow at their barbed ends when accompanied by FH1 domain (Ingouff and Gerald et al., 2005). FH2 domain of another *Arabidopsis* formin, AtFH1, itself can nucleate actin filaments, but afterwards, it binds to barbed ends so tightly that only pointed-end growth is permitted. Addition of the FH1 domain switches the FH2 domain to a mild capper, allowing efficient nucleation and elongation from actin monomers bound to profilin. Interestingly, AtFH1 was shown to associate not only with barbed ends, but also with the side of actin filaments in this study (Michelot and Guérin et al., 2005). Further detailed analysis of AtFH1 action performed by the same team revealed that this protein catalyzes actin filament elongation by a unique mechanism, the nonprocessive elongation. Unlike other formins, AtFH1 does not modify the elongation rates compared to free uncapped filaments, because it slides from the barbed end to the side of the filament after the nucleation event and when attached at the side, it can nucleate new actin filaments from the pre-existing one, generating thus bundles (Michelot et al., 2006). Though interactions of formins with the side of growing filaments were observed earlier in case of FRL1, mDia2 and Bni1p (Harris et al., 2006; Moseley and Goode, 2005), those proteins still behave as processive cappers during elongation process, as proved by direct comparism of AtFH1 with mDia2 (Michelot et al., 2006). The fastest rates of actin elongation were detected recently in case of moss Class II formins, where For2A FH1FH2 domains exceeded 2 times the rates of mouse mDia1, the most efficient conventional formin described (Kovar et al., 2006). Interestingly, when individual FH1 and FH2 domains from the different formins were combined to form chimeric proteins, elongation efficiency of FH2 domains was decreased or abolished compared to non-chimeric constructs, indicating that FH2 domains are not universally compatible with any FH1 domain and that there might be a synergistic elongation activity between FH1 and FH2 domains from a given formin class (Vidali et al., 2009). Analogous conclusions can be made based on the study by Neidt and colleagues, who combined FH domains from fission yeast and the nematode worm formins (Cdc12p and CYK-1, respectivelly) together with different profilin isoforms. It was shown that different formins preferentially utilize distinct profilin isoforms and that both FH1 and FH2 domains are necessary for the interaction specificity (Neidt et al., 2009). Preference for distinct profilin isoforms has been demonstrated also for the plant formin AtFH4 (Deeks and Cvrčková et al., 2005).

For a long time it has been speculated on how do formins aquire energy for processive elongation by their FH2 domains. Romero and colleagues concluded that the FH1FH2 formin fragment accelerates hydrolysis of ATP coupled to profilin-actin and uses the derived free energy for processive polymerization (Romero et al., 2004; Romero et al., 2007). However, other group showed that ATP hydrolysis by polymerized actin was not required for formin action, though the possible acceleration of hydrolysis by formins could not be excluded based on their data (Vavylonis et al., 2006). Furthermore, no stimulation of inorganic phosphate release from polymerizing actin caused by FH1FH2 of Bni1p and profilin was detected, as the gamma-phosphate of ATP from actin subunits was released by

profilin a long time after becoming incorporated into filaments by formin. Moreover, efficient elongation catalyzed by FH1FH2 occured even in the presence of ADP-actin monomers. These data obtained by direct microscopic observations of single molecules of the formin indicate that actin subunit addition alone can provide the energy for processive elongation (Paul and Pollard, 2009b).

2.4.3. Bundlin´it

Apart of nucleation and elongation, some formins are capable of other regulatory functions on the actin cytoskeleton, especially bundling, severing and depolymerization of actin filaments. Severing activity resulting into the fragmentation of actin filaments was observed *in vitro* in the case of mouse formin FRL1 and *Arabidopsis* formin AtFH8 (Harris et al., 2004; Yi et al., 2005) and mouse inverted formin INF2 can even actively depolymerize existing filaments, which is mediated by its WH2 domain (Chhabra and Higgs, 2006; Chhabra et al., 2009). Possible *in vivo* function of actin filament severing is not clear; it could be effectively inhibited by endogenous regulatory mechanisms, however, it might also participate in the formation of actin mesh and other cellular structures together with Arp2/3, which could utilize short filaments as a tempate for branching.

Increasing number of FH2 proteins including DRFs was revealed to bundle actin filaments side by side, creating specialized cell stuctures such as cables or stress fibres. Bundling is mediated by formin molecules attached at the site of actin filaments, that supposedly dissociate and recombine with molecules on other filaments via FH2 domains, resulting in a „glue“ effect. Bundled filaments were found to originate in both parallel and anti-parallel orientations. By now, bundling activity has been proved in case of yeast Bnr1p, mouse mDia2, FRL1, FRL2, FRL3 and Arabidopsis AtFH1 (Moseley and Goode, 2005; Harris et al., 2006; Vaillant et al., 2008; Michelot et al., 2005). Though bundling activity results in formation of identical structures, the mechanism slightly differs among the formins listed. For example, a sole FH2 domain is sufficient for Bnr1p-mediated bundling, whereas FRL3 bundling activity is dependent upon a C-terminal DAD/WH2-like domain. AtFH1 requires the presence of both FH1 and FH2 domains for effective bundling and originally randomly polarized nascent bundles become oriented and mostly parallel as filament elongation proceeds, unlike in FRL1 or mDia2 generated bundles. It also remains to be answered, whether bundling happens simultaneously with or independently of actin filament elongation. The study by Harris and colleagues suggests the later possibility, as a mutation of a conserved residue within FH2, inhibiting barbed end activities of FRL1 and mDia2, did not affect bundling. However, FRL1-mediated bundling seemed to compete with barbed end binding, whereas mDia2-mediated bundling was not. Nevertheless, *in vitro* experiments only suggest behaviour of formins *in vivo*, where endogenous factors regulating nucleation, elongation and bundling processes could be expected.

2.4.4. Linkin´it

Regulation of actin cytoskeleton is tightly bound to microtubule dynamics in living cells. To orchestrate cytoskeletal processes, cells utilize a number of proteins directly interacting with both actin and microtubules, together with a huge set of adjacent regulators (reviewed by Petrášek and Schwarzerová, 2009). Also formins are implicated in actin-microtubule

crosstalk and some of them have been shown to be crucial for microtubule dependent processes *in vivo*, which is described in more detail in chapter 2.3. Moreover, in case of some formins, interactions with microtubule-associated proteins or even direct binding to microtubules has been proven.

In budding yeast, both endogenous formins Bni1p and Bnr1p are involved in microtubule-dependent processes; Bni1p is required for microtubule-dependent nuclear migration (Fujiwara et al., 1999) and also for the control of mitotic spindle position (Lee et al., 1999). In both processes, this formin was suggested to function in a kinesin pathway but not in the dynein pathway of microtubule regulation. Recently, a polarisome complex member Bud6p, known to be involved in spindle pole orientation and also in stimulation of actin cable formation through the formin Bni1p, was shown to bind microtubules and promote their cortical capture. Both Bni1p and Bnr1p contribute to Bud6p localization (Delgehyr et al., 2008). In fission yeast, exhibiting polarized cell growth at cell tips, formin For3p regulates both interphase actin cable formation and microtubule organization in a Bud6p-dependent manner (Feierbach and Chang, 2001; Feierbach et al., 2004; Martin and Chang, 2006). Furthermore, For3p directly interacts with a microtubule-associated polarity factor tea4p and together with tea1p it orchestrates actin assembly at new cell ends (Martin et al., 2005). Apart of that, for3p can regulate microtubule-dependent actin assembly independently of tea1p and tea4p via co-ordination with a microtubule plus end binding protein EB1 and its interactor (Minc and Bratman et al., 2009).

The first study to show that formins can directly interact with microtubules was performed by Palazzo and colleagues who found mDia1 and mDia2 to stabilize microtubules *in vivo* when overexpressed. *In vitro* overexpression also resulted in a formation of stabilized microtubules, and mDia proteins associated with these structures (Palazzo et al., 2001). A further study revealed that mDia forms a complex with EB1 and adenomatous polyposis coli (APC) protein at stable microtubule ends (Wen et al., 2004). FH1FH2 domains of mDia2 proved to be sufficient for this interaction, as well as for direct binding to microtubules. Interestingly, a dimerization-impaired mutant of the mDia2 protein also generated stabilized microtubules in cells, showing that mDia2 activities on actin and microtubules are separable *in vivo*. Purified mDia2 was able to protect microtubules against cold- and dilution-induced disassembly and microtubule shortening rates were found to be markedly reduced in its presence (Bartolini et al., 2008). Amazingly, during osteoclast maturation mDia2 was found to have an opposite effect, as it destabilized microtubules by reduction of their acetylation level, which was achieved by activation of the microtubule deacetylase enzyme (Destaing et al., 2005). Also other DRFs are implicated in microtubule regulation; mDia3 coordinates microtubule attachment to kinetochores during mitosis (Yasuda et al., 2004). Based on mutation experiments, human hDia1 is required for recruitment of APC, EB1 and subsequent capture of microtubules in lymphocytes (Butler and Cooper, 2009). Microtubule stabilization during synaptic growth in *Drosophila* is also Dia dependent (Pawson et al., 2008). These results might suggest a regulatory pathway conserved from yeast to mammals, where DRFs function as scaffold proteins between actin and EB1/microtubules, though it remains unclear how are both of these regulatory functions orchestrated in living cells. It has been speculated that DRFs use binding to microtubule plus ends via the EB1/APC complex as a landmark for polarized actin assembly (Basu and Chang, 2007), but for example, hDia1 was shown to localize first at lytic synapses, before the microtubule-associated proteins that subsequently mediated microtubule capture (Butler and Cooper, 2009).

Formin mediated control of microtubule dynamics appears to be a universal feature of formin function, as it is not restricted to the evolutionarily ancient DRFs subgroup of

FH2 proteins. Endogenous human inverted formin 1 (INF1) directly localizes to microtubules in fibroblasts. Moreover, it induces formation of both bundled, acetylated microtubules and actin stress fibers and mediates coalignment of microtubules with actin filaments when overexpressed (Young et al., 2008). *Drosophila* formin Cappuccino (Capu), originally identified as a crucial factor for microtubule distribution during oocyte development (Emmons et al., 1995), also binds microtubules and crosslinks them with actin *in vitro* (Rosales-Nieves et al., 2006). Similarly, FHOD subfamily members are able to cause microtubule alignment with actin stress fibers (Gasteier et al., 2005) and Formin-1 (Fmn1) from the Fmn subfamily localizes to interphase microtubules in fibroblasts (Zhou et al., 2005). Recently, the first evidence of a plant FH2 protein capable of microtubule association has been described. Overexpressed AtFH4 from *Arabidopsis* predominantly decorates microtubular structures, accumulates at the endoplasmic reticulum and co-aligns it with microtubules. Purified AtFH4 directly binds to microtubules *in vitro*, as proved by co-sedimentation assays that also suggested microtubule bundling activity of AtFH4 (Deeks and Fendrych et al., 2010). Thus, unlike other microtubule-associated formins, AtFH4 and INF1 seem to be the only FH2 proteins reported so far that localize predominantly to microtubules rather than actin filaments.

Though the interaction with microtubules turned out to be quite a common feature of formin action, no conserved region mediating binding to microtubules is shared by known microtubule-associated FH2 proteins. Instead, each family member evolved its own binding site of a different location on a protein molecule. For example, some of the formins mentioned above bind to microtubules through peptide domains located outside any of the FH domains. Such a region corresponds to the second exon upstream of FH3 domain in Fmn1 (Zhou et al., 2005) or to a N-terminal sequence between TM and FH1 domains named the group Ie (GOE) domain in case of AtFH4 (Deeks and Fendrych et al., 2010), whereas a C-terminal polypeptide is sufficient for proper colocalization of INF1 with microtubules (Young et al., 2008). On the contrary, Capu was shown to bind microtubules through its FH2 domain (Rosales-Nieves et al., 2006), and mDia2 binding site maps to a C-terminus of FH2 domain plus a short adjacent downstream sequence (Bartolini et al., 2008).

2.4.5. A detailed insight into processive capping

Hand in hand with the discovery of processive capping of actin filaments, the first suggestions that formins multimerise via the FH2 domain have emerged (Li and Higgs, 2003; Zigmond et al., 2003; Harris et al., 2004). Detailed information about FH2 domain architecture was provided very soon by revealing crystal structure of Bni1p FH2, which turned out to form a “tethered dimer”. Such an intact dimer is required for actin nucleation and processive capping mediated by FH proteins (Xu et al., 2004), as further confirmed by crystalization of the same FH2 domain in the complex with actin (Otomo et al., 2005).

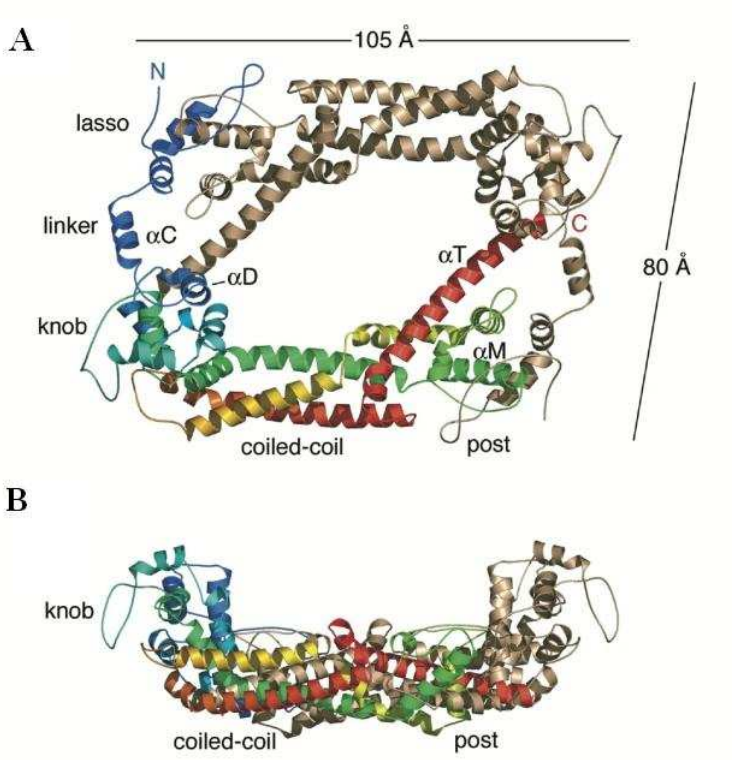

Fig 2.6 Ribbon diagram showing the overall architecture of the FH2 dimer. A: One molecule is colored using the visible spectrum (from blue at th e N terminus to red at the C terminus), the second molecule is colored tan. The lasso, linker, knob, coiled-coil, and post subdomains are labeled, and the approximate dimensions of the dimer are indicated. The N and C termini and selected α helices of one molecule are labeled. Note the manner in which the lasso region of each molecule encircles a portion of the post subdomain of the other molecule in the dimer. **B:** Side view of the FH2 domain dimer (reproduced from Xu et al., 2004).

The FH2 domain fold is almost entirely α helical and it is overally formed into a rod-shape structure. The dimer is formed by a linkage of two FH2 monomers in a head-to-tail orientation, resulting in a donut-like like structure. Starting from its N-terminus, the single FH2 domain consists of a lasso followed by a flexible linker, together providing the dimerization interface with the second FH2 subunit. The linker is joined to a globular knob region, adjacent coiled-coil region and C-terminally located post subdomain, together forming the rod-shaped domain itself (Fig 2.6). When arranged in the head-to-tail orientation with the second FH2 domain, the lasso of one FH2 subunit encircles the post region of the other subunit assuring a very stable contact between them (Xu et al., 2004). Functionally, the dimer is composed of two hemidimers that do not entirely correspond to each FH2 subunit. The hemidimer is formed by the rod-shape domain of one subunit, and the lasso segment of the other. Such a structure represents one functional actin-binding unit, referred to as a bridge element, as it forms a bridge between two actin subunits (Otomo et al., 2005). The interaction with actin is mediated by two highly conserved regions within the hemidimer, one located on Ile 1431 in the knob region and Lys 1601 in the post segment of Bni1p FH2 domain. A mutation of either of these residues is sufficient for a complete impairment of the actin nucleation activity (Xu et al., 2004).

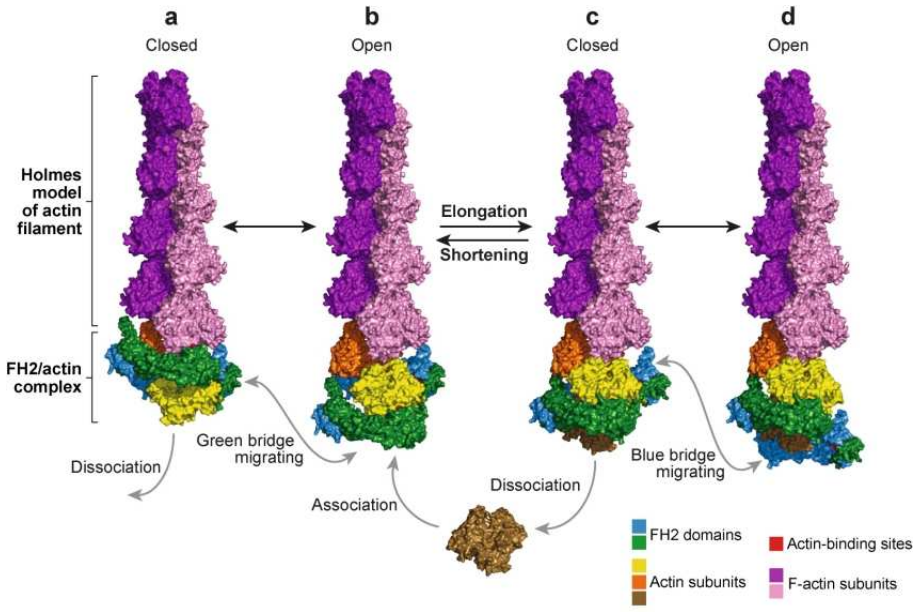

Fig 2.7 Structure-based model of processive capping. The FH2/actin complex is superimposed on the barbed end of the Holmes model of the actin filament. Panels **a** and **b** represent the closed and open configurations, respectively. In both these panels, the green FH2 bridge element is migrating, and the blue bridge is bound. The yellow subunit is in a strained orientation relative to the bulk filament. Panels **c** and **d** represent the (n + 1)th step of elongation and are precisely analogous to steps a and b, respectively, except that the filament is one subunit longer and that the roles of the bridges are reversed—the green bridge is now bound, the blue bridge, migrating. Incorporation of the tan subunit (in the strained orientation) is proposed to induce the now penultimate yellow subunit to adopt F-actin orientation, so that the blue bridge is released to become the migrating bridge. The green bridge is tightly bound because it now makes ideal contacts with the yellow and tan subunits (which are equivalent to the orange and yellow subunits in panels a and b). For more details, see text (adapted form Goode and Eck, 2007).

On the basis of structural and biochemical data, a model of processive capping for FH2 movement at the barbed end of actin filament has been proposed by several authors. Though particular models differ in some details, they basically follow a stair stepping mechanism of FH2 action (Xu et al., 2004; Kozlov and Bershadsky, 2004; Moseley et al., 2004; Otomo et al., 2005; Shemesh et al. 2005; Vavylonis et al., 2006). By combination of the models listed here, Goode and Eck (2007) presented an integrated model of processive capping for either filament polymerization or depolymerization (Fig 2.7). Generally, FH2 domain is proposed to be in a dynamic equilibrium between the open and closed configurations, when one bridge element (hemidimer) is bound and the other is migrating. The bound bridge remains in the tight interaction with two ultimate subunits of the barbed end, while the migrating bridge interacts just weakly, so that it can move and govern addition or dissociation of actin monomers. The addition of a new actin subunit is possible only in an open (accessible) configuration of the migrating bridge, when the hemidimer associates just with the single terminal actin subunit of the filament through the knob region, while its post segment is exposed and capable of actin addition. Actin elongation gets suppressed when the bridge enters a closed (blocked) conformation providing no contact with the terminal subunit. In this state, only dissociation of actin subunits from the

filament can occur. Importantly, actin subunits undergo an orientation shift during the addition process from a strained orientation (in case of newly added subunit) to a F-actin orientation (in case of other previously inserted subunits). FH2 domain binds tightly only to the strained actin subunits, while the interaction with the F-actin oriented ones gets much weaker. Once the new actin subunit is incorporated at the barbed end, the migrating bridge becomes the bound bridge, because it comes into the contact with two actin subunits including the new one with the strained orientation. By this, the preultimate actin subunit turnes into the F-actin orientation, so that the second bridge becomes the migrating bridge, as it now contacts two F-actin oriented subunits. After one cycle (i.e. addition of one subunit), the bridges have reverse roles and after another cycle, the situation is equivalent to the starting point but the filament is two subunits longer. The repeated release of the cap from the end of the nascent fibre may also relax filament torsion that would otherwise soon block filament elongation (Shemesh et al. 2005).

2.5. Regulation of formin action and interacting partners

Regarding the divergences in domain architecture outside the FH1 and FH2 regions, it is not surprising that binding partners implicated in regulatory mechanisms differ among formin subgroups. The only protein interacting with all FH2 proteins tested is profilin, an actin binding protein that sequesters the endogenous pool of actin monomers. Profilin interacts with formins through their FH1 domain that delivers profilin-actin complexes into the proximity of the FH2 domain, thus enhancing its filament elongation efficiency, as described previously.

2.5.1. Regulation by Rho GTPases

One of the best characterized regulatory mechanisms controlling formin action is autoinhibition of DRFs, maintained by intramolecular interaction between N-terminal DID and C-terminal DAD (Alberts, 2001; Li and Higgs, 2003; Wallar et al., 2006; Schonichen et al., 2006). This autoinhibited state effectively impairs the actin nucleation catalytic activity of the FH2 domain, however, the impacts of microtubule-binding or regulation are not clear yet, as constitutivelly active mutant forms of DRFs lacking the N-terminal regulatory elements were usually tested (e.g. Ishizaki and Morishima et al., 2001). In most cases, DID-DAD interaction is released after binding of activated Rho GTPase at the N-terminal GBD. The mechanism of Rho GTPase regulation is indicated in Fig. 2.2. Nevertheless, action of Rho is not always sufficient, as for example RhoA releases inactivated mDia1 only partially (Li and Higgs, 2003), and the formin Daam1 can be activated both in the presence and in the absence of Rho by another factor, Dishevelled (Dvl). Moreover, Daam1 acts upstream of RhoA and is required for its activation (Habas et al., 2001; Liu et al., 2008). In addition to the autoinhibitory potential mediated by the interaction of N- and C-termini, Daam1 is capable also of inter-domain autoinhibition within its FH2 domain, which is provided by a ß-strand located at the end of the linker region. Therefore, purified Daam1 acts as a weak actin nucleator *in vitro*. Crystal structure of the Daam1 FH2 domain revealed that the ß-strand stabilizes FH2 dimer in a locked conformation that constrains its actin binding surfaces. Mutations that disrupt the β-strand lock increase Daam1 nucleation activity about tenfold to a level comparable to other

formins (Lu et al., 2007). The manner of Daam1 autoregulation is potentially very inspiring for plant biologists, as plant formins contain neither of the N-terminal domains typical for DRFs; thus a kind of inter-domain interactions could be implicated in their regulation, which remains still enigmatic.

Apart of release from autoinhibited state, Rho mostly helps to localize formins to the specific cell compartments or regions (Pellegrin and Mellor, 2005; Seth et al., 2006; Wallar et al., 2006; Martin et al., 2007). Genetic interaction between formins and Rho GTPases was originally identified on the basis of yeast mutation studies and confirmed by yeast two-hybrid assay, in which formin Bni1p formed complexed with activated form of Rho GTPase Cdc42 and actin (Evangelista et al., 1997), while the second yeast formin Bnr1p was shown to interact with another GTPase Rho4 and profilin (Imamura et al., 1997). By the same time, similar observations were made for mammalian formin mDia (Watanabe et al., 1997). Many other DRFs bind Rho GTPase proteins and function as their direct effectors in cytoskeleton remodeling processes. This interaction turned out to be highly specific, as particular formins are able to associate only with certain Rho proteins (Imamura et al., 1997; Dong et al., 2003; Gasman et al., 2003; Lammers et al., 2008).

Another class of GTPase-related scaffold proteins identified in yeast and animals, IQGAPs are implicated in activation and recruitment of formins. IQGAPs contain IQ motifs responsible for binding of calmodulin, as well as GTPase activated proteins (GAPs) homology regions (Weissbach et al., 1994; Brandt and Groose, 2007). However, GAP activity seems to be missing in IQGAPs . Instead, they were found to inhibit GTP hydrolysis rates of particular GTPases such as Cdc42, thus stabilizing their activated GTP-bound forms (Brill et al., 1996; Hart et al., 1996; McCallum et al., 1996; Noritake et al., 2004). Moreover, Brill and coleagues (1996) predicted the presence of a WW domain and a F-actin binding domain in IQGAP1 and IQGAP2. Indeed, the association of IQGAPs proteins with actin cytoskeleton through calponin homology domain (CHD) was verified experimentally (Hart et al., 1996; Mateer et al., 2002; Mateer et al., 2004). With respect to actin cytoskeleton, IQGAPs appear to function as master regulators, as they further directly bind and stimulate both Arp2/3 complex activator N-WASP (Bensenor et al., 2007; Le Clainche et al., 2007) and the mammalian formin mDia1. IQGAP1 interacts with mDia1 through a region within the DID domain; the RhoA-mediated release of mDia1 autoinhibition is necessary for its subcellular location (Brandt et al., 2007). This might evoke an idea of a complex regulation of actin assembly, where IQGAP1 stimulates mDia1 nucleation and elongation activity and simultaneously recruits and activates Arp2/3 complex through WASP intaraction to the proximity of pre-existing filaments (Pollard, 2007). To provide a far more complex regulation, IQGAP1 can bridge actin cytoskeleton with microtubules via binding to the microtubule plus end tracking protein CLIP170 (Fukata et al., 2002), which also interacts with mDia1 FH2 domain (Lewkowicz et al., 2008).

Similarly to Daam1 mentioned above, the formin mDia1 can function also upstream of Rho GTPase independently of its downstream behaviour on actin assembly as the Rho effector. This is achieved by binding to the leukemia-associated Rho-GEF (LARG), leading to the activation of RhoA. Thus, mDia1 is a part of positive-feedback loop regulating RhoA activity (Kitzing et al., 2007). In migrating cells, LARG interacts with G protein-coupled receptor and together with mDia1, it transduces extracellular signals and directs cell polarity through microtubule dynamics (Goulimari et al., 2007).

2.5.2. Regulation by post-translational modifications

Arp2/3-mediated nucleation independently of Cdc42 (Fukuoka et al., 2001). Similarly, WASP and Scar/WAVE family proteins known as activators of Arp2/3 complex were reported to modulate formin activity through direct interactions. During filopodium formation, WAVE and Arp2/3 can form the complex with mDia2, resulting in the inhibition of formin function (Beli, Mascheroni and Xu et al., 2008). *Drosophila* WASP family member Wash acts downstream of Rho1 and further genetically interacts with three different actin nucleators, the formin Cappuccino (Capu), Spire and Arp2/3 complex. Wash was shown to nucleate actin in an Arp2/3-dependent manner and to control actin and microtubule dynamics through Spire and Capu (Liu et al., 2009). These data indicate that scaffold proteins such as DIP or WASP/WAVE might inhibit formin activity while simultaneously stimulating Arp2/3 complex and vice versa, thus balancing the action of different cytoskeleton regulating proteins. A common regulatory feature, phosphorylation, plays a crucial role in the activation of some formins. In yeast, Bni1p was shown to be activated by the Fus3p kinase. Phosphorylation of Bni1p by Fus3p was proved *in vitro* and *in vivo*, where it turned out to be necessary for Bni1p localization and activation during the pheromone response (Matheos et al., 2004). Recently, phosphorylation of the Bni1p formin by another kinase Prk1p was found to be sufficient for disruption of its intramolecular interaction and subsequent activation (Wang et al., 2009). Regulation of FH2 proteins by phosphorylation occurs also in mammals, where human formin FHOD1 is modified at its C-terminus by Rho-dependent protein kinase ROCK1, resulting in disruption of the autoinhibitory interaction. FHOD1 phosphorylation-mediated release is sufficient for a full restoration of formin activity, so that no further activation by RhoGTPase is required (Takeya et al., 2008).

Another very interesting regulatory interactions were discribed in case of the inverted formin INF1, which does not lose the actin nucleation potency when its DID and DAD (represented here by WH2) domains associate, whereas this inhibitory interaction impairs the actin depolymerization activity. Furthermore, INF1 associates with endoplasmic reticulum due to the farnesylation of its C-terminus, though ER binding depends only partly on the C-terminal prenyl group and ionic interactions between INF1 and ER might be also important (Chhabra et al., 2009). Membrane localization of another formin, FMNL1, is achieved by myristoylation of its N-terminal region (Han and Eppinger et al., 2009) suggesting that formins evolved various Rho-independent mechanisms for their activation and recruitment.

2.5.3. Other localization partners and interactions with scaffold proteins

In many species ranging from flatworms to mammals, Src tyrosine kinase signalling was found to coordinate cellular processes through formin proteins that mostly bridge Src kinases with the RhoGTPase pathway and trigger Src activation. Src family nonreceptor tyrosine kinases have multiple roles in cellular signaling. They are activated by mitogens, such as lysophosphatidic acid (LPA) that induce significant changes in Rho-dependent actin dynamics (Ridley and Hall, 1992; Rodriguez-Fernandez and Rozengurt, 1996). Src binds to the FH1 domain of formin proteins through its SH3 domain. Following FH2

proteins have been identified as direct binding partners for Src in animal cells: mouse DRFs mDia1 and mDia3 (Tominaga et al., 2000; Gasman et al., 2003; Yamana and Arakawa et al., 2006), delphilin (Miyagi et al., 2002); DAAM1 (Aspenstrom et al., 2006), FHOD1 (Hannemann et al., 2008), FMN1 (Uetz et al., 1996) and schistosomal SmDia (Quack et al., 2009). In case of FHOD1, Src kinase activity is required for physical and functional interactions between the formin and ROCK1 kinase during plasma membrane blebbing (Hannemann et al., 2008). mDia1 regulates polarization in migrating cells by delivering APC and active Rho-GTPase Cdc42 in microtubule-dependent manner and Src in actin-dependent manner to their respective sites of action (Yamana and Arakawa et al., 2006). Besides the direct interaction with mDia, activation of Src kinase was also found to be modified by a SH3 domain-containing Dia-interacting protein (DIP) acting downstream of mDia (Satoh and Tominaga, 2001). Another SH3 containing protein, an insulin receptor substrate p53, binds to FH1 domain of mDia1 (Fujiwara et al., 2000), suggesting that FH1 domain provides a lot more regulatory interactions besides its profilin/actin binding activity.

The recently described interacting protein DIP (alternatively termed WISH from WASP interacting SH3 protein), binds the FH1 domain of mDia through its SH3. It can further directly target FH2 domains of mDia1 and mDia2, where in the later case it inhibits formin-mediated actin filament assembly and bundling *in vitro*. This interaction is mediated by the leucine-rich region (LRR) of DIP and provides a Rho-independent regulatory mechanism of formin inhibition and activation (Eisenmann et al., 2007). Moreover, DIP was shown to directly interact with N-WASP, the activator of another actin nucleation factor, Arp2/3 complex. Upon binding to N-WASP, DIP stimulates Arp2/3-mediated nucleation independently of Cdc42 (Fukuoka et al., 2001). Similarly, WASP and Scar/WAVE family proteins known as activators of Arp2/3 complex were reported to modulate formin activity through direct interactions. During filopodium formation, WAVE and Arp2/3 can form the complex with mDia2, resulting in the inhibition of formin function (Beli, Mascheroni and Xu et al., 2008). *Drosophila* WASP family member Wash acts downstream of Rho1 and further genetically interacts with three different actin nucleators, the formin Cappuccino (Capu), Spire and Arp2/3 complex. Wash was shown to nucleate actin in an Arp2/3-dependent manner and to control actin and microtubule dynamics through Spire and Capu (Liu et al., 2009). These data indicate that scaffold proteins such as DIP or WASP/WAVE might inhibit formin activity while simultaneously stimulating Arp2/3 complex and vice versa, thus balancing the action of different cytoskeleton regulating proteins.

Lately referred protein Capu, the member of FMN formin subgroup, forms a complex with another actin nucleator Spire, which also catalyzes the formation of unbranched filaments. Spire binds directly to the FH2 domain of Capu and this interaction impairs formin nucleation activity. In contrast, formation of Spire–Capu complex enhances actin nucleation by Spire (Quinlan et al., 2007). Based on bioinformatic data, there is evidence linking the two proteins in other organisms, as in sequenced metazoan genomes, Capu family formins appear only in organisms that also contain Spire family genes (Higgs and Peterson, 2005). Recently, analogous cooperation has been also reported in case of the mammalian homologs Spir-1 and Spir-2, which interact with formin-1 and formin-2 , though in this case, the interaction is not mediated by the FH2 domain of formin proteins (Pechlivanis et al., 2009).

Bud14p, a yeast multifaceted cytoskeletal regulator that coordinates microtubule- and actin-based functions via separate domains, was shown to rapidly displace the Bnr1p formin FH2 domain from growing barbed ends, enabling a continuous production of short

actin filaments at the bud neck (Chesarone et al., 2009). Though other formins, such as fission yeast For3p or budding yeast Bni1p were also observed to undergo a rapid retrograde movement shortly after their attachment at the site of action, i.e. membrane (Martin and Chang, 2006; Buttery and Yoshida et al., 2007), this is the first direct observation of active formin removal by the displacement factor followed by attenuation of actin filament elongation. Recently, mDia2 was found to be targeted by post-translational ubiquitin modification and degraded at the end of mitosis. A forced expression of activated mDia2 resulted in failure of cytokinesis (DeWard and Alberts, 2009), indicating the necessity of switch-off mechanisms regulating formin activities.

2.5.4. Localization mechanisms of plant formins

Unfortunately, nearly nothing is known about regulation and interacting partners of plant formins on the cellular level. However, at least in some cases, such as Class I formins with transmembrane domains, they do not necessarily need to bind proteins providing their localization as do yeast and animal formins, because their localization-mediating elements are already incorporated at the N-terminus of the protein. The localization of standard Class I formins (see type A in Fig 2.8) to the plasma membrane has been proven experimentally in case of *Arabidopsis* family members AtFH1, AtFH4, AtFH5, AtFH6 and AtFH8. In a primary work by Banno and Chua (2000), AtFH1 remained in a microsomal fraction after cell fractionation, indicating a possible membrane association. When overexpressed in pollen tubes, AtFH1 decorated the plasma membrane and caused severe membrane deformations (Cheung and Wu, 2004). For AtFH4, localization data of the endogenous protein are available, where AtFH4 accumulates at cell-to-cell borders between adjoining cells, as shown by indirect immunofluorescence. In the same work, N-terminal region of a related formin, AtFH8, attached to GFP labeled cell membrane zones in *Arabidopsis* roots (Deeks and Cvrčková et al., 2005). Also AtFH6 is targeted to the plasma membrane, as shown by both localization of a GFP fusion protein in protoplasts, BY-2 culture cells or *Arabidopsis* roots and by immunolocalization of the endogenous formin (Favery and Chelysheva et al., 2004; Van Damme et al., 2004). Unlike those, stably overexpressed AtFH5-GFP accumulates in the cell plate of dividing root cells and the signal reduces after contact is made between the cell plate and the parent cell wall, while no plasma membrane association is evident, as would be expected (Ingouff and Gerald et al., 2005). This suggests the presence of endogenous regulatory factors that orchestrate spatio-temporal localization of AtFH5 and restrict its localization to a specific spatio-temporal domain; further analysis of such a behaviour wold be appreciated. In plant formins, the only non-cytoskeletal interactor published so far came from yeast two-hybrid screen using C-terminal region of AtFH1 as a bait. This novel protein, named FIP2, shares a partial homology to animal K^+ ATPases and bacterial putative membrane proteins (Banno and Chua, 2000), but nothing is known about its effect on formin behaviour and no further studies characterizing this interaction has been reported.

The PTEN-like domain of many Class II formins (type D in Fig 2.8) may also provide an interface for various regulatory elements. Its role in formin recruitment was shown in case of the moss *Physcomitrella*, where it mediated apical localization of formins For2A and For2B in growing cells (Vidali et al., 2009). Animal PTENs usually exhibit phospholipid phosphatase activity, however, plant PTEN-related domains apparently lack conserved residues required for this activity (Cvrčková et al., 2004). Nevertheless, many regulatory interactions of animal PTENs are mediated by other than catalytic regions. For

example, intracellular localization of PTEN in leukocytes and kidney cells is regulated by Rho GTPases RhoA and Cdc42 (Li and Dong and Wang et al., 2005) and human PTEN is stabilized by association with PDZ domain-containing proteins (Valiente et al., 2005). Just to remind, PDZ domain is also found in the FH2 protein delphilin. No experimental data are available yet for the Class III group of plant formins, which contain RhoGAP-related domain, however, localization and regulation function of this region could be expected as well (Grunt et al., 2008).

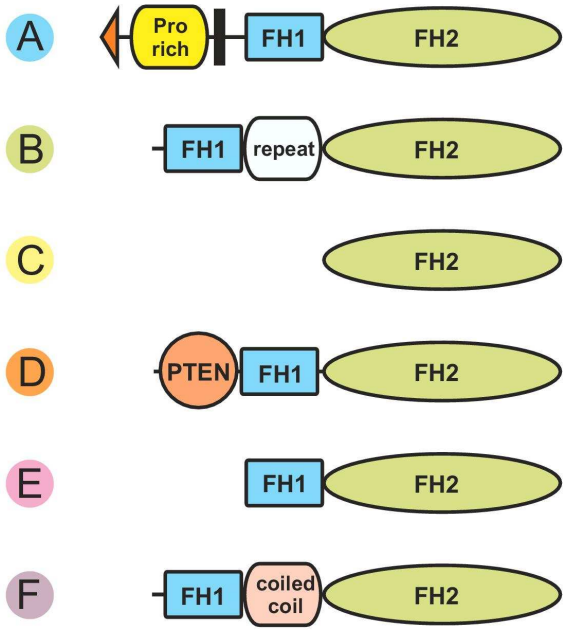

Fig 2.8 Domain composition of FH2 proteins in higher plants. Schematic representation of the domain composition and order encountered in plant FH2 proteins (domains of variable size, such as FH1, and unique sequences not to scale). Note that only structures E and F correspond to those found outside the plant kingdom (Cvrčková et al., 2004).

Chapter 3

MATERIAL AND METHODS

3.1. Biological material

Bacterial strains were used as follows: *Escherichia coli* XL1-Blue, *Escherichia coli* DH5α, *Escherichia coli* DB3.1, *Escherichia coli* Rossett, *Escherichia coli* Codon+, *Agrobacterium tumefaciens* GV3101, all grown on LB medium.

Suspension culture Bright Yellow-2 (BY-2) from *Nicotiana tabacum* was cultivated in LS medium (Linsmaier-Skoog), whereas *Arabidopsis thaliana* suspension culture was grown on MS medium (Murashige-Skoog, Duchefa) containing Gamborg B5 vitamins (Duchefa). For extracts isolation, cells were harvested at the late exponential phase after 4-7 days.

3.2. Plant cultivation

Arabidopsis plant were cultivated directly *ex vitro* or *in vitro*. For *in vitro* cultivation, *Arabidopsis* seeds were sterilized for 3 min. by 70% ethanol followed by 10% household bleach treatment (2 x 3 min.) and washed 3 times in sterile water. Seeds were vernalized in 4°C for 3 days. Plantlets were cultivated in 20°C under long day light period (16 hours light, 8 hours dark) on half strenght MS medium (Murashige-Skoog, Duchefa) containing 1% sucrose and 0.8% agar or 1.6% agar for vertical plates, respectively. Medium was supplemented with selection agents and other chemicals as required: kanamycin in concentration 50 mg/l, hygromycin 25 mg/l, Basta [PPT, ammonium 2-amino-4-(hydroxymethylphosphinyle) butyrate] 20 mg/l or claforan (sephotac) 100 mg/l. After development of true leaves (10-14 days), plantlets were transfered into Magenta boxes GA7 (Sigma) and finally removed on soil (mixture of „Zahradnický substrát B“ with sand 2:1) and further cultivated under long day conditions.

Tobacco (*Nicotiana tabacum* and *N. benthamiana*) plants were sown on soil and cultivated under the same conditions as *Arabidopsis* plants.

3.3. Genotyping analysis of T-DNA insertional mutants

Plant DNA for genotyping was isolated either according to DNazol Reagent protocol (GibcoBRL, Invitrogen) from 5-30 mg of plant tissue, or using sodium hydroxide treatment of inflorescences (Klimyuk et al., 1993). Briefly, several flowers and flower buds were collected in a test tube with 40 µl 0.25 M NaOH. Samples were boiled for 3 min and neutralized by addition of 40 µl 0.25 M HCl together with 20 µl 0.5 M Tris- HCl and

0.25% Nonidet NP-40. The mixture was boiled for another 3 min and than immediately chilled on ice. If necessary, DNA isolates were stored at 4°C.

PCR was carried out with the Biometra aparatus, parameters were set on 58-66°C, 50 sec for annealing and 72°C 30-100 sec for elongation using Taq polymerase or DreamTaq polymerase (MBI). Temperatures and times have been optimized for each set of primers and PCR product lenght. 0.5 µl of DNazol miniprep or 1 µl of hydroxide DNA preparation were used as a template in 20 µl of total reaction volume. List of T-DNA mutant lines and primers used for genotypic analysis are shown in Tab 3.1, sequences in Supplemental data 1.

Table 3.1 T-DNA insertion lines in *Arabidopsis* formin genes.

[1]Used together with LB3-short primer (CATCTGAATTTCATAACCAATCTCG) for SAIL lines or with LBb1 primer (GCGTGGACCGCTTGCTGCAACT) for SALK lines to detect the gene-specific T-DNA insertion. [2] Used together with the corresponding primer for T-DNA detection to detect the presence of WT alelle. ND = not designed.

gene	locus	mutant name	T-DNA line	primer for T-DNA detection[1]	primer for wt detection[2]
AtFH1	At3g25500	***atfh1***	SALK_032981.52	AtFH1	AtFH1aA
AtFH2	At2g43800	***atfh2***	SAIL_615_E03	AtFH2	AtFH2aA
AtFH3	At4g15200	***atfh3***	SAIL_426_F05	AtFH3	AtFH3aA
		atfh3-2	SALK_150350.38	AtFH3-2	AtFH3-2aA
AtFH4	At1g24150	***atfh4***	SALK_005937.42.20	AtFH4	AtFH4aA
AtFH5	At5g54650	***atfh5***	SALK_044455.48.95	AtFH5	AtFH5aA
		atfh5-2	SALK_044464.17.30	AtFH5-2	AtFH5-2aA
AtFH6	At5g67470	***atfh6***	SALK_031051.46	AtFH6	AtFH6aA
AtFH7	At1g59910	***atfh7***	SAIL_677_E08	AtFH7	AtFH7aA
AtFH8	At1g70140	***atfh8***	SAIL_93b_D11	AtFH8	AtFH8aA
AtFH10	At3g07540	***atfh10***	SAIL_530_H05	AtFH10	ND
AtFH11	At3g05470	***atfh11***	SAIL_37_A10	AtFH11	ND
AtFH12	At1g42980	***atfh12***	SALK_004741.53	AtFH12	AtFH12aA
AtFH13	At5g58160	***atfh13***	SALK_046433.47	AtFH13	AtFH13aA
AtFH14	At1g31810	***atfh14***	SALK_058886.40	AtFH14	AtFH14aA
AtFH15	At5g07650	***atfh15a***	SAIL_700_D04	AtFH15a	AtFH15a-aA
		atfh15b	SAIL_1230_C10	AtFH15b	ND
AtFH16	At5g07770	***atfh16***	SAIL_720_F01	AtFH16	AtFH16aA
		atfh16-2	SALK_092364.40	AtFH16-2	AtFH16-Bgl
AtFH17	At3g32400	***atfh17***	SAIL_618_B12	AtFH17	AtFH17aA
AtFH18	At2g25050	***atfh18***	SAIL_204_E11	AtFH18	AtFH18aA
AtFH20	At5g07740	***atfh20***	SAIL_1237_B06	AtFH20	ND

3.4. Crossing of *Arabidopsis* plants

After removal of already opened flowers, young flower buds and developing siliques, closed flower buds of 1-1.2 mm in lenght with immature anthers were emasculated by tweezers continuously sterilized with 70% ethanol. Mature anthers from donor plant were placed on the stigma and covered by foil wrapper to avoid stigma dessication and undesired pollination.

3.5. Gene expression data analysis

Public expression data from experiments using the Affymetrix ATH1 *Arabidopsis* genome array available at the Genevestigator database (https://www.genevestigator.ethz.ch; Zimmermann et al., 2004; Hruz et al., 2008) were used. For general anatomy analysis, arrays from wild-type plants grown under physiological conditions were selected. List of experiments used for the analysis is shown in Supplemental data 2. Average values of normalized signal intensities were determined. For representational purposes we grouped expression values into six categories.

For more detailed expression analysis of selected formins in roots and under dark conditions, significant data ($p>0.06$) of untreated WT samples from following experiments were used, annotation databases are in brackets: AT 00029 (NASC), AT 00079 (NASC), AT 00093 (AtGene Express), AT 00191 (NASC), AT 00286 (GEO) for roots and AT 00002 (FGCZ), AT 00109 (AtGene Express), AT 00206 (GEO), AT 00153 (NASC), AT 00276 (GEO), AT 00300 (GEO). Following experiments contain data for induced PCD and stress-related mutants: AT-00026 (NASC), AT-00175 (NASC), AT-00180 (ArrayExpress), AT-00291 (GEO).

3.6. RNA isolation and reverse transcription

RNA for reverse transcription was prepared usually from 100 mg of fresh material using the RNeasy plant mini kit (Qiagen) according to manufacturer protocol. RNA concentration was measured spectroscopically. The first strand cDNA synthesis was performed using the BioBasic RT-PCR kit following manufacturer´s instructions except the reverse transcriptase enzyme (Sigma). Ordinarily, 1-4 μl of total RNA preparation was preincubated for 10 min at 70°C together with oligo(dT) primer and dNTP mixture followed by chilling on ice. After that, other chemicals including AMV reverse transcriptase were added into 20 μl of total reaction volume and incubated for 40 min at 48°C followed by 20 min at 55°C.

3.7. Cloning of selected formin genes

Standard molecular cloning methods have been used throughout, with minor modifications; the Gateway cloning-by-recombination system (Invitrogen) has been used according to manufacturer´s instructions.

3.7.1. *AtFH3*

Whereas no cDNA or partial ESTs of *AtFH3* gene were publicly available, N-terminally truncated version of the gene was obtained from reverse transcription. For RT-PCR, RNA from *Arabidopsis* flowers and flower buds was isolated, reverse transcription was performed with oligo(dT) primer and for *AtFH3* amplification, gene specific primers AtFH3-ATG and AtFH3-re-Eco were used. High-fidelity Accu Taq polymerase (Sigma) or Phusion Polymerase (Finnzymes) were used for all PCR amplifications. As 5´-end has not been reliably predicted (latest prediction does not include Met as the first amino-acid indicating another upstream part as a possible gene coding region), a 5´-primer was therefore designed according to the first predicted in-frame Met. Such a version still contains the transmembrane domain and conserved formin homology domains FH1 and FH2. Based on this template, three different domain variants were amplifiend using AtFH3-re-Pci 3´-reverse primer together with 5´-forward primers AtFH3-ATG-Pci, AtFH3-1+2-Pci or AtFH3-2D-Pci, cloned under Lat52 promoter into pCAMBIA-Lat52-GFP (a kind gift of David Twell), thus creating Lat52::AtFH3t:GFP, Lat52::AtFH3[FH1FH2]:GFP and Lat52::AtFH3[FH2]:GFP. Sequencing of Lat52::AtFH3t:GFP revealed unexpected differences in gene structure (described in section 4.2.1) that abolished predicted reading frame. Constructs with a contigueous AtFH3 reading frame were used for stable transformation of *Arabidopsis* plants.

Furthermore, parts of *AtFH3* devoid of transmembrane domain were amplified with 3´-AtFH3-re-Y2H-Pst primer together with AtFH3-1+2-Y2H-Eco or AtFH3-2D-Y2H-Eco 5´-primers and cloned via introduced EcoRI+PstI sites into the yeast two-hybrid vectors pGAD containing activation domain and pGBT bearing bait domain, respectively (both obtained from Clontech). BD-AtFH3[FH1FH2] has been used by the time of writing for yeast two-hybrid interaction screen. The sequences of all primers are shown in the Supplemental data 1.

3.7.2. *AtFH16*

To obtain full-length cDNA of the *AtFH16* gene, we have first sequenced the presumably complete cDNA corresponding to the EST clone APZL29g02 (Kazusa), expected to contain a complete AtFH16 region corresponding to gene predictions. For amplification, a set of gene-specific primers AtFH16-fb-Eco and AtFH16-re-Xho introducing EcoRI and XhoI sites, respectively was used. The full-lenght cDNA of AtFH16 was digested with EcoRI and XhoI enzymes, cloned into pBluescript KS+ vector and sequenced. Within its N-terminus, the cDNA turned out to contain a retained second intron resulting in a premature STOP codon. In order to replace the error-containing part of the gene and to

avoid any sequence changes, an inner ~930 bp long gene fragment was cut out of the construct using restriction enzymes SalI and BglII recognizing endogenous cleavage sites. The corresponding part of the cDNA was obtained by RT-PCR, for which RNA isolated from whole 7 days-old *Arabidopsis* seedlings and transcribed by reverse transcriptase from the oligo(dT) primer was used as a template. The inner fragment was than amplified with a pair of primers AtFH16-Sal and AtFH16-Bgl derived from the endogenous sequence, digested with SalI and BglII restrictases and re-cloned instead of the incompletely spliced region into pBluescript KS+ containing original N- and C-termini of *AtFH16*. The corrected full-lenght cDNA was excised by EcoRI and XhoI enzymes, cloned into the pENTR3C (Gateway entry vector; Invitrogen) digested with the same restriction enzyme pair and verified by sequencing in case of both pBluescript KS+ and pENTR3C derived constructs.

To generate constructs for GFP fusions, six additional subfragments besides the full-lenght *AtFH16* gene were amplified using primer pairs as shown in Tab 3.2, where the 5´-end primer introduces EcoRI site, whereas the 3´-end primer introduces XhoI site. Via the corresponding sites designed in the primers, the subfragments were cloned into the Gateway pENTR3C vector and further recombined by LR reaction using LR clonase mix (Invitriogen) into the Gateway destination binary vectors pGWB5 (designed for C-terminally located GFP) or pGWB6 (for N-terminally located GFP), kindly provided by T. Nakagawa, Research Institute of Molecular Genetics, Shimane University, Japan. Subfragment GFP:AtFH16Δ1 was cloned by Matyáš Fendrych. For generation of RFP fusions, the subfragments were amplified using SmaI site containing primers, digested with the Cfr9I restrictase (a SmaI analogue that creates cohesion ends) and cloned into the binary vector pBAR:RFP (constructed by Michal Hála) digested with the same enzyme. The cDNA sequences were verified by sequencing after the cloning and by restriction analysis after the LR reactions.

Table 3.2 List of primers and vectors used for cloning of *AtFH16* and its subfragments. Primer sequences are shown in Supplemental data 1.

subfragment	cloning vector	5´- forward primer	3´- reverse primer
GFP:AtFH16	pENTR3C	AtFH16-fb-Eco	AtFH16-re-Xho
AtFH16:GFP	pENTR3C	AtFH16-fb-Eco	AtFH16-re-os-Xho
GFP:AtFH16Δ1	pENTR3C	AtFH16-fb-Eco	AtFH16-N-re-Xho
GFP:AtFH16Δ2	pENTR3C	AtFH16-2D-Eco	AtFH16-2D-re-Xho
AtFH16Δ2:GFP	pENTR3C	AtFH16-2D-Eco	AtFH16-2D-re-Xho
RFP:AtFH16Δ3	pBAR:RFP	AtFH16-2D-Sma	AtFH16-re-Sma
AtFH16Δ3:GFP	pENTR3C	AtFH16-2D-Eco	AtFH16-re-os-Xho
RFP:AtFH16Δ4	pBAR:RFP	AtFH16-fb-Sma	AtFH16-2D-re-Sma
AtFH16Δ4:GFP	pENTR3C	AtFH16-fb-Eco	AtFH16-2D-re-Xho
GFP:AtFH16Δ5	pENTR3C	AtFH16-1+2-Eco	AtFH16-re-Xho
AtFH16Δ5:GFP	pENTR3C	AtFH16-1+2-ATG-Eco	AtFH16-re-os-Xho
GFP:AtFH16Δ6	pENTR3C	AtFH16-1+2-Eco	AtFH16-2D-re-Xho
AtFH16Δ6:GFP	pENTR3C	AtFH16-1+2-ATG-Eco	AtFH16-2D-re-Xho

For antibody production, a 462 bp long N-terminal part of FH2 domain was excised from AtFH16Δ3 subfragment using EcoRI (introduced by AtFH16-2D-Eco primer) and HindIII (internal cleavage site) and cloned into bacterial expression vector pET30a+ (Qiagen). In order to obtain recombinant proteins for *in vitro* experiments, additional variants of AtFH16 were transferred into bacterial expression vectors as follows: The full-lenght cDNA of *AtFH16* was amplified using AtFH16-fb-Sma and AtFH16-re-Sma primers containing SmaI site, digested by Cfr9I and cloned into the pQE32a vector (Qiagen). AtFH16Δ4 and AtFH16Δ5 amplified with the same sets of primers as used for AtFH16Δ4:GFP and AtFH16Δ5:GFP, respectively were digested by EcoRI and XhoI and ligated into pET30a+. At last, recombination by LR clonase was used for delivery of the full-lenght *AtFH16* and AtFH16Δ3 fragment from the pENTR3C entry vector into the Gateway pDEST17 vector.

3.8. Pollen harvesting and germination

Arabidopsis pollen was fliped off mature anthers into pollen germination medium (20% sucrose, 3% PEG 3350, 0.01% H_3BO_3, 0.07% $CaCl_2.2H_2O$) and germinated in dark for 4-10 hours at 24°C. To achieve better germination efficiency, whole anthers disrupted by injection needle together with stigma were added and co-cultivated.

Tobacco pollen was harvested from *Nicotiana tabacum* plants cv. Samsun grown in a greenhouse. Isolated anthers were dessicated on filter paper for 1 day, pollen was collected and stored at -20°C. Before germination, pollen grains were rehydrated for 10 min at room temperature, resuspended in a medium consisting of 10% sucrose and 0.1% H_3BO_3 and cultured for 1-2 h on a shaker.

3.9. Isolation and labeling of *Arabidopsis* microspore and pollen stages

Flower buds were sorted according to their lenght; whole flower buds were fixed in 2% glutaraldehyde in 0.05 M PIPES buffer at pH 7.2 containing 5 mM $MgSO_4$ and 5 mM EGTA for 1 h at room temperature, followed by postfixation in 1% (w/v) osmium tetraoxide in water. Samples were dehydrated in ethanol and propylene oxide and embedded in Spurr's resin. For light microscopy, sections of 1 μm were stained by toluidine blue (0.1% in 1% borax).

For nuclei staining, whole inflorescence or sorted flower buds were fixed in ethanol: acetic acid 3:1 and incubated overnight in 4°C. Before microscopic examination, anther sacs were ruptured using needle and mounted in 5% DMSO, 1% Tween 20 and 1 mM DAPI (Sigma) for 20 min.

3.10. Design of antisense oligodeoxynucleotides (ODNs) and pollen transfection

For analysis of knock-down effect of pollen Class I formins, sequences of partial cDNAs of tobacco (*Nicotiana tabacum*) *NtFH3, Nicotiana benthamiana NbFH6* and other *Solanaceae* homologs of *AtFH3* and *AtFH5* were analyzed with Soligo software (http://sfold.wadsworth.org/soligo.pl) for suitable target regions for antisense ODNs. Three best-scoring antisense ODNs and corresponding sense control ODNs were synthesized (Tab. 3.3) and tested for their effect on tobacco pollen tube growth.

ODNs delivery into growing pollen tubes was done as described previously (Moutinho et al., 2001). Briefly, the stock ODNs and cytofectin were incubated for 20 min at room temperature and the mixture was then diluted with germination medium consisting of 20% (w/v) PEG 3350 and 0.01% (w/v) H_3BO_3 and containing rehydrated pollen to achieve a final concentration of 30 μM ODNs and 15 μg/ml cytofectin. Observations were recorded 2 and 4 h after germination.

Table 3.3 The sequences of ODNs targeting tobacco Class I formins. AS means antisense orientation, S corresponding sense orientation.

oligonucleotide	sequence
NtFH-S1	5´-AAT GYR ACA ACW GAR GAA-3´
NtFH-AS1	5´-TTC YTC WGT TGT YRC ATT-3´
NtFH-S2	5´-GAA GAR RAR AGA ATH ATG-3´
NtFH-AS2	5´-CAT DAT TCT YTY YTC TTC-3´
NtFH-S3	5´-CTY CHA AAA CWA ARC TRA-3´
NtFH-AS3	5´-TYA GYT TWG TTT TDG RAG-3´

3.11. *In situ* immunolabeling of pollen tubes

Pollen tubes were fixed by mixing equal volumes of pollen tube culture with 3.7% paraformaldehyde in 2x concentrated PEM buffer (100mM PIPES, 10mM EGTA, 10mM $MgSO_4$, pH 6.9), vacuum-infiltrated for the first 5 min and then gently shaked in the fixation medium for 1 h. After two washing steps held in PEM and one in PBS buffer, cell walls were permeabilized by 0.3% cellulase, 0.3% pektinase and 0.05% driselase (Sigma) in PBS for 20 min on a rotator followed by 3x washing in PEM and further treatment by 0.1% Triton X-100 in PEM. After 3x washing steps in PBS, pollen tubes were incubated overnight at 4°C with the primary antibody diluted in PBS with 1% BSA in the concentration of 1:200, washed 3x in PBS and further incubated with the secondary antibody (1:350 in PBS with 1% BSA) at room temperature for 1h. Washed samples were mounted on slides in 50% glycerol with 0.1% p-PPD (para-phenylenediamine) to avoid bleaching, directly microscoped or stored in -20°C.

3.12. Design of peptide antigens

For formin-derived antigens, sequence conservation and predicted 3D-structure were taken into account as primary criteria for antigenic peptide selection as described in Results, section 4.2. 3D models of the AtFH3 and AtFH16 FH2 domains, used for designing FH2 domain peptides, were generated by threading the antigen sequence onto the published crystal structure of the yeast Bni1 FH2 domain (Xu et al., 2004) using methods described elsewhere (Cvrčková et al., 2004; Grunt et al., 2008). The template and the target structures were aligned with ClustalW (Thompson et al., 1994) and the resulting alignment was manually edited with help of the secondary structure prediction outputs. For modeling, WHAT IF program (Vriend, 1990) was used. Hydrophilicity determined using a modification of the Hopp and Woods method (Hopp and Woods, 1981) at http://www.innovagen.se/custom-peptide-synthesis/peptide-property-calculator/peptide-property-calculator.asp has been considered as a secondary criterion to eliminate potentially insoluble peptides.

For the remaining antigens, predictions of hydropathy (Kyte and Doolittle, 1982) and antigenicity (Welling et al., 1985) performed at http://www.expasy.org/tools/pscale were compared with antigenicity prediction using Kolaskar and Tongaonkar´s method (Kolaskar and Tongaonkar, 1990) at http://bio.dfci.harvard.edu/Tools/antigenic.pl. Secondary structure prediction and prediction of exposed vs. buried residues, performed at the Predict Protein server (Rost et al., 2003; www.predictprotein.org) were considered as secondary criteria.

3.13. Production of anti-oligopeptide antibodies

Peptides were synthesized and polyclonal rat antibodies were produced commercially using standard immunization protocols by Moravian Biotechnology (Brno, Czech Republic) using KLH-conjugated peptides shown in Tab 4.1; the peptide CLN was conjugated to BSA at the same time via an additional cysteine to improve solubility. For each peptide, three rats were immunized. To remove antibodies against the KLH carrier, selected antisera were commercially affinity-purified on a KLH-containing column (Hena s.r.o., www.hena.cz).

Additionally, two rabbits were immunized by CLN peptide conjugated to KLH by Exbio Antibodies (Vestec, Czech Republic; www.exbio.cz) and at the same place, both antisera were affinity-purified on a KLH-containing column.

3.14. Protein extracts isolation and western blotting

All steps were performed at 4°C unless otherwise stated. For total protein extracts, suspension cultures or tobacco pollen tubes were freshly harvested by filtration and homogenized in a mortar with addition of acid-washed sand and ice-cold extraction buffer (70 mM Tris-Cl, pH 7.5, containing 250 mM sucrose, 3 mM EDTA, 5 mM DTT and Protease Inhibitor Coctail for plant cell and tissue extracts (Sigma P9599). Cell debris were

removed by centrifugation at 7500 x g for 10 min. Protein extracts were stored at –80°C until use.

Arabidopsis seedlings were collected from vertical plates, frozen in liquid nitrogen, ground in a mortar and treated as described above.

Proteins in all extracts or fractions were quantified using the Bio-Rad DC Protein Assay prior to separaton on SDS/10-12.5% (w/v) PAGE and transferred onto a nitrocellulose membrane (BioRad). Immunological detection of protein-antibody complexes was performed as recommended by ECL Western blotting protocols (Amersham) with 5% (w/v) non-fat dry milk as a blocking agent and 0.5% (v/v) Tween-20 in PBS. Primary antibodies were used in dilution 1:1000, secondary horseradish peroxidase-conjugated goat anti-rat (Sigma A9037) or anti-rabbit (Promega) antibodies in dilution 1:10 000.

3.15. Purification of AtFH16 fragment and anti-AtFH16 antibody production

A 18 kDa part of FH2 domain with N- and C-terminally located 6xHis tags was expressed in *Escherichia coli* Rossette cells. Since all the recombinant protein resided in insoluble inclusion bodies, batch purification under denaturing conditions using Ni-NTA resin (Quiagen) pefrormed according to the manufacturer protocol was chosen as purification method. The purified protein was used for immunization of five mice in BioPharm (Jílové u Prahy). Neither of the obtained antisera recognized a desired antigen in plant extracts.

3.16. Subcellular fractionation of suspension cultures

After rapid removal of culture medium, 4-5 g of 7 days old *Arabidopsis* suspension culture cells were forzen in liquid nitrogen and homogenized to a fine powder with a mortar and pestle together with small amount of a sea sand and all subsequent steps were performed at 4 °C. For fractionation, the homogenate was mixed with 2-3 ml of buffer TS (10 mM Tris-Cl, pH 7.4, 250 mM sucrose) and centrifuged at 800 x g for 5 min. Supernatant was collected and pellet washed twice in the same buffer, resulting in a pellet fraction referred to as CW (cell walls and nuclei). Combined supernatant (9 ml) was centrifuged at 30 000 g for 7.5 min, and pellet was resuspended in 1.5 ml of TS yielding the M (plasma membrane) fraction. Supernatant was further centrifuged at 100 000 x g for 1h, resulting in the microsomal fraction P (pellet resuspended in 1.2 ml of TS) and the cytosolic fraction S (supernatant).

3.17. Size exclusion chromatography (SEC)

For SEC, the homogenate was mixed with 5 ml of buffer (20 mM HEPES, pH 6.8; 150 mM NaCl; 1 mM EDTA; 1 mM DTT; 0.5% Tween20) supplemented with Protease

Inhibitor Cocktail (Sigma P9599) and sequentially centrifuged at 5000 g, 10 min, and 30 000 g, 30 min. 80mg of total protein were applied on a Superdex300 HiLoad 26/60 column (Pharmacia) equilibrated with the same buffer, flow rate 60 ml/min. Protein concentration was monitored by measuring absorbance at 254 nm; 5 ml fractions were collected.

3.18. Microscopy

Microscopic pictures were acquired with the DP50 camera (Olympus) attached to Olympus BX51 microscope. Images of seedlings and whole plants were taken by Olympus C-4040 Zoom camera or Nikon D90 camera. Confocal laser-scanning microscopes Leica TCS SP2 or Zeiss LSM 5 Duo were used for CLSM pictures. For simultaneous green and red channel imaging, the multitracking function was utilized and each laser was activated one at a time.

Cryo-scanning electron microscopy was performed by Prof. Jan Derksen. Briefly, disrupted anthers were glued onto a stub with colloidal carbon adhesive and frozen in liquid nitrogen. The samples were transferred in a transfer holder under vacuum at liquid-nitrogen temperature to the cold stage at -95°C into a cryopreparation chamber CT 1500 HF (Oxford Instruments, High Wycomb, UK). The specimens were sputter coated with 5 nm platinum. The specimens were conveyed under high vacuum to the cold stage of a scanning electron microscope equipped with a cold-field emission electron gun (JSM 6300F; Jeol, Tokyo), analyzed, and recorded at -180°C using a 5-kV accelerating voltage.

3.19. *Arabidopsis* root and hypocotyl lengths measurement

Images of seedlings on plates were taken by Nikon D60 digital camera, lengths and angles were measured with Image J software (http://rsbweb.nih.gov/ij/). For the estimation of the significance of differences between experimental datasets of normal data distribution, Bonferroni and Duncan´s multiple comparison tests were used, while Kruskal-Wallis Z test was applied when the assumption of normality was rejected using the NCSS software (NCSS Statistical Software, USA).

3.20. *Agrobacterium*-mediated transient expression of fusion proteins

The *Agrobacterium tumefaciens* strain GV3101 was transformed by electroporation. For transformation, cells were grown overnight at 28°C, sedimented and washed twice with infiltration buffer (50 mM MES pH 5.6, 2 mM Na_3PO_4, 0.5% glucose, 20 mM $MgSO_4$). Alternativelly, sole 20 mM $MgSO_4$ solution was used instead of infiltration buffer with the same results. The final cell density was adjusted to $O.D._{600}$ ranging from 0.07 to 2 and the medium was supplied with 100 mM acetosyringone (Sigma).

Before infiltration, suspension of transformed agrobacteria was mixed with the equal volume of *Agrobacterium* cells bearing a plasmid expressing the p19 protein from *bushy stunt tomato virus* (Voinnet et al., 2003) to reduce silencing of delivered genes (Voinnet et al. 2003; the 35S:p19 plasmid was kindly provided by PBL Technologies, Ltd.). Young leaves of *Nicotiana benthamiana* were infiltrated with the suspension through stomata of the lower epidermis and observed within 1.5-3 days after infiltration.

Chapter 4

EXPERIMENTAL PART I

As a routine approach for studying protein function, we attempted to produce various polyclonal antibodies recognizing either universally FH2 domain-containing proteins or specifically particular members of *Arabidopsis* formin family. As neither of the antisera obtained after immunization of mice with purified protein parts (anti-AtFH5, done previoulsy by Fatima Cvrčková and Viktor Žárský; anti-AtFH16 as described in chapter 3.15) brought satisfactory results, we produced additional antibodies against synthetic KLH-conjugated oligopeptides in rats. However, most rat antisera recognized the same background KLH-related plant antigen (KRAP) in *Arabidopsis* and tobacco. We characterized KRAP with respect to size and cellular localization and examined possible antigen-specific reasons for the failure of most immunizations (Oulehlová et al., 2009; Appendix 2). Below I will summarize these experiments.

4.1. Rationale for using the KLH-peptide approach

Polyclonal antibodies against synthetic oligopeptides have become routinely used instruments of biochemistry and molecular biology. In contrast to recombinant protein antigens, a synthetic peptide based on any region of the protein of interest is easily produced in desired amounts, simplifying production of a specific antibody. Since molecules smaller than 12 kDa do not efficiently elicit vertebrate immune response, oligopeptides have to be conjugated to a suitable carrier (for a review see Harlow and Lane, 1988; Maloy et al., 1991; van Regenmortel, 2001). Common methods include either chemical coupling to larger carrier molecules such as bovine serum albumin (BSA) or keyhole limpet hemocyanin (KLH), or the Multiple Antigen Peptide (MAP) Conjugation System (Tam, 1988) in which several peptide antigens are anchored onto branching lysine dendrites of a small immunologically inert core molecule.

KLH (keyhole limpet hemocyanin) is a large copper-containing glycoprotein from the marine mollusk *Megatura crenulata*. KLH carries a number of lysine residues suitable for conjugation of peptide antigens, and triggers a strong immune response in vertebrates. The resulting antibodies have been reported to exhibit very low, if any, non-specific crossreactivity (Dixon et al., 1966; Harlow and Lane, 1988). Unlike BSA, KLH does not share epitopes with commonly used ELISA or Western Blots blocking reagents.

Most animals commonly used for immunization, including rabbits and chicken, are herbivorous, resulting in non-specific background reaction of their polyclonal antisera (or immunoglobulin fractions thereof) towards plant antigens. Affinity purification of antisera using immobilized antigen usually leads to loss of high affinity antibodies. However, rat antisera exhibit minimal non-specific crossreactivity with plant material, which makes rats the animals of choice for production of antibodies to be used in plant biology. Moreover, the amount of antigen needed for immunization is relatively small, the yield of both preimmune and hyperimmune sera is sufficient for most applications, and commercially

available anti-rat secondary antibodies do not crossreact with anti-mouse primary antibodies, making double labeling experiments possible.

4.2. Antigens and peptide design

We attempted to produce rat polyclonal antibodies against five protein antigens. The pilot antigen of our study was the plant Class I formin AtFH3. According to publicly available microarray data (Honys and Twell, 2004; Pina et al., 2005; Zimmermann et al., 2004), *AtFH3* mRNA is preferentially present in mature and germinating pollen similarly to its close homologue *AtFH5* (see chapter 5.1.1 and Fig. 5.1). Two of the remaining antigens also represent members of the *Arabidopsis* formin family (Deeks *et al.*, 2002; Cvrčková *et al.*, 2004), namely the cytoplasmic Class II formin AtFH16, and a conserved portion of a PTEN-related domain shared by several Class II formins. The last two antigens were the *Arabidopsis* Exo70A1 subunit of the exocyst complex (Synek et al., 2006) and the *Nicotiana tabacum* phospholipase PLDδ (Pleskot et al., 2010).

Table 4.1 Summary of peptides and corresponding antigens used in this study. NtPLDδ corresponds to the translation of an incomplete cDNA cloned in our laboratory (Pleskot et al., 2010), so that predicted size of full-lenght version is not available (N.A.); tobacco has at least two PLDδ isoforms; Arabidopsis homologue has m.w. of 90 kDa).

name	antigen	domain	predicted size	sequence
NVT	AtFH3 (At4g15200)	FH2 (specific)	65 - 70+	NVTTEEVVDAIKEGNELPVELL
GRS	AtFH3 (At4g15200)	FH2 (specific)		GRSSLTWPAERFLKIL
DEL	AtFH16 (At5g07770)	FH2 (specific)	79	DELQIQYGESQTAE
TED	AtFH16 (At5g07770)	FH2 (specific)		TEDVFGGPDHNIDD
CLN	AtFH13 (At5g58160)	PTEN (conserved)	140	CLNRDEVDTLWHIKE
GEG	AtFH18 (At2g25050)	PTEN (conserved)	123	GEGGCRPIFRIYGQD
LFL	AtExo70A1 (At5g03540)	internal	72	LFLEFGNGDDSNSQLASVT
LER	AtExo70A1 (At5g03540)	C-terminal		LERLLGELFEGKSMNEPR
GDL	NtPLDδ	N-terminal	N.A.	GDLELHIVHARHLPN
QEL	NtPLDδ	internal		QELKSSQLKDVHPSD

For each protein antigen, two short peptides were synthesized, coupled to KLH and used for rat immunization. In case of *Arabidopsis* formins, 3D models of the relevant domains were used in order to design peptides from accessible areas on the protein surface. Models of the AtFH3 and AtFH16 FH2 domains were constructed by Fatima Cvrčková as described in Materials and Methods (chapter 3.12); for the PTEN antigen, a previously published model (Cvrčková et al., 2004) has been used. To avoid cross-reactivity of the FH2 antibodies with other members of the extensive plant formin family, peptide sequences unique to each protein were used, even if their overall properties (solubility and predicted antigenicity) were somewhat suboptimal. On the contrary, conserved sequences were taken into account for PTEN peptide candidates with the aim to produce a wide-spectrum antibody against any PTEN-containing formin.

For the remaining antigens, Exo70A1 and PLDδ, antigenic peptides were selected by Martin Potocký from complete protein sequences, taking into account hydropathy, antigenicity, secondary structure and algorithmic prediction of surface localization (see Materials and Methods, chapter 3.15). The sequences and other properties of peptides used for immunization are summarized in Tables 4.1 and 4.2.

Table 4.2 Outcome of immunization with the peptides from Table 4.1. For each peptide/recognized antigen combination, the number indicates the number of positive antisera (out of three rats). Relevant peptide parameters determined as described in Materials and Methods (section 3.12) are shown for each peptide; antigenicity (KT) stands for average antigenic propensity according to (Kolaskar and Tongaonkar, 1990), position on the molecule (exposed) is predicted based on 3D modeling.

	recognized antigen			**peptide parameters**				
peptide	**KRAP 75**	**KRAP 90**	**specific**	**Welling**	**KT**	**KT epitopes**	**hydrop.**	**exposed**
NVT	3	1	0	-0.2	1.06	TEEVVDA; NELPVELL	0.04	yes
GRS	3	1	0	-0.18	1.07	AERFLKIL	0.04	yes
DEL	1	1	0	-0.49	1.01	DELQIQY	-0.61	yes
TED	2	0	0	-0.22	0.97	TEDVFG	-0.85	yes
CLN	2	1	0	-0.13	1.02	VDTLWHIK	-0.6	yes
GEG	1	0	0	-1	1.01	GCRPIFRIYG	-0.42	yes
LFL	3	1	0	-0.38	1.00	NSQLASVT	-0.4	N.A.
LER	3	3	0	-0.36	0.98	LERLLGE	-0.57	N.A.
GDL	1(weak)	0	2	0.49	1.08	GDLELHIVHAR	-0.06	N.A.
QEL	0	0	1(weak)	0.39	1.06	whole peptide	-0.83	N.A.

4.3. Antibodies against KLH-coupled antigens recognize a conserved protein in *Arabidopsis* and tobacco

Antibodies against two peptides derived from AtFH3 (GRS and NVT; Tab.4.1), but not the corresponding pre-immune sera, detected a single band of approximately 75 kDa on Western blots of *Arabidopsis* and tobacco suspension cultures and tobacco pollen tubes (Fig.4.1A). All three rats immunized by the GRS peptide exhibited a very good response to this protein, while sera from rats immunized by the NVT peptide exhibited somewhat weaker reaction (Tab.4.2 and not shown). In addition, two antibodies (GRS3 and NVT9) recognized also a 90 kDa protein in *Arabidopsis* extracts (Fig.4.1A, right panel). The apparent size of the shared antigen approximately corresponds to that expected for AtFH3 (~70 kDa depending on gene structure prediction available at the time of experiments). We thus started a more thorough characterization of the 75 kDa antigen using the GRS2 antiserum, while waiting for antibodies against the remaining peptides.

4.4. Intracellular localization of the KLH-related antigen KRAP75

The GRS2 antiserum recognizing KRAP75 has been used for immunostaining of chemically fixed tobacco pollen tubes, where it decorated intracellular fibrous or membraneous structures (Fig. 4.3C), while cells stained with preimmune serum exhibited no signal (Fig. 4.3A). In emerging tubes shorter than two diameters of the pollen grain, the signal was abundant only in the proximal part of pollen tubes (Fig. 4.3D), whereas in longer tubes, the immunolabeled structures were located in the distal region as well. Although AtFH3 is predicted to be a transmembrane protein, no staining was observed at the plasmalemma, including the pollen tube tip where formin-specific signal was expected. This also alerted us to the possibility that the GRS2 antibody recognizes something else than AtFH3.

In cell fractionation experiments, the majority of KRAP75 was detected in the soluble cytosolic fraction of protein extracts from *Arabidopsis* suspension culture (Fig. 4.1B). Fractionation of the soluble proteins by size exclusion chromatography, where native protein complexes are sorted by size, revealed only one peak detected by GRS2, corresponding to a 440 kDa protein complex in *Arabidopsis* suspension (Fig. 4.1C). This indicates that only antibodies against KRAP75, but not against AtFH3, are present in the immune sera, because the presence of both a masking non-specific background and the specific (AtFH3) signal in the same protein fraction is extremely unlikely.

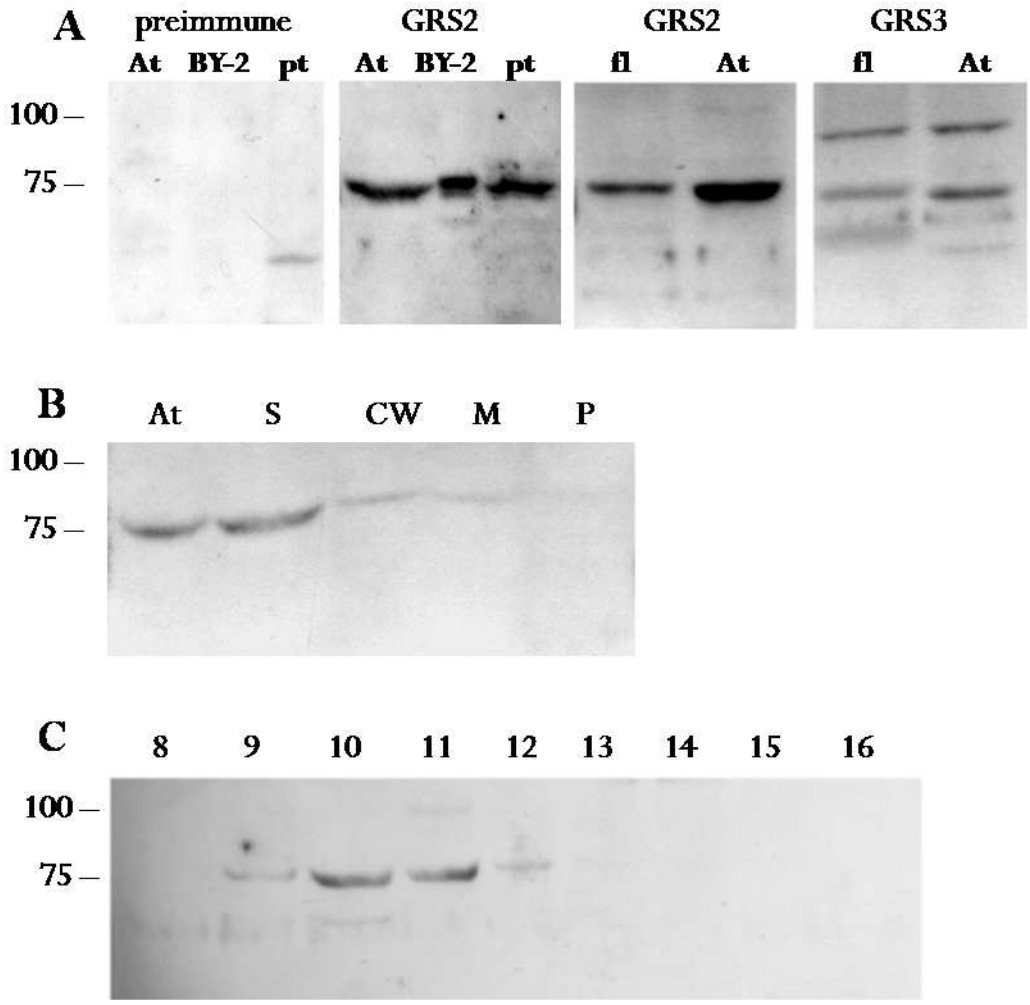

Fig 4.1 KRAP75 is a cytosolic protein and participates in an approx. 440 kDa complex. A: Western blot of extracts from *Arabidopsis* suspension cells (At), tobacco BY2 cells (BY2) and tobacco pollen tubes (pt) probed with the GRS2 antibody (right) and the corresponding preimmune serum (left). Further right, western blots probed with two antibodies against the GRS peptide: GRS2 (left) and GRS3 (right). Extracts were from *Arabidopsis* flowers (fl) and *Arabidopsis* suspension (At). Positions of marker proteins and their sizes (in kDa) are indicated next to all blots. **B:** Distribution of KRAP75 in subcellular fractions of *Arabidopsis* suspension cells. At – whole extract, S – cytosol, CW – cell walls, M – 30 000 g pellet, P – 100 000 g pellet **C:** A single protein complex of 440 kDa detected by GRS2 in size exclusion chromatography fractions from *Arabidopsis* suspension. Column fraction numbers are shown above the lanes. The starting fraction 8 corresponds to elution volume of 150 ml, the peak of KRAP75 corresponds to fractions containing complexes of approximately 440 kDa.

4.5. Only highly antigenic peptides induce specific rat antibodies in the presence of KLH

For two peptides derived from the tobacco phospholipase D (PLDδ), we managed to obtain antibodies reacting to specific antigens. In particular, the GDL5 antiserum recognized, in

addition to a very weak KRAP75 signal, two bands which may correspond to PLDδ variants and which persist even after removal of KLH-interacting antibodies by purification of the crude antisera over a KLH affinity column. This also documents that KRAP75 indeed corresponds to an epitope cross-reacting with KLH, as the KRAP75 signal disappears after antibody purification. Absence of the presumed PLDδ signal in *Arabidopsis* extracts (Fig. 4.2A) further supports its specificity since no *Arabidopsis* protein contains a sequence corresponding to the GDL peptide.

After fractionation of tobacco BY-2 suspension culture, PLDδ variants were detected in both soluble and membraneous fractions. The smaller PLDδ isoform was nearly absent in M fraction (pellet after 30 000g consisting predominantly of plasma membranes), while proportion of both variants in P fraction (pellet after 100 000g enriched in microsomes) was equal (Fig. 4.2B).

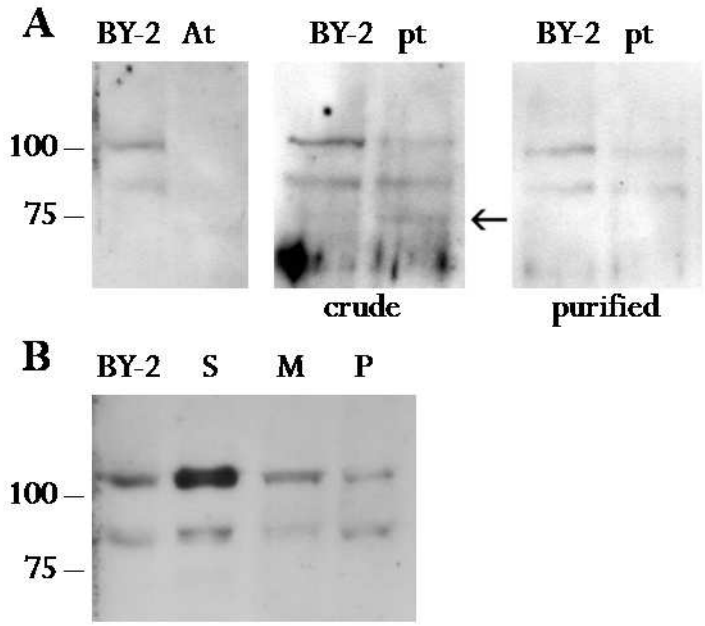

Fig 4.2 Specific antibodies against the GDL peptide recognize an antigen with predicted properties of tobacco PLDδ. A: The antigen recognized by GDL5 is tobacco-specific; the left panel shows comparison of Western blots of tobacco (BY2) and *Arabidopsis* (At) suspension extracts. Western blots of tobacco BY2 suspension (BY2) and tobacco pollen tubes (pt) probed with crude GDL5 antiserum (middle) and GDL5 purified on a column with immobilized KLH (right). Arrow shows a weak KRAP75 signal that is removed by purification. **B:** Distribution of PLDδ in subcellular fractions of tobacco suspension cells. BY-2 – whole extract, S – cytosol, M – 30 000 g pellet, P – 100 000 g pellet.

Several parameters possibly influencing the outcome of immunization have been determined either in the process of peptide design or subsequently (Tab. 4.2). The only major difference between the successful peptides and the failed ones in the rat system was the antigenicity parameter established by the method of Welling et al. (1985); surprisingly, the newer approach developed by Kolaskar and Tongaonkar (1990) suggested comparably

good antigenicity for the successful peptides against PLDδ as well as for the failed ones (especially for the NVT and GRS peptides).

4.6. Low antigenic peptides induce a response in rabbits

To test whether the null responsiveness of rats to the low antigenic peptides (determined by the method of Welling) conjugated to KLH is also shared by other animals routinely used for antibody production, rabbits were immunized by one of the peptides showing a failure in the rat system. For rabbit immunization, the CLN peptide (derived from the formin AtFH13) with the best antigenicity prediction among the previously failed peptides was chosen. Nevertheless, its predicted antigenicity response was slightly negative and worse than in the successful peptides. The two rabbit antisera prepared against CLN peptide were directly commercially purified against KLH so that the proportion of peptide- and KLH-induced antigens could not be evaluated.

The antisera together with the preimmune sera were tested on protein extracts prepared of *Arabidopsis* suspension culture, as well as light-grown and dark-grown *Arabidopsis* seedlings. Both antisera recognized a 100 kDa protein not detected by preimmune sera in the extracts prepared of suspension culture cells and green seedlings, but not etiolated seedlings (not shown). However, *Arabidopsis* contains no predicted Class II PTEN-containing formin of such size and also a presence of this protein in *atfh13* mutant signifies a nonspecificity of the signal.

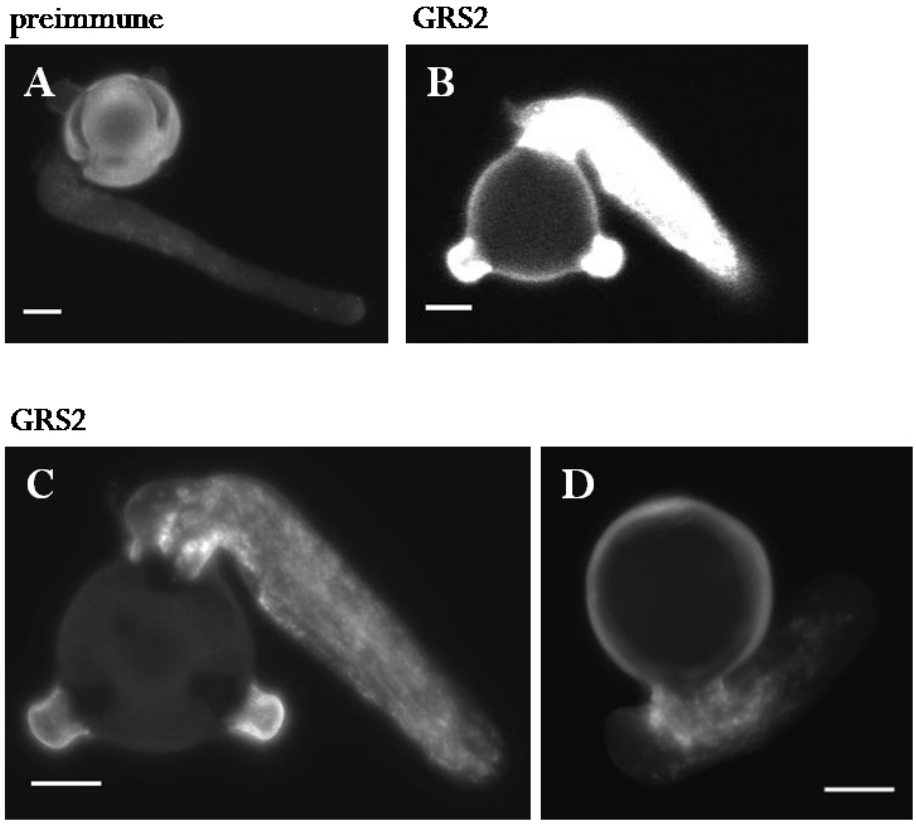

Fig 4.3 Structures resembling the endomembrane system are recognized by the GRS2 antibody in tobacco pollen tubes. A: Z-projection of pollen tube stained by preimmune serum. **B:** Single stack of pollen tube stained by the GRS2 antibody captured using the same microscope settings as for the preimmune serum. **C, D:** Endomembrane-like structures recognized by the GRS2. Scale bars represent 10 μm.

Chapter 5

EXPERIMENTAL PART II

5.1. Expression analysis of *Arabidopsis* formin genes

To gain insight into the developmental and organ-specific regulation of the expression of individual *Arabidopsis* genes encoding formin family members we analyzed the publicly available Affymetrix ATH1 *Arabidopsis* genome array data in the Genevestigator database (Zimmermann et al., 2004; Hruz et al., 2008). For the general expression analysis, we selected only experiments on different organs/tissues from WT plants grown under physiological conditions. For the analysis of expression in dark-grown seedlings, data for untreated WT plants were processed.

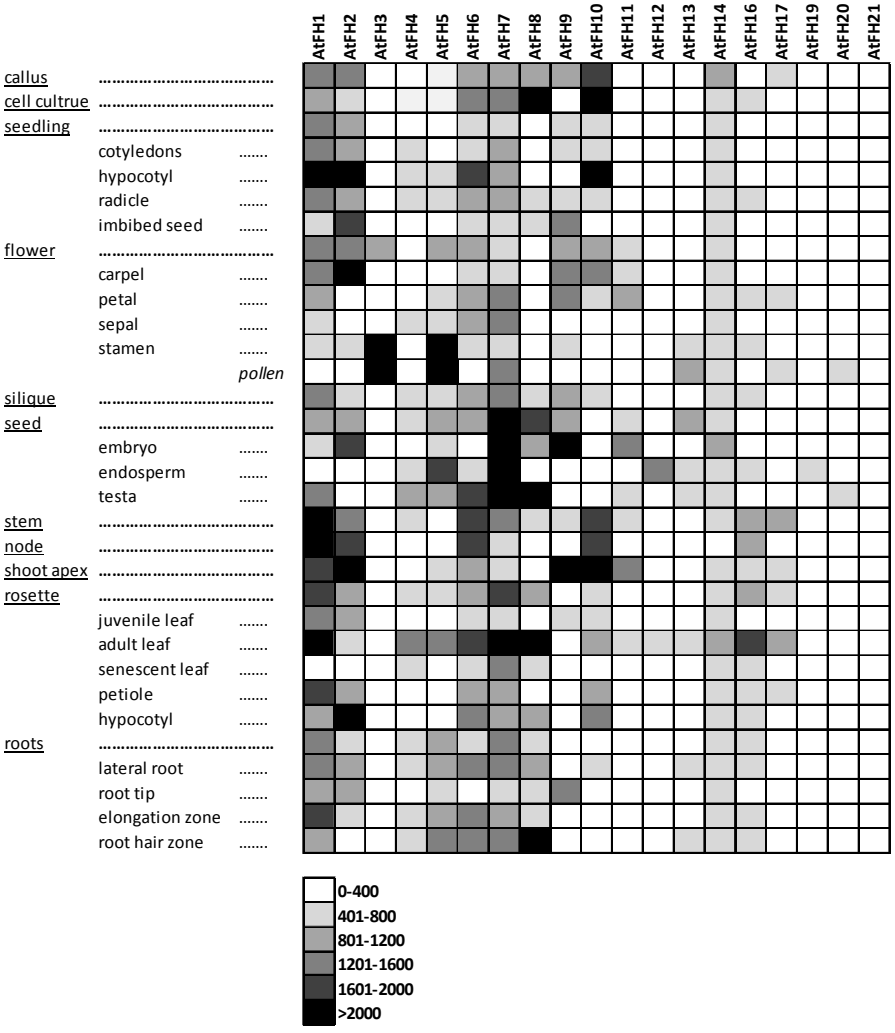

Fig 5.1 Expression analysis of *Arabidopsis* formin genes. Expression data for *Arabidopsis* formins were retrieved from Genevestigator database. Particular microarray experiments (chips) included in this analysis are listed in Supplemental data 2.

Expression data were collected for 19 out of 21 *Arabidopsis* formin genes (Fig. 5.1), as no probe sets for *AtFH15* and *AtFH18* are included in ATH1 chip. Nevertheless, ESTs are available for both these genes (though only from *AtFH15a* part in case of *AtFH15* locus), indicating that *AtFH15* and *AtFH18* are transcriptionally active. For more information about cDNAs/ESTs of *Arabidopsis* formins, see Cvrčková et al. (2004, Appendix 1). Under standard conditions, no significant expression was detected in case of *AtFH21*, and only marginal expression was allocated to *AtFH12*, *AtFH19* and *AtFH20* genes. However, *AtFH12* was recently found to be expressed e.g. in chalazal endosperm during certain stages of embryo development (study AT-00298, GSE11262), after viral infection (study AT-00324, E-MEXP-509) or in roots under salt stress conditions (experiment AT-00120, TAIR-ME00328). Besides a weak expression in roots verified by several other experiments (e.g. AT-00023, GSE10323; AT-00087, TAIR-ME00319), *AtFH19* transcript was detected also in cellular endosperm of globular emryo stage (study AT-00298, GSE11262). *AtFH20* is upregulated during *in vitro* tracheary element transdifferentiation of suspension cells (AT-00174, ME00377) or expressed in roots under various stress conditions (AT-00120), where low levels of *AtFH21* are present as well. As a whole, all *Arabidopsis* formin genes seem to be transcriptionally active, though their expression levels and patterns differ vastly.

5.1.1. *AtFH3* and *AtFH5* are prevailing formins expressed in mature pollen

A majority of *Arabidopsis* organs usually contain transcripts of several formins belonging to the both family classes, however, there are only two strongly expressed formin genes in mature pollen (Fig. 5.1); *AtFH3* and *AtFH5*, the closely related formins from Class I group (Cvrčková et al., 2004). Moreover, *AtFH3* is almost exclusively expressed in pollen, so that implication of both these formins during pollen germination and polarized tube growth could be suggested. Besides, PTEN domain-containig Class II formins *AtFH13*, *AtFH14* and *AtFH17* are significantly expressed in pollen, though the two later ones are rather present in immature microspores and their transcript levels are much lower compared to *AtFH3* or *AtFH5*. Finally, *AtFH7*, the only Class I *Arabidopsis* formin lacking TM domain is moderately expressed in mature pollen, which means that there are no other transcriptionally active conventional Class I formins besides *AtFH3* and *AtFH5* in *Arabidopsis* mature pollen.

5.1.2. *AtFH16* and PTEN domain-containig formins are abundantly expressed in root hairs

Besides pollen tubes, root hairs represent another example of extremely polarized cell type elongating by so called tip growth (Cole and Fowler, 2006). Substantially more formin genes including *AtFH16*, the Class II member of our interest, were found to be expressed in root hairs compared to the situation in mature pollen (Fig. 5.1), though these data are not fully comparable, as expression of additional genes could be expected after the pollen tube growth onset. Since Class I and Class II formins might have different functions in cell polarization (Vidali et al., 2009), we analyzed expression pattern of the formin groups

separately as well. In root hairs, transcript of *AtFH16* is the most abundant one among Class II formin genes (Fig. 5.2), closely followed by *AtFH13* and *AtFH14*, i.e. the same PTEN domain-containig Class II formins expressed in mature pollen. Transcripts of these three formins prevail also in lateral roots and root elongation zone.

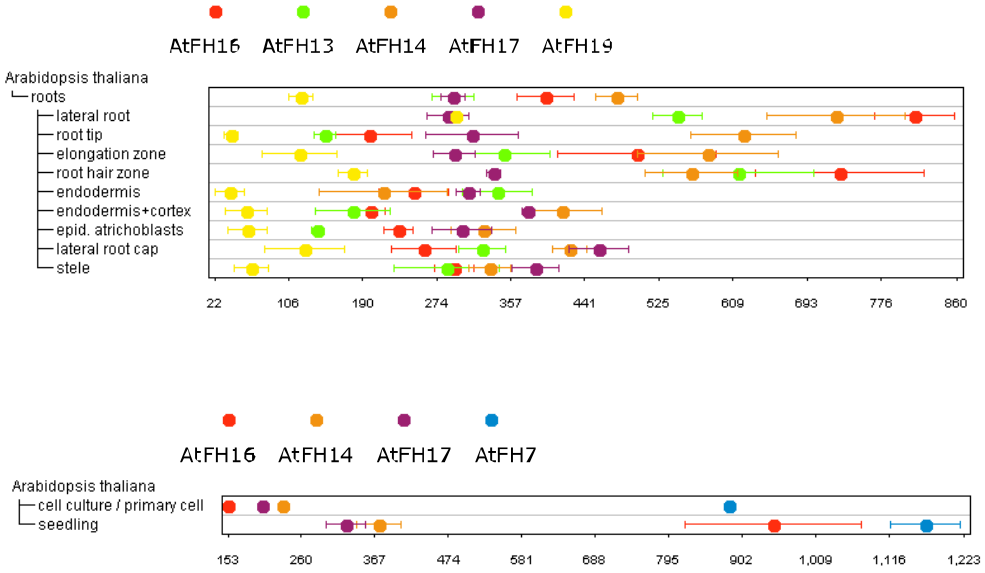

Fig 5.2 Expression of Class II formins in roots and during dark growth. The upper panel shows Class II formins significantly expressed in roots sorted according to the root anatomy. The lower panel shows expression of Class II formins significantly expressed under the growth in dark conditions, where a Class I member *AtFH7*, the only Arabidopsis type B formin besides *AtFH16* is also included. Expression values are represented by x-axis, particular microarray experiments (chips) included in this analysis are listed in Material and Methods, chapter 3.5.

5.1.3. *AtFH16* expression is induced in dark-grown seedlings

AtFH16 expression levels in various plant organs or under different conditions are rather steady and no stimuli triggering any outstanding induction of expression were found. However, *AtFH16* expression levels increase after induction of PCD (programmed cell death) and furthermore, they are consistently elevated in *Arabidopsis* mutants in stress-responsive genes related to ethylene signaling with constitutive defense response concomitant with constitutive expression of PR (pathogen-related) genes such as *mkk1*, *mkk2*, *mpk4*, *ctr1* or *cpr5* (Kieber et al., 1993; Jing et al., 2007; Qiu et al., 2008).

Next, *AtFH16* is upregulated in etiolated seedlings, where only two other Class II formins, *AtFH13* and *AtFH17* containing PTEN-domain are significantly expressed (Fig. 5.2). Expression levels of *AtFH16* are three-times higher than that of *AtFH13* or *AtFH17*, making *AtFH16* the predominantly expressed Class II member in dark-grown *Arabidopsis* plants. For comparison, expression of *AtFH7* sharing the similar domain architecture with *AtFH16* is included in figure 5.2, showing that *AtFH7* levels are comparable in both dark-grown suspension culture and seedlings, whereas *AtFH16* is upregulated in seedlings only.

5.2. Characterisation of *Arabidopsis* T-DNA insertional mutants

At the beginning of this project in our laboratory, almost nothing was known about the function of particular plant formins and no loss-of-function phenotypes have been described. To elucidate a function of formins in *Arabidopsis thaliana*, a collection of publicly available T-DNA insertional mutants covering the majority of both Class I and Class II genes was put together (Fig. 5.3).

T-DNA insertional mutants were ordered from two sources; the first part of the mutants was obtained from European *Arabidopsis* Stock Centre NASC database providing kanamycine-resistant mutants created by SALK institute (Alonso et al., 2003) and the second batch named SAIL lines (Syngenta Arabidopsis Insertion Library) bearing Basta resistance was obtained from Torrey Mesa Research Institute (TMRI), formerly being a part of Garlic database, now available from SALK (Sessions et al., 2002), see Tab. 3.1. Seeds from the original stocks were sown both on selection or selection-less medium and plants carying T-DNA insert were further checked by PCR method (see chapter 3.3). A progeny of the mutant plants was once more propagated on the selection medium and the resulting segregation ratio was taken into account as an indicator for detecting possible extra T-DNA insertions within given genomes. Segregation ratio of the PCR-verified mutation frequency in the population near to 1:2:1 (homozygous:heterozygous:WT) corresponding with the particular resistance suggested the presence of a single insertion in the gene of interest. Resistance of the mutant plants to the selection marker differed with respect to a selection-resistance gene present, where *NPTII* gene of SALK lines was usually affected by silencing, so that only few or even no generations of plants could be cultivated on the kanamycine selection medium.

In T3 and T4 generations, homozygous mutant lines were selected in following genes: *AtFH1*, AtFH2, AtFH3* (2 lines), *AtFH4*, AtFH5* (2 lines), *AtFH6*, AtFH7, AtFH8, AtFH12*, AtFH13*, AtFH14, AtFH15, AtFH16* (2 lines) and *AtFH18*. Asterisks indicate genes, in which the homozygots were selected by Fatima Cvrčková. All the plants were screened by the PCR method using primers summarized in Tab.3.1 that enables an identification of both mutated and WT alleles (Fig.5.4). The presence of T-DNA insertion in the desired locus was not confirmed by the PCR approach in case of genes *AtFH11*, *AtFH15* (mutant *atfh15b*, SAIL_1230_C10) and *AtFH20*, in which no PCR product specific for the mutated allele could be amplified from the resistant plants. For *atfh10* with T-DNA insertion located in the 5´-UTR, PCR verification was used only for the detection of mutated alleles, as their presence entirely correlated with the Basta resistance. Homozygous mutants in *AtFH10* were therefore identified based on the segregation ratio on the selection medium (indicating the presence of the single T-DNA insertion). By the time of writing the thesis, only *AtFH17* WT plants or heterozygous *atfh17* mutants were found within Basta resistant progeny grown from the original SAIL seeds indicating a presence of extra T-DNA insertion and homozygous mutants in *AtFH17* are to be identified in the next generation.

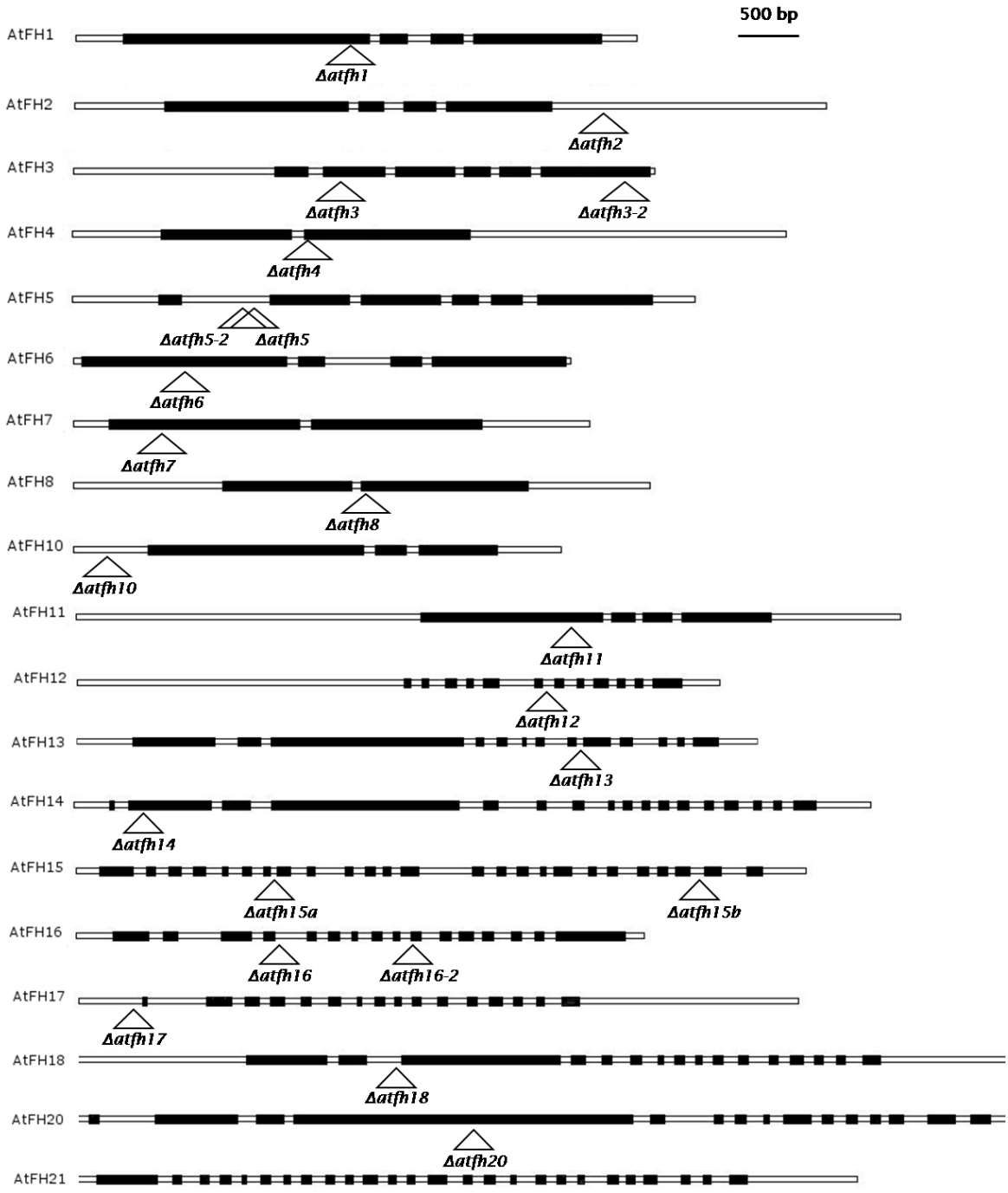

Fig 5.3 Schematic picture of T-DNA insertional mutant lines characterized in this study. *Arabidopsis* formin genes are schematicaly pictured in their exon/intron structure and position of particular T-DNA insertions within the genes is shown. Accession numbers of mutant lines and primers used for genotypic analysis are shown in table 3.1.

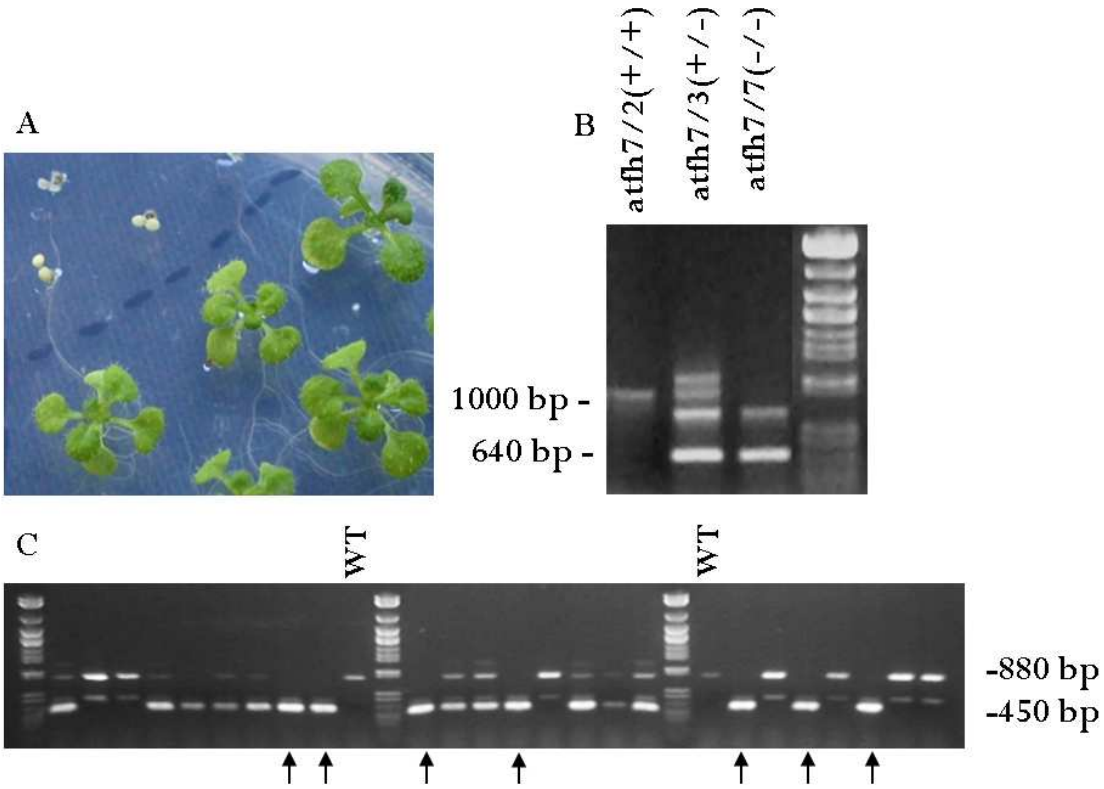

Fig 5.4 Example of mutant selection and genotyping. A: Basta resistant seedlings of *atfh2*-/- (right), sensitive plants of *atfh2*+/+ are shown on left. **B:** PCR analysis showing distribution of WT and mutated alleles of *AtFH7* gene. **C:** Genotyping of *atfh3-2* progeny; samples from *atfh3-2*-/- homozygous plants are marked by arrows.

A slightly modified approach for the WT and mutated allele discrimination was applied in case of *atfh5* (SALK_044455.48.95), where mutant plants had to be identified indirectly. In this line, combination of the allele-specific "genotyping" primer and the LB primer (LBb1 or LB-SALK) gave no PCR product. However, PCR with getotyping primer and primer for the detection of WT allele amplified a product of the expected size. These results suggest rearrangements within the T-DNA left border sequence, sometimes originating during insertion of T-DNA into the host genome (Tax and Vernon, 2001) that block annealing of the LB primer. As the *NPTII* gene for kanamycin selection was not silenced in this mutant line, resistant plants with 100% resistant progeny and no PCR product for WT allele were considered as *atfh5* homozygots. Later, additional mutant in the *AtFH5* gene (*atfh5-2*, SALK_044464.17.30) with the T-DNA insertion located at the same intron as *atfh5* was ordered and successfully verified with the same set of genotyping primers.

Phenotypes of the selected homozygous mutants presented above were generally morphologically characterized and no obvious differences from WT were observed except of *atfh14* and *atfh3* and one allele of *atfh16*. In the first case, a mutant phenotype (smaller or missing petals, shorter siliques) was caused by the presence of extra T-DNA insertion as confirmed by back-crossing with WT plants, after which the phenoytpe was exhibited also by kanamycine-resistant plants homozygous in *AtFH14* WT alleles. The remaining two mutation lines are described in more detail below in the chapters 5.2.1 and 5.2.2.

5.2.1. Impairment of major pollen formins does not affect microspore development and pollen tube growth

Compared to *atfh14*, the situation was more complicated in the case of *atfh3*, where pollen of selected mutant plants contained a portion of aberrant grains that failed to germinate (Fig. 5.5 A, B). *atfh3* mutant was generated in *QUARTET* mutation (*qrt1-1*) background, where even mature pollen grains remain attached in tetrades, thus providing a useful tool for segregation analysis (Rhee and Somerville, 1998). In the first generation, a percentage of aberrant pollen grains differed among individual plants, nevertheless, it correlated with the loss of *AtFH3* function. However, an extra T-DNA insertion was present in *atfh3* based on the segregation ratio of heterozygotes on Basta-containing plates. In order to remove any other T-DNA inserts besides the one in *AtFH3* gene, homozygous *atfh3* mutants were back-crossed with *Arabidopsis* Columbia WT plants and homozygotes were selected from the progeny of heterozygous plants exhibiting expected segregation ratio 1:2:1 on Basta, that correlated with the presence of mutated allele of *AtFH3* confirmed by PCR-genotyping analysis. Even after the removal of the additional T-DNA insertion, the mutant phenotype could be still observed, but was not exclusively bound to *atfh3* mutation in the following generations.

AtFH3 is almost exclusively expressed in pollen, mainly in mature stage (see chapter 5.1.1), so that hardly any other mutant phenotype except the some kind of pollen interference had been expected. The pollen developmental defect occurring in *atfh3* mutants was therefore briefly characterized. To indentify, in which developmental stage do microspores start to collapse, individual anther stages were collected; all flower buds were picked off the individual inflorescences, numbered according to their position on the stems and further sorted according to their lenght in milimeters. Whole buds were chemically fixed and overall microspore development was observed both at embeded sections of whole anthers (sectioned by Mieke Walters-Arts) and at DAPI (4',6-diamidino-2-phenylindole) stained microspores released from anther-sacs. Both approaches revealed that the tetrades of haploid micropores had formed, but some of the early microspores failed to polarize, persisted in the one-nuclear stage even when other microspores from the same tetrad already underwent Pollen Mitosis I (PMI) and subsequently shrunk (Fig. 5.5 C-H). Remaining microspores fully developed and germinated *in vitro* at the same rate as WT (60-70%) with no significant differences in pollen tubes architecture. Meanwhile, homozygot plants in additional *AtFH3* allele (*atfh3-2*) were selected. No abnormalities in pollen development were found in this line, indicating that the phenotype described above was contingent on other factors within the *atfh3* background than T-DNA insertions.

In order to impair function of two major formins expressed in pollen, *atfh3atfh5* mutant was generated. Nevertheless, both microspore development and pollen germination processes remained unaffected (Fig. 5.6). Developmental stages of microspores were examined microscopically after DAPI staining of nuclei, pollen tubes were incubated *in vitro* and observed after 5 to 15 hours.

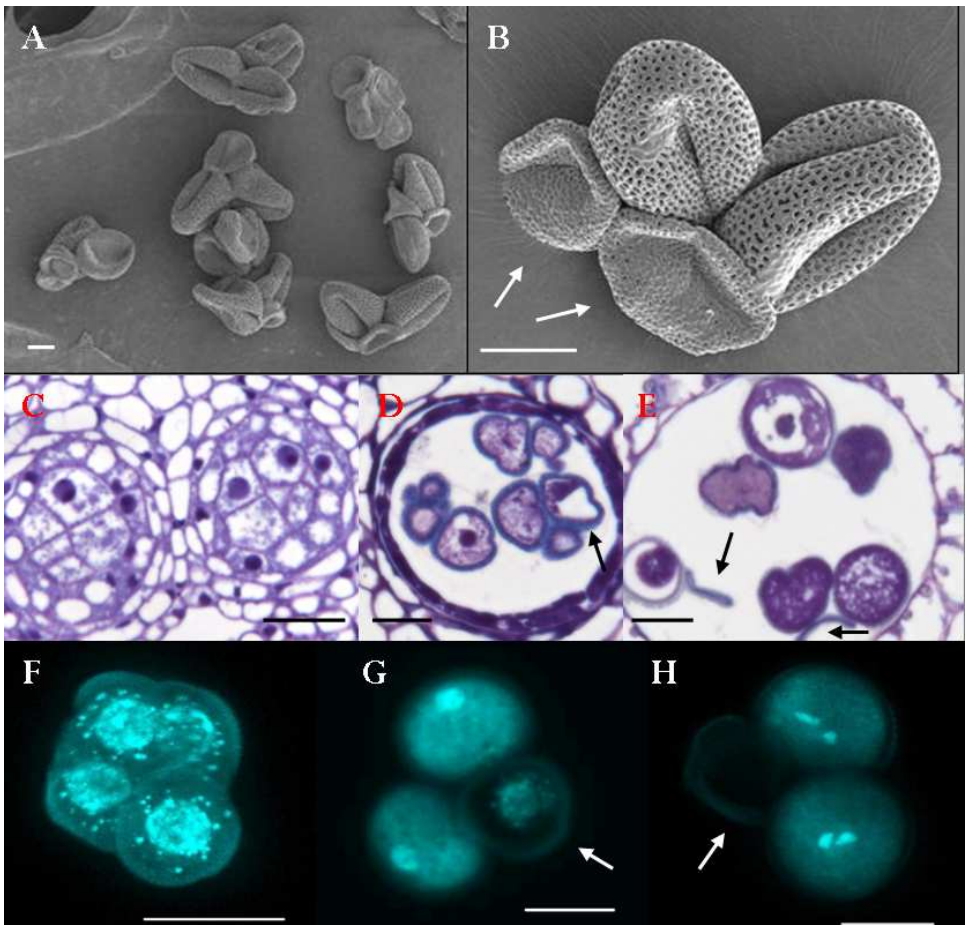

Fig 5.5 Defects of microspore development in *atfh3* background. A: Scanning electron microscop photogpraphy of tetrads with collapsed pollen grains. **B:** *atfh3* pollen in detail, collapsed grains are marked by arrows **C, D, E:** Sections of chemically fixed anthers. Formation of haploid microspores attached in tetrades within 0.2mm anthers (C), binuclear stage in 0.5mm anthers, where collapsing microspores are already present (D), mature pollen (E). **F, G, H:** Corresponding developmental stages of microspores stained with DAPI for nuclei visualization, arrows show aborted micropsores. Scale bars represent 10 μm.

To test downregulation effect of *AtFH3* and *AtFH5* tobacco homologues in pollen, 3 pairs of sense/antisense degenerated oligonucleotides based on available sequences of *Nicotiana* formins were synthetized (Tab. 3.3) and delivered into germinating tobacco pollen (*Nicotiana tabacum* cv. Samsun), where the incubation with the sense oligonucleotide is considered as a control treatment. Design of all oligonucleotides was done by Martin Potocký (as described in the section 3.13). Pollen tubes were incubated in the presence of particular oligonucleotides together with cytofectin in dark conditions and the temperatures of 19°C, 22°C and 26°C. Pollen tubes were than microscoped 2 hours and 4 hours after germination and measured. Neither of antisense oligonucleotides caused perturbations in pollen tube growth.

Fig 5.6 Appearance of *atfh3atfh5* pollen tubes. Right and middle images show *in vitro* germinated pollen from mutant plants. Pollen tubes did not differ in lenght and shape from WT (left), except of infrequent presence of abnormal, short, thick or branched tubes indicating affected polarity (arrow). *atfh3* mutant was generated in *qrt1* background, pollen grains of the mutant are therefore attached in tetrades. Scale bars represent 10 μm.

5.2.2. Mutation in one of *atfh16* alleles leads to slight perturbations in the growth of etiolated hypocotyls and light grown roots

AtFH16 represents the only type B formin within the Class II family (Cvrčková et al., 2004) and as described in chapters 5.1.2 and 5.1.3, microarray data indicate *AtFH16* to be slightly upregulated in roots and root hairs, in etiolated seedlings and in senescence- and defense-related processes. Therefore, we examined morphology of *atfh16* (SAIL_720_F01) seedlings grown on vertical agar plates both under the standard cultivation conditions and in the dark.

As the segregation ratio of heterozygotes (characterized by the PCR genotyping) on the selection medium containing Basta indicated the presence of an extra T-DNA insertion, the selected homozygous plants were first back-crossed in order to remove it. Originally, no major morphological differences were observed during the first routine experiments with this mutant line, thus we used another mutant line without any extra insertion, *atfh2* (SAIL_615_E03), to create the double mutant *atfh2atfh16* that was intended to be used for further crossing with other formin mutants. Later on, when localization of AtFH16-derived fusion proteins brought the interesting results (see below, chapter 5.3.4), *atfh16* was once again more carefully examined and distinct differences compared to WT were found. To exclude the eventual influence of the additional T-DNA insertion on the phenotype, *atfh2atfh16* plants were finally used for the study. As T-DNA insertion of *atfh2* is located in 3´UTR of *AtFH2* gene and *atfh2* homozygots do not exhibit any phenotype aberration corresponding to *atfh16*, the effect of *atfh2* on any features studied seem highly improbable. Moreover, the same phenotype correlating with *atfh16* mutation was noticed

also in case of a double mutant with the Rho-GDI deficient mutant *buddy 1-1* (*atfh16bdy1-1*), showing that the phenotype is bound to the *atfh16* allele and can be transmitted to next generations and other backgrounds (Fig. 5.7 A, 5.9 A).

To test the effect of the *atfh16* mutation on a course of senescence, seedlings were sown directly on soil or pre-grown on agar plates containing 50 mM NaCl in order to induce early stress conditions, and after 10 days, they were individually planted out to peaty tablets and grown in the greenhouse. To avoid a position effect, mutant and WT plants were randomly distributed within a shelf. After 30 and 40 days, leaf senescence was evaluated. Since no differences between the mutant and WT plants were noticed with respect to the number of yellowing leaves, their appearance or the timing of flowering, no further characterization such as chlorophyl content measurements etc. were done.

Besides, the influence of following treatments, especially plant hormones, on the growth of young 7d seedlings was also tested: sucrose as an osmotic stress-inducing compound (suc, 4%), sodium chloride (NaCl, 50 mM), inhibitor of retrograde transport brefeldin A (BFA), abscisic acid (ABA, 0.3 μM), ethylen precursor 1-aminocyclopropane-1-carboxylic acid (ACC, 25 μM), methyl jasmonate (MeJA, 20 μM and 100 μM) and salicylic acid (SA, 2.5 μM and 50 μM). Osmotic stress had no effect on the root growth, especially on the appearance of root hairs. Similarly, salt stress conditions did not severely influence the overall morphology of the plants, where the light-grown seedlings showed slightly more wavy roots and the dark-grown seedlings had shorter hypocotyls and increased root waving compared to WT. The similar phenotype was observed in case of ABA and SA, where etiolated hypocotyles appeared more wavy compared to WT. ACC and MeJA notably affected even the growth of WT plants that had markedly reduced lenghts of both hypocotyls and roots to the same extent as *atfh16* seedlings. No other abnormalities, such as lack of apical hook formation, were observed in *atfh16* mutants (not shown).

The same phenotype noticed on sucrose, NaCl, BFA, ABA and SA appeared on the control half-MS medium as well, indicating that probably some cytoskeleton-related processes (Ishida et al., 2007; Oliva and Dunand, 2007) could be affected by the loss of AtFH16. In order to test this hypothesis, *atfh16* mutants were sown on additional set of vertical plates supplied with cytoskeletal drugs as follows: taxol (0.5 μM and 0.75 μM), amiprophos-methyl (APM, 1 μM and 2.5 μM), 1-butanol (0.4% and 1% and 3-butanol of the same concentrations as a control), all affecting microtubules dynamics, and jasplakinolide (jasp, 0.1 μM and 0.4 μM) together with latrunculin B (LatB, 0.1 μM and 0.3 μM) influencing actin cytoskeleton. After 3 days, roots of both light- and dark-grown seedlings already elongated, whereas elongation of etiolated hypocotyls accelerated within 4-7 days after germination and after 7 days, the maximum hypocotyl lenght was attained. Under the light conditions, 7d seedlings had already emerging primary leaves, while no lateral roots usually appeared by that time, so the measurements were performed 7 days after germination for all experimental conditions.

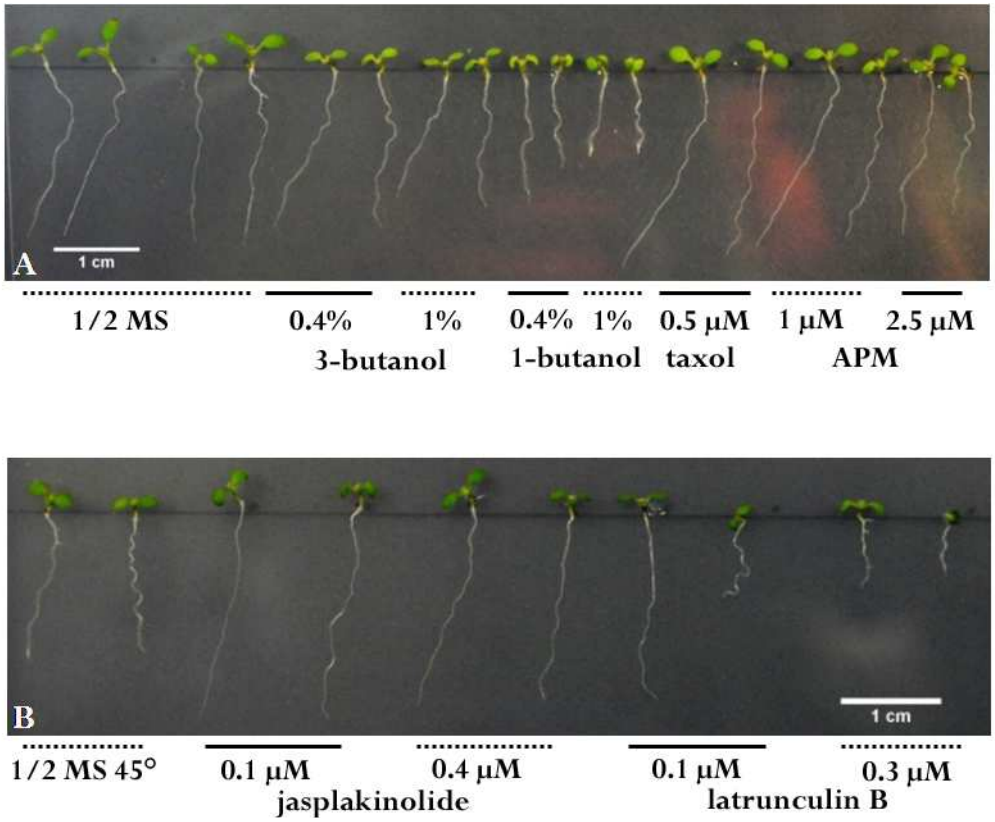

Fig 5.7 Mutant phenotype of light-grown *atfh16*. A: Representative seedlings grown in the presence of microtubule-affecting drugs. For illustration, plants treated for 4 days with 1-butanol (together with control treatment by 3-butanol) are included as well, though the measurements are not available yet. The first four plants from the left are grown on the control half-MS medium as follows: WT, *bdy1-1*, *atfh16*, *atfh16bdy1-1*. To the right, pairs of WT and *atfh16* seedlings grown on particular treatments are underlined. **B:** Phenotype of *atfh16* on hard tilted agar plates and on actin-affecting drugs. Pairs of WT followed by *atfh16* seedling are underlined. Scale bars represent 1 cm.

For the light-grown seedlings, three features describing root growth were measured and statistically analyzed. I measured the lenght of primary roots, their skewing, i.e. a root angle with respect to the the gravity vector. Finally I compared the intensity of root waving, which was determined as the ratio of linear distance between root base and root tip divided by the overall root lenght, so the ratio value of a hypothetical absolutely straight root would be 1. In the absence of any cytoskeleton-affecting compounds on the control half-MS medium, *atfh16* roots did not differ in the lenght and waving intensity from WT, however, they turned out to grow straight down compared to WT roots, that always skewed slightly leftwards, when viewed from above the plates (Fig. 5.7 A). The average difference between WT and mutant root angle was not dramatic, approximately 7 degrees, but evident (graphs on Fig 5.8). The differences in root skewing, usually accompanied by root twisting, are often observed in case of microtubule-associated mutants and they can be highlighted on a tilted hard agar growth medium (Ishida et al., 2007; Sedbrook and Kaloriti, 2008) When subjected to such conditions, root length of mutants still corresponded to WT, however, the intensity of waving significantly increased (Fig. 5.7 B and 5.8 A, B). The direction of root growth drew slightly nearer the vertical line

representing the gravity vector in case of both *atfh16* and WT, but the differences in root angles between them persisted (10 degrees on average), Fig. 5.8 C.

More interesting phenotypes occurred, when the growing medium was supplemented with low doses of drugs interfering with microtubule dynamics. Microtubule-stabilizing agens taxol in the concentration of 0.5 μM affected neither root lenght of all seedlings, nor the waving intensity of WT roots that remained at the same levels (around 0.95) as on the control medium, but increased waving of *atfh16* roots. As expected, all roots skewed markedly leftwards as a result of microtubule stabilization, nevertheless, the difference in skewing corresponded to the half-MS medium (10 degrees). Similar results were acquired on a slightly higher taxol concentration of 0.75 μM, though it already modestly influenced the root lenght of the mutant seedlings (Fig. 5.7 A and 5.8). When the plants were grown in the presence of 1 μM APM that induces microtubule depolymerization, both mutant and WT seedlings behaved in a similar manner, where roots of the mutant plantlets were slightly shorter, wavier and grew under the distinct root angle. However, on a higher APM concentration of 2.5 μM, roots of WT plants became more wavy as well and the difference in root skewing deminished to less than 5 degrees on average, though it remained statisticaly significant (Fig. 5.7 A and 5.8).

Formins are known to play crucial roles in regulation of actin cytoskeleton, and therefore, I tested the effect of actin-affecting drugs as well and there, the most dramatic impact on *atfh16* phenotype was observed. Jasplakinolide, the actin-stabilizing agens used in concentrations of 0.1 μM and 0.4 μM influenced the phenotype of *atfh16* only moderately on the level of the root lenght and skewing, while no significant variations in root waving intensity occured, compared to the control half-MS medium (Fig. 5.7 B and 5.8). I emphasize that the results obtained on jasplakinolide treatment are only preliminary for both light- and dark-grown plants, as the experiment was not repeated (mainly because of the high price of jasplakinolide drug, which would be probably needed in the higher concentrations than tested). By contrast, disruption of actin cytoskeleton by 0.1 μM latrunculin B led to the prominent shortening of *atfh16* roots that exhibited shortening of 40% compared to WT. Furthermore, mutant roots waved more intensively on 0.1 μM LatB than on any other treatment tested. The roots of both mutant and WT plantlets directed straightly down with no differences in root skewing. Application of 0.3 μM LatB severely influenced even the growth of WT plants, so that their roots waved dramatically (root ratio of 0.88) and remained three times shorter than the control plates. The phenotype of mutant plants on 0.3 μM LatB was analogous to that on lower LatB concentration, characterized by the immense root shortening and by the intensive waving, where root ratio measurements gave the same results of 0.8 for both LatB concentrations (Fig. 5.7 B and 5.8).

As a whole, *atfh16* seedlings grown on vertical plates slightly but significantly differed from WT with respect to the certain root growth parameters, especially root skewing and waving. Skewing of *atfh16* roots was consistently smaller compared to WT both on the control medium and on the most cytoskeletal drugs tested except of the higher concentration of APM, where WT roots behaved more like the mutant ones, and also except of LatB that dramatically influenced the skewing of WT roots as well. On 2.5 μM APM, WT roots exhibited intensive waving similar to the mutant ones, whereas taxol, the drug with the opposite effect on microtubules, emphasized waving intensity only in case of *atfh16*. The utmost differences between the mutants and WT occured when seedlings were treated with the low concentration of LatB, where *atfh16* exhibited intensively shortened and wavy roots.

Root skewing and waving is very often accompanied by root twisting (Ishida et al., 2007), however, the detailed analysis of this feature has not been done yet, thought routine microscopy of root cells was performed and no obvious abnormalities in root cells shape and root hair growth were noticed. Nevertheless, the root skewing phenotype is relatively mild, so that eventual enhanced twisting of *atfh16* roots would need to be thoroughly analyzed to uncover possible differences.

Apparently, the measurements performed on light-grown seedlings indicate a slight aberration in the cytoskeleton-related pathways of *atfh16.* Cytoskeleton mutants with abnormalities in root growth parameters usually exhibit also twisting and waving of aboveground organs, especially petioles, resulting in the spirality of rossetes, and of etiolated hypocotyls (Thitamadee et al., 2002; Sedbrook et al., 2004). Rossetes of *atfh16* plants grown under the standart conditions resembled those of WT and no distinctive twisting was observed, however, the dark-grown seedlings exhibited significanly enhanced waving of etiolated hypocotyls. The intensity of hypocotyl waving was quantified as a ratio of the direct distance between hypocotyl base and hypocotyl top divided by the overall hypocotyl length, analogously to the root ratio estimated for the light-grown seedlings as described above. Moreover, the measurements of 7d plants grown on the vertical half-MS medium uncovered that hypocotyls of the mutants were 15% shorter on the average compared to the WT ones. On the contrary, roots of etiolated *atfh16* seedlings were of 18% longer than WT and their waving intensity was significantly higher (Fig. 5.9 A and 5.10 A-D). When the ratio of hypocotyl length vs. root length was calculated for particular seedlings, it turned out that WT plants invested more to the elongation of hypocotyls rather than to the elongation of roots compared to the *atfh16* mutants (Fig. 5.10 E). Specifically, the hypocotyl/root lenght ratio calculated for WT plants was 1.86, whereas it reached only 1.29 value in case of *atfh16*.

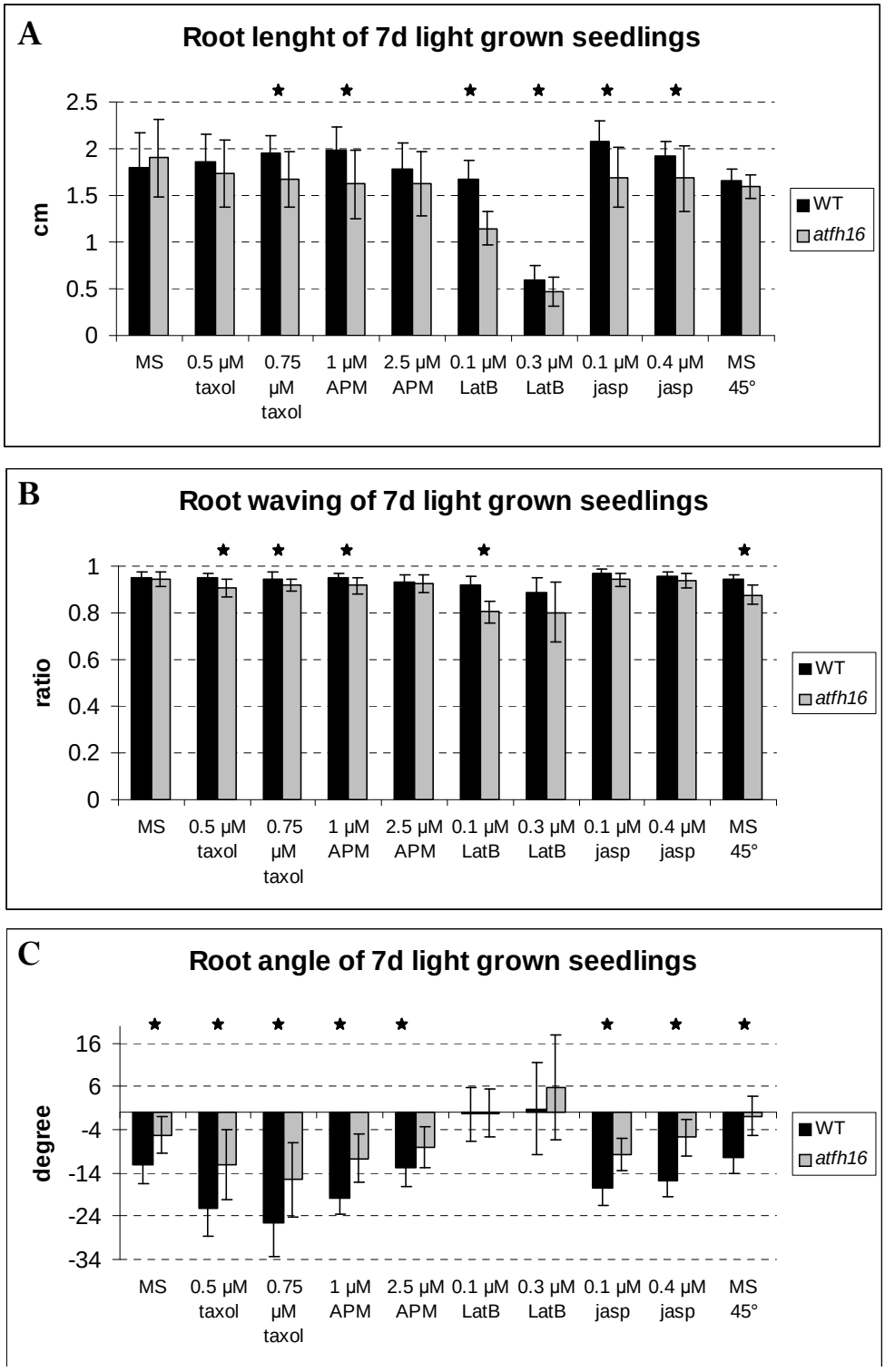

Fig 5.8 Root parameters of *atfh16* light-grown seedlings. A: Lenghts of WT and *atfh16* primary roots measured on 7d seedlings grown on vertical plates supplied with cytoskeleton-affecting drugs. **B:** Root waving determined as the ratio of linear distance between root base and root tip divided by the overall root lenght. **C:** Root skewing (bending) measured as a root angle with respect to the the gravity vector. Statistically significant differences between WT and *atfh16* ($p<0.01$) are marked by asterisk. Error bars represent the standard deviation, with $n>20$.

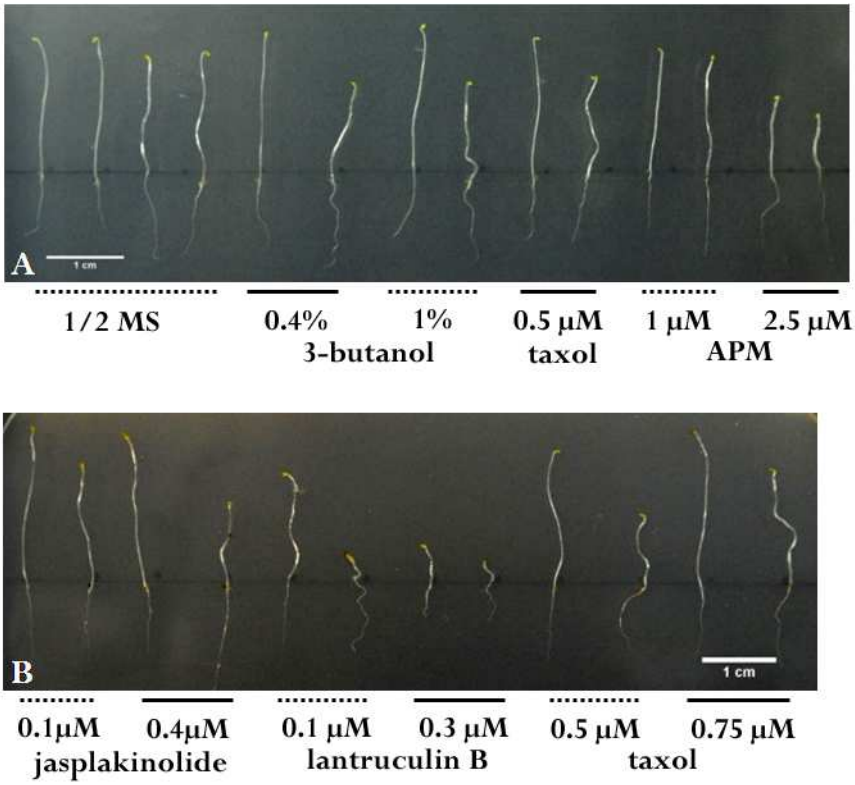

Fig 5.9 Mutant phenotype of dark-grown *atfh16*. A: Representative etiolated 7d seedlings grown on the control medium and in the presence of microtubule affecting drugs. For illustration, plants cultivated on 3-butanol are shown as well; its active isomer 1-butanol aborted germination, so that its effect on etiolated growth could not be examined. The first four plants from the left are grown on the control half-MS medium as follows: WT, *bdy1-1*, *atfh16*, *atfh16bdy1-1*. To the right, pairs of WT and atfh16 seedlings grown on particular treatments are underlined. **B:** Phenotype of *atfh16* in the presence of actin-affecting drugs and taxol; pairs of WT followed by *atfh16* seedling are underlined. Scale bars represent 1 cm.

Similarly to the light-grown plants, etiolation process was monitored using the same cytoskeleton-affecting drugs as well. Application of 0.5 µM taxol pronounced the overall differences between the mutant and WT plants, where the etiolated hypocotyls of *atfh16* were 20% shorter than WT and their intensity of waving slightly increased compared to the control medium (Fig. 5.9 A and 5.10 A, B). Furthermore, the roots of *atfh16* were wavier, but taxol caused slightly increased waving in WT roots as well, so the difference in the waving intensity between mutants and WT remained at the same level. All other features as the root lenght and the hypocotyl/root ratio were comparable to the control medium (Fig. 5.10 C-E). Further reduction of *atfh16* hypocotyls lenght was observed on 0.75 µM taxol, where the mutant hypocotyls reached only 70% of WT hypocotyl lenght. The shortening of *atfh16* hypocotyls affected hypocotyl/root ratio calculated, where the average values were 2.06 for WT and only 1.15 for *atfh16*, respectively. Despite the more intensive waving of WT hypocotyls caused by the higher taxol concentration, the difference between WT and mutant hypocotyl ratio further increased depending on the taxol concentration (Fig. 5.10 B). Besides, the root lenght of both WT and mutant plantlets remained similar compared to the values measured on the

control medium. Although the waving was generally strengthened on 0.75 μM taxol, the difference between root ratios of *atfh16* and WT was not affected (Fig. 5.10 D).

The oposite effect, mainly on the growth of the etiolated hypocotyls, was induced by the microtubule-destabilizing drug APM. In the concentration of 1 μM, the length of *atfh16* hypocotyls was only slightly reduced compared to the half-MS medium and it remained nearly at the same level as on taxol treatments. On the other hand, the hypocotyls of WT plants exhibited noticeable shortening in contrast to the control medium, so that the hypocotyl length of WT and mutants was not significantly different. A further reduction of both *atfh16* and WT hypocotyl lenght occured on 2.5 μM APM, where all the plants reached comparable values (around 0.9 cm) and they were also very similar in waving intensity (Fig. 5.9 A and 5.10 A, B). Such a shortening of WT hypocotyls resulted in the dramatic decline of hypocotyl/root ratio (from 1.86 on MS to 1.03 on 2.5 μM APM), which already did not significantly vary from the ratio of *atfh16* (Fig 5.10 E). Despite the slight overall reduction of the root lenght caused by APM, the variation of *atfh16* from WT remained unchanged, just as for the root waving intensity that did not differ from the control medium (Fig 5.10 C, D).

When dark-grown (etiolating) seedlings were subjected to the drugs influencing actin cytoskeleton, the phenotype of *atfh16* nearly copied the situation in the light-grown plants. The differences of hypocotyl lenght between WT and mutants remained significant on both 0.1 μM and 0.4 μM jasplakinolide and varied around 22%. The waving of hypocotyls seemed not to be affected by jasplakinolide and it was fully comparable with the half-MS medium; still showing the significant difference between WT and mutant (Fig. 5.9 B and 5.10 A, B). Any other perturbations in the root growth were invoked by 0.1 μM and 0.4 μM jasplakinolide. The difference between hypocotyl/root ratio of *atfh16* and WT seedlings was higher that on the control medium in case of both concentrations of jasplakinolide (Fig. 5.10 E).

In contrast to all the other cytoskeletal drugs tested, the appearance of *atfh16* etiolated hypocotyls was affected to the greatest extend by the low concentration of LatB, like in the roots of light-grown mutant plants. On 0.1 μM LatB, even the WT hypocotyls were markedly shortened and reached only 80% of their length on the control medium, however, the hypocotyls of *atfh16* elongated only to 30% of the control medium lenght and varied extensively in their waving intensity compared to the mutant plants on half-MS plates (Fig. 5.9 B and 5.10 A, B). The same concentration of LatB had only a mild effect on the root length of the etiolated seedlings; their roots remained nearly unaffected with only a negligible shortening in case of *atfh16* roots, nevertheless, the mutant roots exhibited increased waving intensity on 0.1 μM LatB compared to the control medium (Fig. 5.10 C, D). The higher concentration of 0.3 μM LatB had severe effect on the growth of all the etiolated seedlings, as it impaired the elongation of hypocotyls and caused overall immense growth defects.

To sum up, the etiolated hypocotyls of *atfh16* plants behaved in the similar way as the light-grown roots, especially with respect to the variation in length and in the intensity of waving. Analogously to the previous experiments, the differences between mutant and WT plants were more distinct on microtubule-stabilizing taxol, whereas APM with the opposite effect evoked *atfh16* resembling phenotype even in case of the WT plants. Nevertheless, the most prominent disturbances in the growth of etiolated *atfh16* seedlings were caused by the low doses of actin-destabilizing latrunculin B.

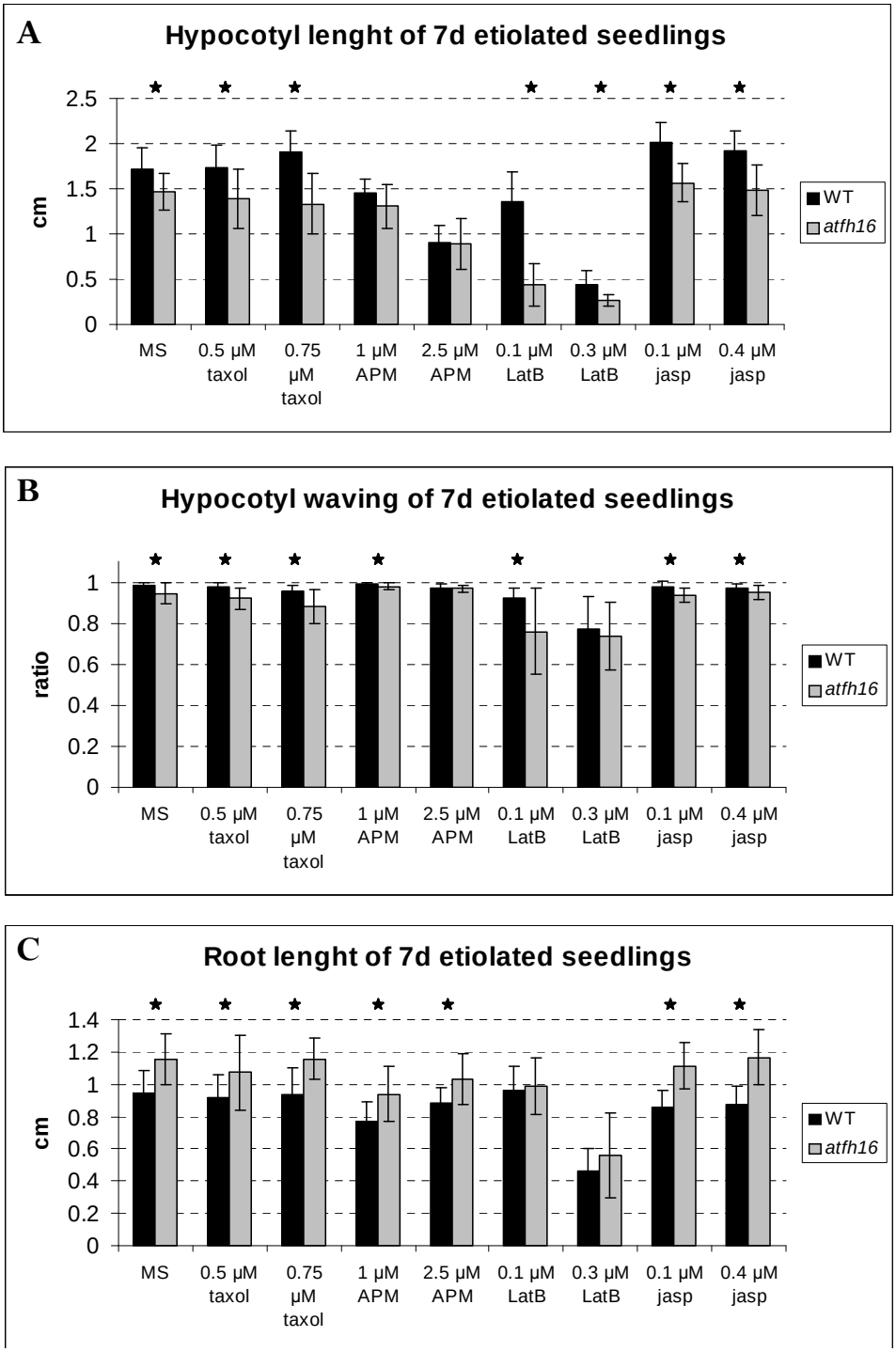

Fig 5.10 Hypocotyl and root parameters of *atfh16* dark-grown seedlings. A: Lenghts of WT and *atfh16* etiolated hypocotyls measured on 7d seedlings grown on vertical plates supplied with cytoskeleton-affecting drugs. **B:** Waving intensity of etiolated hypocotyls determined as the ratio of linear distance between hypocotyl base and hypocotyl top divided by the overall hypocotyl lenght. **C:** Root lenght of etiolated seedlings. **D:** Root waving intensity of dark-grown seedlings measured as the ratio of linear distance between root base and root tip divided by the overall root lenght. **E:** Average ratio of hypocotyl/root lenght that was determined for each individual seedling indicates, which of these organs is preferentially elongated. Statistically significant differences between WT and *atfh16* ($p<0.01$) are marked by asterisk. Error bars represent the standard deviation, with $n>20$.

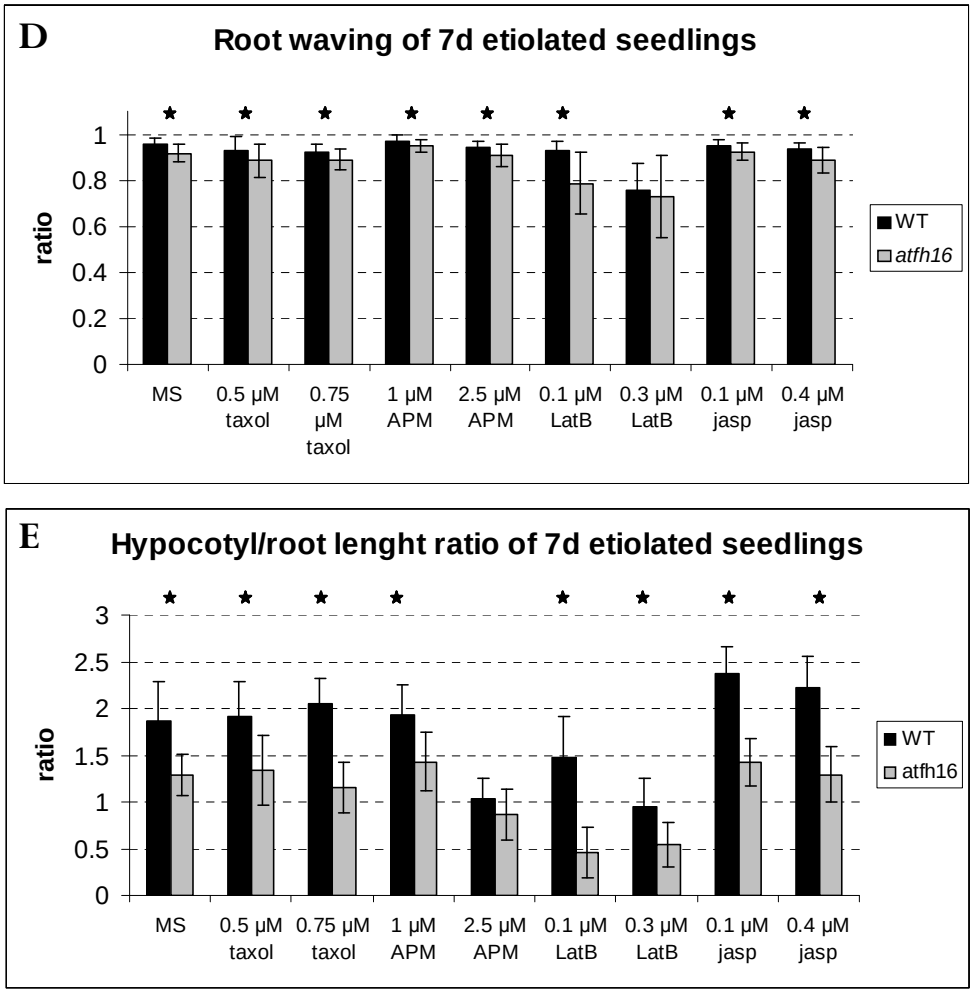

Fig 5.10 (continue) Hypocotyl and root parameters of *atfh16* dark-grown seedlings. A: Lenghts of WT and *atfh16* etiolated hypocotyls measured on 7d seedlings grown on vertical plates supplied with cytoskeleton-affecting drugs. **B:** Waving intensity of etiolated hypocotyls determined as the ratio of linear distance between hypocotyl base and hypocotyl top divided by the overall hypocotyl lenght. **C:** Root lenght of etiolated seedlings. **D:** Root waving intensity of dark-grown seedlings measured as the ratio of linear distance between root base and root tip divided by the overall root lenght. **E:** Average ratio of hypocotyl/root lenght that was determined for each individual seedling indicates, which of these organs is preferentially elongated. Statistically significant differences between WT and *atfh16* ($p<0.01$) are marked by asterisk. Error bars represent the standard deviation, with $n>20$.

To visualize a state of cytoskeletal structures in the *Arabidopsis* plants with impaired *AtFH16* function, *atfh16* mutants were crossed with transformants expressing GFP:mTalin, a marker for actin cytoskeleton (Kost et al., 1998) and with GFP:MAP4, which decorates microtubular strucures (Marc et al., 1998; plants were a gift from Richard Anthony). Homozygous plants for *atfh16* were selected by PCR analysis and the presence of the reporter marker for cytoskeleton was verified microscopically. Since both GFP:mTalin and GFP:MAP4 are constitutively expressed under the 35S promoter, homozygous plants can be easily identified according to their overexpression phenotype. Appearance of the cytoskeleton system was examined microscopically in 7d seedlings

grown on the vertical plates, both at light and in dark. As the overexpression of both cytoskeletar markers causes several morphological abberations (Kost et al., 1998), especially in the homozygous state, *atfh16* homozygotes were therefore observed on both homozygous and heterozygous background of each cytoskeleton marker. However, even the expression of GFP:mTalin or GFP:MAP4 in heterozygous plants induced the marker-related morphological changes that masked the moderate mutant phenotype of *atfh16.* No differences in the architecture of cortical microtubules were apparent in *atfh16*GFP:MAP4 plants (not shown). In case of *atfh16*GFP:mTalin, several discrepancies in actin organization such as helical arrays of filaments, markedly thick filament bundles or randomly distrubuted short, curved filaments were noticed compared to the control GFP:mTalin (Fig 5.11). Albeit all these abnormalities were already observed as artifacts caused by the accumulation of GFP:mTalin (Sheanan et al., 2004b; Voigt et al., 2005), disruption of *AtFH16* seems to enhance formation of such discrepancies in actin network; more detailed analysis would be needed to decide whether this indeed is the case.

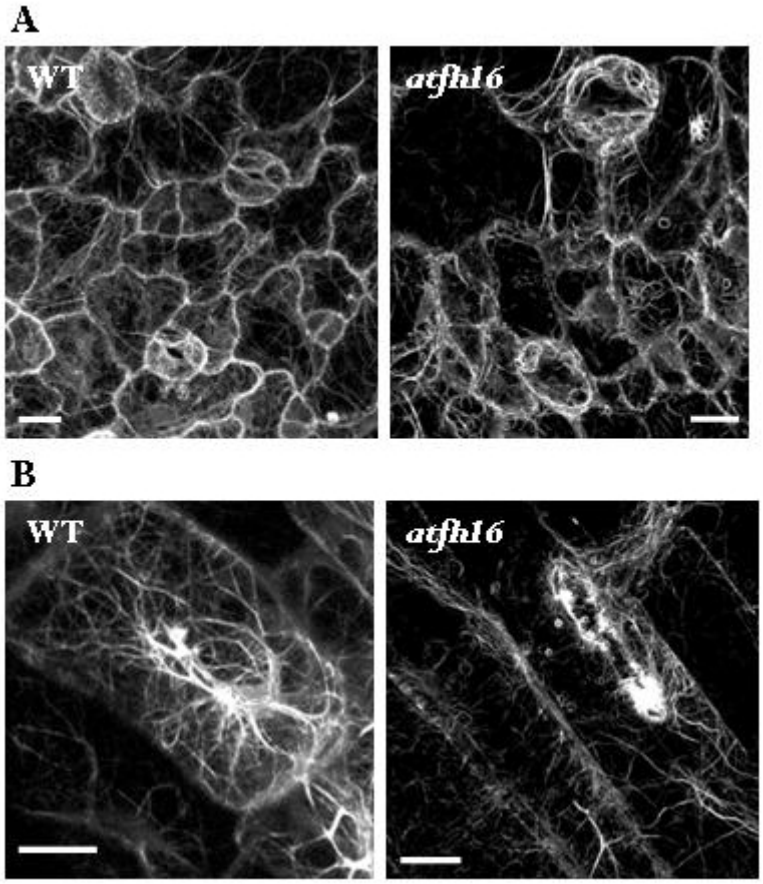

Fig 5.11 Visualization of actin cytoskeleton in *atfh16* mutants by GFP:mTalin. Dark-grown 7d seedlings homozygous in atfh16 expressing GFP:mTalin were microscopically examined; **A:** cotyledon surface, **B:** etiolated hypocotyls. Scale bars represent 10 μm.

Besides genotyping analysis, disruption of *AtFH16* allele by mutation was verified by RT-PCR, where no full-lenght *AtFH16* transcript was detected in 7d *atfh16* seedlings (Fig. 5.12). Nevertheless, a direct connection between the observed phenotype of *atfh16*

and *AtFH16* impairment needs to be further verified, as the recently selected homozygots in the second allele *atfh16-2* do not exhibit comparable phenotypic changes (so far only briefly tested on the half-MS and 0.1 μM LatB media) and transgenic mutant plants stably expressing GFP:AtFH16 or AtFH16:GFP under the 35S promoter were not suitable for a complementation analysis because of mosaic distribution and early silencing of the transgene (see 5.3.3)

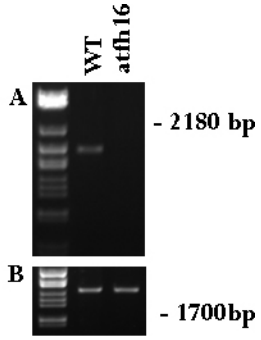

Fig 5.12 Verification of *atfh16* mutants by RT-PCR. Total RNA from *Arabidopsis* WT Col-0 and *atfh16* plants was reverse-transcribed and PCR amplified using primers for full-lenght *AtFH16* **(A)**. Primers specific for *ACT7* amplification (constitutively transcribed gene) were used as an internal control **(B)**.

5.3. Cloning and characterization of selected formins

5.3.1. Structure of *AtFH3* differs from the theoretical gene prediction.

As the impairment of *AtFH3* and *AtFH5* did not affect pollen development, truncated versions of the *AtFH3* gene were cloned by RT-PCR under Lat52 promoter to test the overexpression effect in pollen. Now, there are recently modified gene predictions available on TAIR (1818 bp and 2271 bp, www.arabidopsis.org). Gene structure predictions available by the time of cloning experiments have been subjected to a critical review in our previous publication (Cvrčková et al., 2004) resulting in suggestion of a previously unpredicted N terminal domain, but still predicting only a N-terminally truncated ORF of 2496 bp starting with AAA instead of ATG. The later prediction was used for primers design, where 5´ primer was located within the first ATG codon downstream in frame of AAA codon, consistently with the recent TAIR predictions that have been confirmed by cloning of *AtFH3* gene done by Ye, Zheng et al. (2009). 3´primer was located on the TAG termination codon predicted by Cvrčková et al. (2004), assuming the existence of sequencing error in genome database and thus prolonging the existing gene model from TAIR. Additional set of 5´primers was designed to amplify also two shortened versions of *AtFH3* containing either FH1FH2 domains or FH2 domain itself. With all the primer sets, cDNA products of expected sizes corresponding to the prediction made by Cvrčková et al. (2004) were amplified. As a template, total RNA isolated from *Arabidopsis* inflorescence and transcribed by reverse transcriptase using oligo(dT) primer was used.

Sequencing of the construct Lat52::*AtFH3*t:GFP uncovered some differences compared to the prediction; a short N-terminally located deletion of four nucleotides that surprisingly does not necessarily lead to a premature abortion of AtFH3 protein translation. Translation of such full-lenght *AtFH3* sequence obtained by sequencing in a different reading frame leads only to the protein sequence changes within the N-terminus, whereas the other downstream regions remain unaltered. The sequencing further revealed a presence of mistakes in the genomic sequence of *Arabidopsis*, especially in CG-rich regions that had led to the wrong prediction of two short aminoacid sequences within FH2 domain. Furthermore, the cloned version of *AtFH3* showed that both versions predicted by TAIR lack important parts of FH2 domain and are in fact C-terminally truncated. This fact has been recently confirmed also by Ye, Zheng et al. (2009), who cloned the full lenght cDNA of *AtFH3* using similar approach.

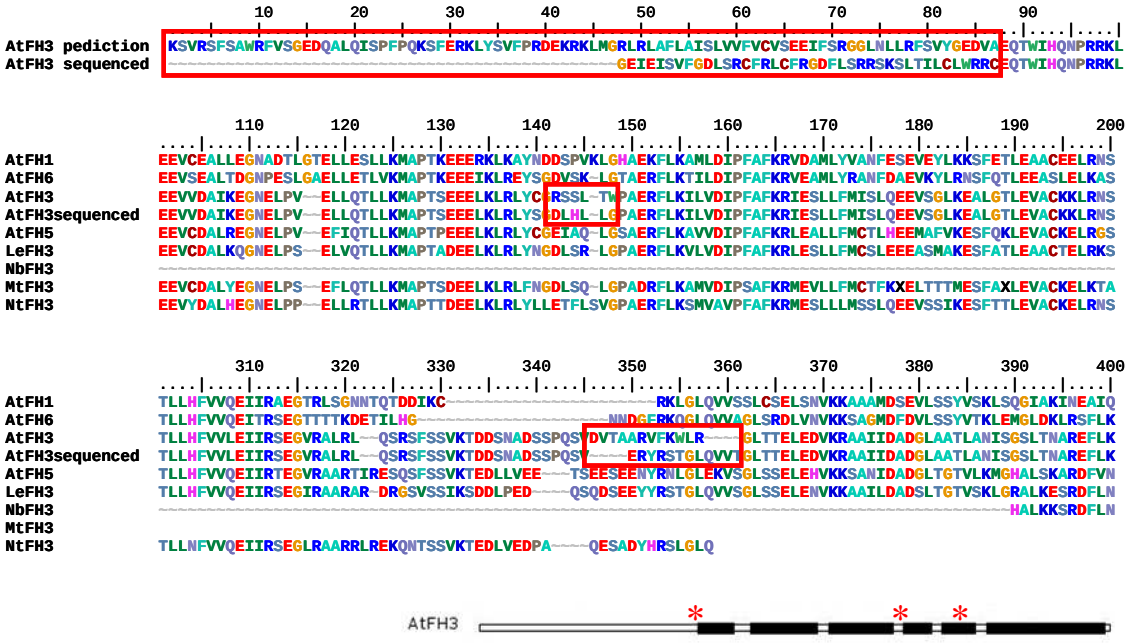

Fig 5.13 Revision of AtFH3 protein sequence within N-terminus and FH2 domain. Comparison of incomplete AtFH3 N-termini (RT-PCR amplified version vs. prediction of Cvrčková et al., 2004) and FH2 domains alignment of AtFH3 and related formins. Differences between predicted and cloned versions are highlighted by red boxes. Asterisks at schematic picture show their position within *AtFH3* gene prediction.

Compared to the short 1818 bp TAIR prediction in detail, the cDNA amplified by RT-PCR lacks four amino acids on the positions 124-127. Translation in the original reading frame would lead to the premature abortion of translation, however, translation in the reading frame 3 starting from the first ATG codon would result in a 42 aa long N-terminal sequence substitution that differs from both all the predictions and the recently cloned gene of *AtFH3*, but corresponds with them from the amino acid on the position 43 onwards (Fig. 5.13). In my sequence, T replaces C on the position 213, which does not alter amino acid composition. Positions 508 and 561, that differ in Ye and Zheng´s clone, match prediction in my case. Furthermore, nucleotides 516-518 are missing, so that Phe 173 on the TAIR protein prediction is absent and preceding Met changes to Ile, while reading frame remains unchanged. Following substitutions that do not change amino acid sequence and could be thought as polymorphism are further present: T on 834 → A, A on

897 → G, T on 900 → A, A on 1437 → C, T on 1521 → C, T on 1671 → C, A on 1673 → G.

An extra G on 1360 proposed in our 2004 paper was not confirmed, while an additional C emerged at 1385 position resulting in the addition of 47 bp, previously considered to be an intron according to the TAIR prediction. Similarly, G on 1760 of TAIR sequence is absent, as predicted in our paper, while G on 1765 was confirmed. This leads to a sequence differing in 12 amino acids compared to our 2004 prediction (Fig. 5.13). The same findings were also described by Ye and Zheng (2009). Near the C terminus, two substitutions different from both our 2004 prediction and the Ye and Zheng version occur within my cDNA that cause changes in protein sequence, where Ile 674 of my sequence replaces Phe and Gly 713 occures instead of Asp. The first substitution leads to the incorporation of a similar amino acid, which can be also found at the same position in the majority of AtFH3 homologues from other plants. These facts make a polymorphism origin of the substitution highly probable. In the second case, the acidic amino acid replaces a hydrophobic one and does not occur in AtFH3 partial constructs prepared for yeast two-hybrid experiments, so that I consider the later substitution as a result of RT- or PCR-introduced mutation. The new edited amino acid sequence of AtFH3 is consistent with the corresponding regions of selected related genes, (Fig. 5.13, Supplemental data 3).

Besides the non-functional N-terminally truncated version that turned out to be cloned out of frame, individual conserved domains of *AtFH3*, Lat52::*AtFH3*[FH1FH2]-GFP and Lat52::*AtFH3*[FH2]-GFP, were transformed into *Agrobacterium* and subsequently into *Arabidopsis* plants by the floral dip method. About 30 individual primary transformants from each transformation were grown and their *in vitro* germinated pollen tubes were microscoped. However, GFP fluorescence was not observed in any of the transformants.

5.3.2. Cloning of *AtFH16*, a member of Class II family.

A cDNA of *AtFH16* was amplified combining the Riken clone APZL29g02 and a reversely transcribed inner fragment. Sequencing of the full lenght cDNA amplified from APZL29g02 revealed the presence of an incorrectly spliced 5´end of the second intron, resulting in the incorporation of an extra intron part together with STOP codon into the cDNA sequence. Thus, the whole problematic region of ~ 930 bp was cut out using the inner cleavage sites and replaced by a RT-PCR amplified fragment. For the fragment amplification, total RNA isolated from the whole 7 days old *Arabidopsis* seedlings subsequently transcribed by the reverse transcriptase was used as a template. Such a reconstituted cDNA of *AtFH16* was cloned into pBluescript KS+ and Gateway pENTR3C vectors and used for further cloning experiments.

Compared to our published prediction (Cvrčková et al., 2004), some clones of the newly amplified cDNA of *AtFH16* contain an extra insertion of 12 nucleotides (four amino acids) located on a boundary of the third exon indicating the presence of alternatively spliced area (shown on Fig. 5.14). Moreover, another sequence corresponding to the extraneous loop encoded by the last exon (belonging to FH2 domain coding region) appeared to be an intron, confirming the older predictions. Besides, four nucleotide substitution compared to the TAIR prediction NM_120859 were found within the cloned cDNA: T 389 → C (Phe → Ser), T 525 → C, A 1609 → G (Thr → Arg) and A 1698 → T (Glu → Asp). The second substitution does not change the protein sequence and as well as

the fourth substitution, it is located on the third place of the codon. The later one results in the exchange of amino acid, where acidic glutamine is replaced by asparagine of the similar chemical character. Therefore, I consider these two substitutions as a polymorphism effect. On the contrary, the first togehter with the third substitution leads to the incorporation of the chemically different amino acids and supposedly originated as RT- or PCR-introduced mutations (complete sequence is shown in Supplemental data 4).

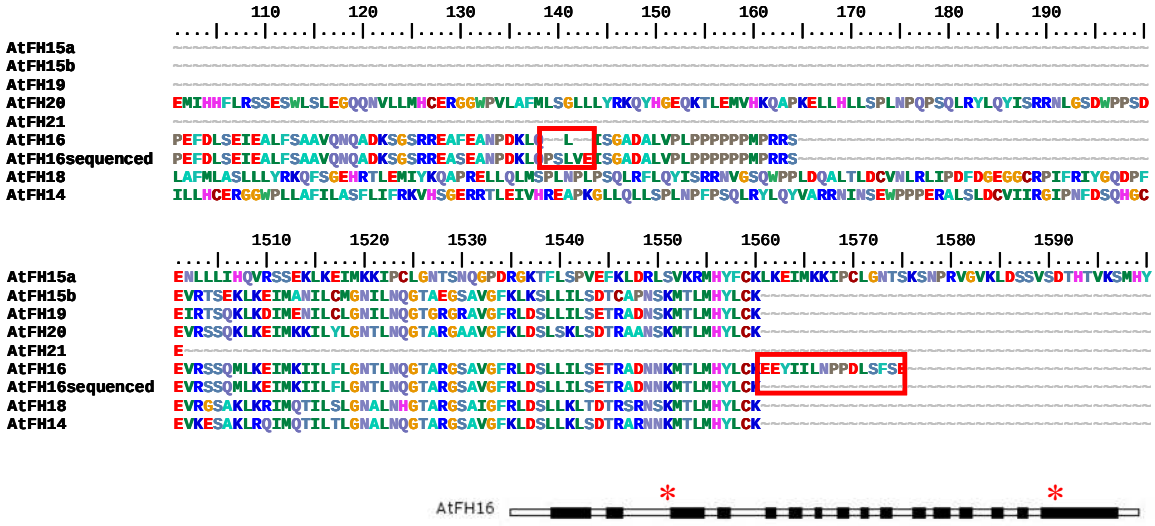

Fig 5.14 AtFH16 contains alternatively spliced N-terminus. Four extra amino-acids are inserted in the third exon as a consequence of alternative splicing. Recently predicted loop within FH2 domain was not confirmed by *AtFH16* cloning. Both divergences are shown in red boxes. Asterisks at schematic picture show their position within *AtFH16* gene prediction.

5.3.3. AtFH16 fusion proteins expressed under 35S promoter localize to root cells and root hairs and do not impair developmental processes in *Arabidopsis*.

Overexpression of plant formins may lead to the formation of abnormal cytoskeletal patterns resulting in the perturbances in cell polarity and morphogenesis (Cheung and Wu, 2004; Deeks and Cvrčková et al., 2005) To study overexpression effects of *AtFH16* in *Arabodopsis*, GFP-fusion proteins expressed under the 35S promoter (35S::GFP:*AtFH16*, 35S::*AtFH16*:GFP) were introduced into *Arabodopsis thaliana* cv. Columbia 0 plants using the floral dip method. From each transformation, about 60 primary transformants were selected and microscopically examined. GFP signal, which was detected only in the minority of the resistant seedlings, exhibited the same localization pattern in case of both N-terminally and C-terminally fused AtFH16 proteins. GFP-fused AtFH16 was predominantly localized in root hairs (Fig. 5.15 B), especially within the long root hairs growing from the root base. This localization pattern was often accompanied by the weaker signal in root epidermal cells (Fig. 5.15 A), with a characteristic "mosaic" appearance, where fluorescent cells were unequally distributed within the root. In both cell types, AtFH16 resided in net-like structures of interconnected strands with obvious dynamic movement comprising rapid vesicle-like directional migration and slower rearrangement of

the whole strands (Fig. 5.16 A, B). The most intensive GFP fluorescence could be observed in perinuclear area with exclusion of the nucleus, indicating absence of free GFP in the first days after germination. No signal was detected in aboveground organs, except of one plant expressing 35S::GFP:*AtFH16* showing a very weak GFP fluorescence with diffuse pattern that was restricted to stomatal cells of leaves (not shown).

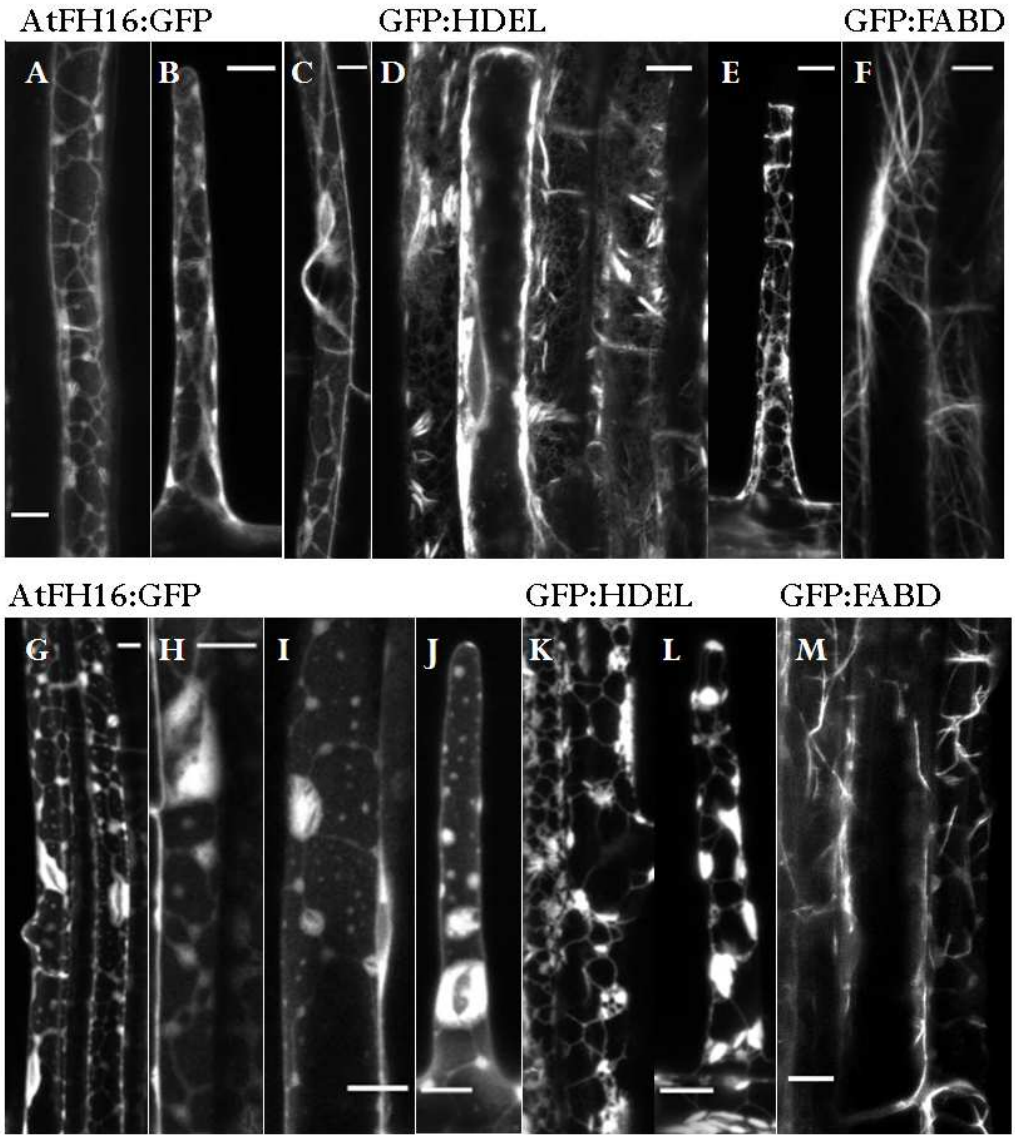

Fig 5.15 35S::AtFH16:GFP expressed in *Arabidopsis* roots resembles ER pattern and is latrunculin B sensitive. AtFH16:GFP appeares as a net-like structure composed of dense perinuclear system, together with thick and thinner interconnected strands in roots of stable transgenic *Arabodpsis* seedlings. Pictures show root cell **(A)**, root hair **(B)** and root cell with emerging root hair **(C)**. GFP:HDEL, a marker of ER, is organized in simmilar, yet finer and more complex system **(D, E)**. Rice grains-like structures are considered as artefacts. **F:** GFP:FABD root cells with decorated actin filaments. The second row of pictures shows same proteins after 2 hours of LatB treatment (10 μM). Fragmentation of actin cytoskeleton was used as a control of LatB action **(M)**. AtFH16:GFP signal looses from thick strait strands, whereas disconnected punctated structures appear **(G, H)**. The effect becomes more evident after 4 hours **(I, J)**. Similarly, GFP:HDEL localization changes, the network becomes less complex and the signal aggregates around sheets of ER. However, no punctated structures originate. Scale bars represent 10 μm.

Originally, the formin-labeled structures were thought to be cytoplasmic strands only, because AtFH16 protein lacks both transmembrane or PTEN domain that could mediate its anchorage to membrane compartments. However, the closer look on the root hairs indicated that the signal is present also in other celullar structures besides cytoplasm. During elongation of root hairs, a specialized type of extension called the tip growth occurs, in which all growth takes place in the apical part of the tip-growing cell. Here, so-called clear zone forms, consisting of a dense cytoplasm containing vesicles. Furthermore, the tip growth is supported by intensive cytoplasmic streaming inside the root hair (Cole and Fowler, 2006). Although the root hairs observed were in good physiological conditions as indicated i.e. by non-swelling tips with the presence of clear zone or rapidly moving cytoplasm, AtFH16-fusion protein localized neither diffusely to the tip of the root hairs, nor copied the tracts of streaming cytoplasm visible under the root hairs surface. Similarly, when free GFP, known to linger in the cytoplasm, occurred in some root cells as a result of the fusion protein degradation, the localization pattern was diffuse and different from the formin signal.

To clarify the identity of cellular compartments stained by GFP:AtFH16 and AtFH16:GFP, characterized stable transformants expressing markers for actin, microtubules, endoplasmic reticulum (ER) and vacuole were used for comparison. It turned out that AtFH16 localization at least in root hairs corresponds to the pattern of GFP:HDEL, a marker for ER (Haseloff et al., 1997; Fig. 5.15 E). In case of root cells, GFP:HDEL stained a similar, but finer network of endomembranes than AtFH16 with analogous velocity of movement and rearrangement (Fig 5.15 D and 5.16 C). Distinct domains of ER were shown to be attached to actin filament network, so that disruption of actin by LatB leads consequently to disorder in ER (Sheahan et al., 2004). To test, whether actin disruption influences character and dynamics of formin-labeled structures, 5d transgenic plants expressing AtFH16:GFP were incubated with 10 μM LatB for 1 to 12 hours (Fig. 5.15 G-M). The progress of actin filaments fragmentation was monitored in parallel on roots of plants expressing GFP:FABD, the second actin-binding domain (fABD2) of *Arabidopsis* fimbrin, AtFIM1 (Sheahan et al., 2004b). The effect of 10 μM LatB was apparent already after 10 min of the treatment, however, the majority of thicker actin filaments remained intact. When the incubation was prolonged, nearly all actin fibers in root cells became fractured or even disappeared after 2 hours. By the same time, changes in localization pattern of both GFP:HDEL and AtFH16:GFP occurred as well; fine structures of the ER network were no longer visible and instead, cisternae of low complexity organization together with the strong GFP signal aggregated around ER sheets were observed. In case of AtFH16:GFP, the originally cross-linked thick strands disappeared, while only few finer strands remained and a kind of disconnected punctated structures appeared. The dynamic transport previously occurring alongside the interconnected strands nearly stopped in case of the persisting disordered trails.

Later on, usually 7-10 days after germination, AtFH16 fusion proteins underwent progressive degradation resulting in the increase of free GFP content followed by loss of the fluorescent signal, which unfortunately disabled further observations of formin localization at maturing plants.

Besides the transformation of WT plants, 35S::GFP:*AtFH16*, as well as 35S::*AtFH16*:GFP were also transformed into *atfh16* background in order to observe the localization of GFP-fused AtFH16 in the absence of the endogenous protein. Among isolated primary transformants, up to 20 plants with GFP positive signal were selected and

transplanted into peaty tablets for seed production. According to microscopic examination of the T1 plants, which was only brief in order to avoid damage of seedlings, the majority of plantlets with fluorescent signal seemed to exhibit the same type of localization as observed on WT background. Although two seedlings transformed with 35S::GFP:*AtFH16* also displayed the GFP signal in aboveground organs, including for example cotyledon epidermal cells, their further growth was restricted compared to other transformants, and after few days, both seedlings became yellowish and finally died. This suggests that silencing of ectopically expressed GFP:AtFH16 or AtFH16:GFP in most of young plant organs is crucial for the successful progress of growth and development. Once overexpression of AtFH16 inside the whole plant is allowed, in leads to the growth restriction and overall plant weakening. However, further experiments, especially detailed microscopic analysis of the higher number of transformed plants showing no silencing effect would be needed to make any conclusions.

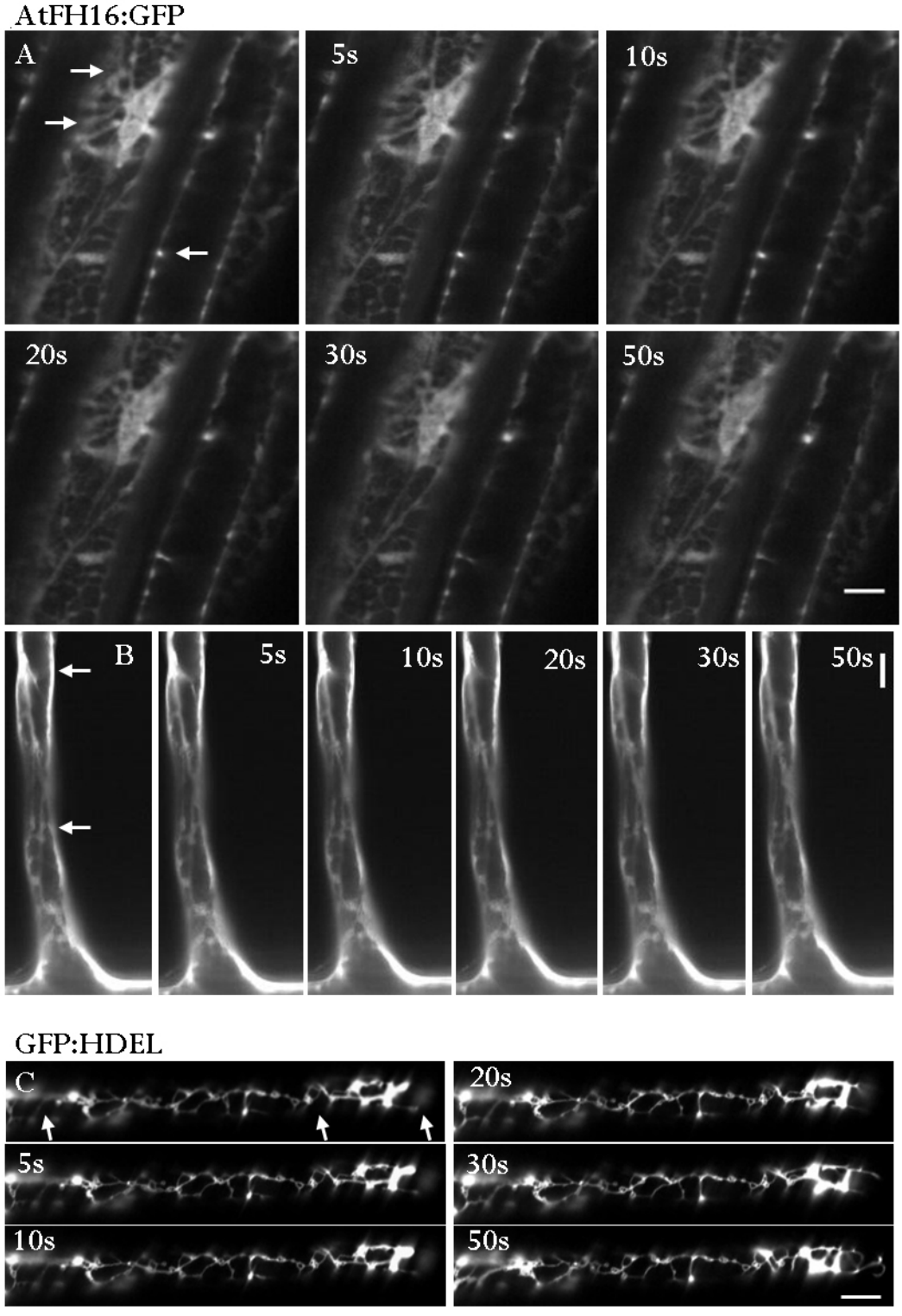

Fig 5.16 35S::AtFH16:GFP decorated structures constantly remodel. On time-lapse photographs, intensive vesicle trafficing together with remodeling of network strands is apparent. Remodeling of AtFH16:GFP in perinuclear area of root cells **(A)** or root hair base **(B)** within 50 seconds. Analogous rearrangement of GFP:HDEL occures inside root hair **(C)**. Examples of mobile strands are depicted by arrows (quick movements of vesicles can be hardly seen on selected pictures). Scale bars represent 10 μm.

5.3.4. Transiently expressed AtFH16 protein decorates cytoskeletal structures in *Nicotiana bentamiana* leaves

To examine AtFH16 subcellular localization *in vivo*, a set of *AtFH16* subfragments were cloned into binary vectors allowing their expression with the fluorescent marker (GFP or RFP) under the the 35S promoter. AtFH16-derived fusion proteins were than transiently expressed in epidermal cells of *Nicotiana bentamiana* leaves after *Agrobacterium*-mediated transformation. All AtFH16 subfragments except of N-terminal part of the formin (GFP:AtFH16Δ1, cloned by Matyáš Fendrych) were attached to the fluorescent tag both N-terminally and C-terminally, giving rise to the collection of 13 different fusion proteins summarized in Fig. 5.17. Unlike all other *Arabidopsis* formins, C-terminus of AtFH16 protein is formed by a non-conserved proline-rich region located behind the FH2 domain. In order to test its influence on the subcellular localization, following versions lacking this part were cloned; GFP:AtFH16Δ2, AtFH16Δ2:GFP, RFP:AtFH16Δ4, AtFH16Δ4:GFP, GFP:AtFH16Δ6 and AtFH16Δ6:GFP. The proline-rich FH1 domain of AtFH16 consists of two shorter regions partitioned by an internal repetitive sequence. Subfragments lacking either one part or the whole FH1 region were prepared as follows: N-terminal part of the FH1 domain was removed in constructs GFP:AtFH16Δ5, AtFH16Δ5:GFP, GFP:AtFH16Δ6 and AtFH16Δ6:GFP, whereas the whole FH1 domain is missing in case of GFP:AtFH16Δ2, AtFH16Δ2:GFP, RFP:AtFH16Δ3 and AtFH16Δ3:GFP.

Table 5.1 Summary of AtFH16 localization pattern. * = only in the presence of dsRED:FABD N = nucleus, no cyt = no staining of cytoplasm, NT = not tested

construct	actin*	MT	spots	other
GFP:AtFH16	+	+	+	
AtFH16:GFP	+	+	+	
GFP:AtFH16Δ1	+	-	-	
GFP:AtFH16Δ2	NT	+	+	
AtFH16Δ2:GFP	NT	-	-	N, cortex, no cyt
RFP:AtFH16Δ3	NT	+	+	
AtFH16Δ3:GFP	-	+	+	
RFP:AtFH16Δ4	NT	+	+	
AtFH16Δ4:GFP	NT	+	+	
GFP:AtFH16Δ5	NT	+	+	
AtFH16Δ5:GFP	NT	+	+	
GFP:AtFH16Δ6	NT	-	-	
AtFH16Δ6:GFP	NT	+	-	N with spots, no cyt

In transiently transformed leaves of *Nicotiana bentamiana*, both GFP:AtFH16 and AtFH16:GFP exhibited several localization patterns ranging from a weak cytoplasmic

signal (with exclusion from the nucleus), through brighter dots of a different size and mobility, apparently cytoskeletal fibrous structures to structures reminiscent of the endoplasmic reticulum (ER). Distribution of localization patterns was not homogenous and varied within a single infiltrated leaf, depending on its ontogenic stage. In the cells of young leaves (about 3cm in length), AtFH16 predominantly localized into spots, dots and fibrous structures, whereas cytoplasmic signal prevailed in the cells of mature leaves. The similar pattern of localization was observed when individual AtFH16 subfragments were expressed on their own, except the AtFH16Δ2:GFP and AtFH16Δ6:GFP, which resided mostly in the nucleus. A weaker signal of AtFH16Δ2:GFP was usually also present at the cell periphery, whereas AtFH16Δ6:GFP strongly accumulated inside the nucleus in the form of bright bodies, whereas only the minority of the cells exhibited an extra-nuclear signal, among which the filamentous strucures prevailed. The localization patterns of GFP or RFP-tagged versions of AtFH16 are shown on Fig. 5.18 and summarized in Tab 5.1.

Fig 5.17 AtFH16 fusion protein and its derived truncated versions used in localization studies. Full-lenght AtFH16 protein and various combinations of domains were attached to GFP or RFP creating a set of both N-terminally and C-terminally fused proteins. N-terminus of AtFH16 contains polyproline rich FH1 domain consisting of two parts (green boxes) followed by a conserved FH2 domain (ochre box). Two internal repetitive motifs located between the two parts of FH1 domain and also at the N-terminus of FH2 domain are depicted as spotted boxes. C-terminal part of the protein consists of non-conserved polyproline rich region (pink box). Numbers indicate initial amino acid of particular domain or region according to AtFH16 variant without 4 amino acids insertion originated from aletrnative splicing of N-terminus.

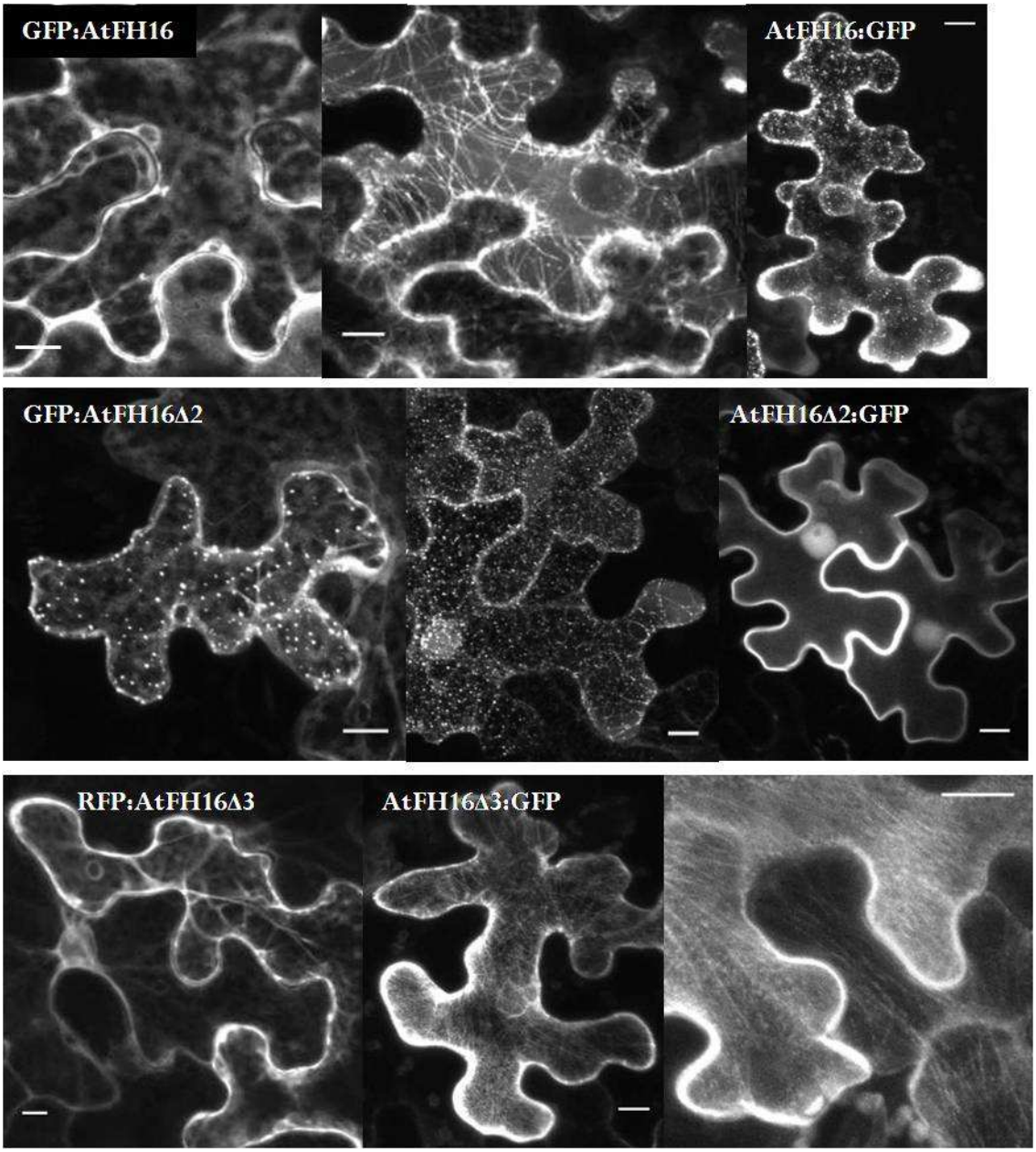

Fig 5.18 A localization overview of transiently expressed AtFH16 and its subfragments. Both full-lenght AtFH16 protein and its derived truncated variants localize to various cellular structures. Each picture line shows representive localization patterns of one particular subfragment except of GFP:AtFH16Δ1 with mostly uniform localization pattern, which can be seen on Fig. 5.19. Scale bars represent 10 μm.

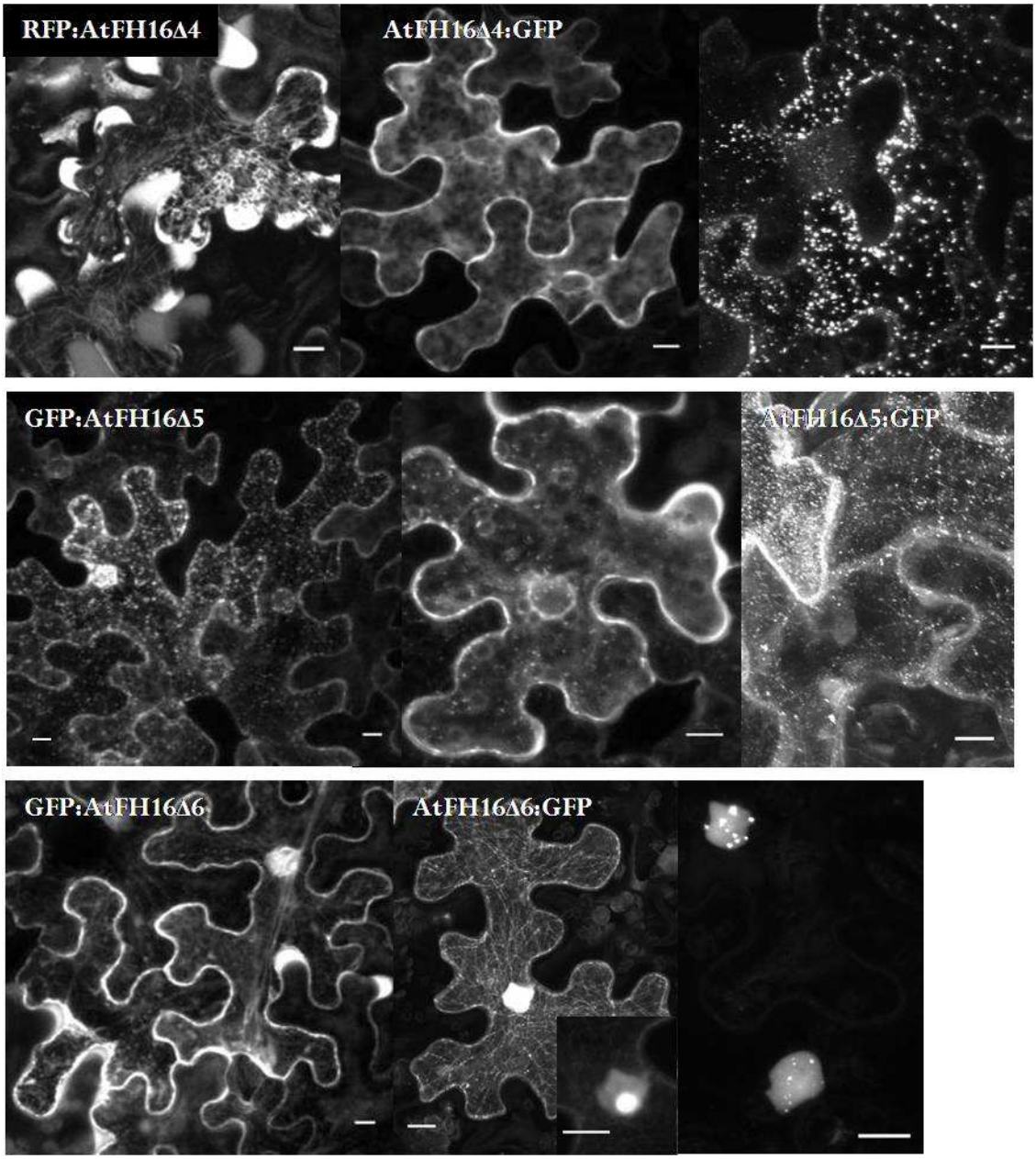

Fig 5.18 (continue) A localization overview of transiently expressed AtFH16 and its subfragments. Both full-lenght AtFH16 protein and its derived truncated variants localize to various cellular structures. Each picture line shows representive localization patterns of one particular subfragment except of GFP:AtFH16Δ1 with mostly uniform localization pattern, which can be seen on Fig. 5.19. Scale bars represent 10 μm.

To determine a character of the filaments decorated by AtFH16, co-localization of the formin together with cytoskeletal fluorescent markers was tested. The full-lenght protein (GFP:AtFH16, AtFH16:GFP), as well as its selected subfragments (GFP:AtFH16Δ1 - done by Matyáš Fendrych, AtFH16Δ3:GFP) were co-infiltrated with dsRED:FABD (a gift from Boris Voigt) containing the actin-binding domain of *Arabidopsis* fimbrin. Both full-lenght AtFH16 and its N-terminal part were able to co-localize in some portion of the cells with dsRED:FABD (Fig. 5.19, 5.20), whereas in case of AtFH16Δ3:GFP, no co-localization was observed (Fig 5.20). Moreover, except of

GFP:AtFH16Δ1, all the other three fusion proteins of AtFH16 often bound to fibrous structures different from the red-labeled actin filaments and sometimes, both types of fibers were labeled by AtFH16 within the single cell (Fig. 5.19, bottom line).

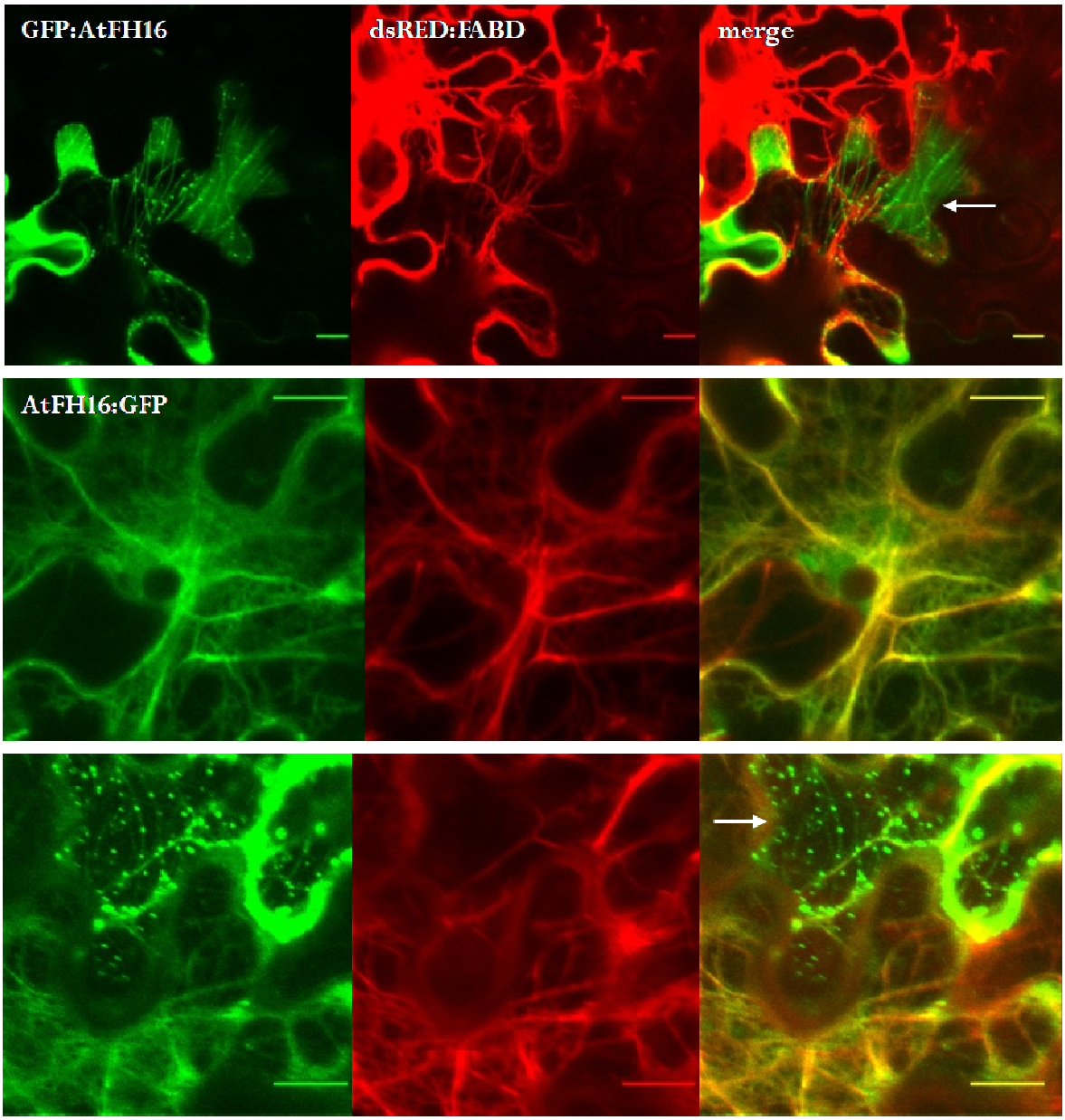

Fig 5.19 Co-localization expriment of AtFH16 with actin. *N.bentamiana* leaves were co-infiltrated with the actin marker dsRED:FABD together with GFP:AtFH16 (upper row of pictures) or AtFH16:GFP (middle and lower rows). Arrows point to filamentous structures that do not co-localize with actin. Scale bars represent 10 μm.

The second type of filaments decorated by AtFH16 resembled the cortical microtubule network. The identity of this filamentous system was tested by the additional co-localization experiments using GFP:TUB6 (a gift fromTakehide Kato) or KMD:RFP (Deeks, Fendrych et al., 2010) as the green or red microtubule marker, respectively. When I co-expressed GFP:AtFH16 together with the microtubule marker KMD:RFP, cellular

distribution of the formin remained unchanged compared to its localization pattern when expressed individually. All the filamentous structures decorated by GFP:AtFH16 fully co-localized with the red signal of KMD:RFP. Similarly, the fibres decorated by the RFP:AtFH16Δ4 subfragment thorougly traced microtubules labeled by GFP:TUB6 (Fig 5.21), which is in contrast to the previous experiments with the actin co-localization that showed at least partial overlap of dsRED:FABD and AtFH16 (GFP:AtFH16, AtFH16:GFP or GFP:AtFH16Δ1) signals.

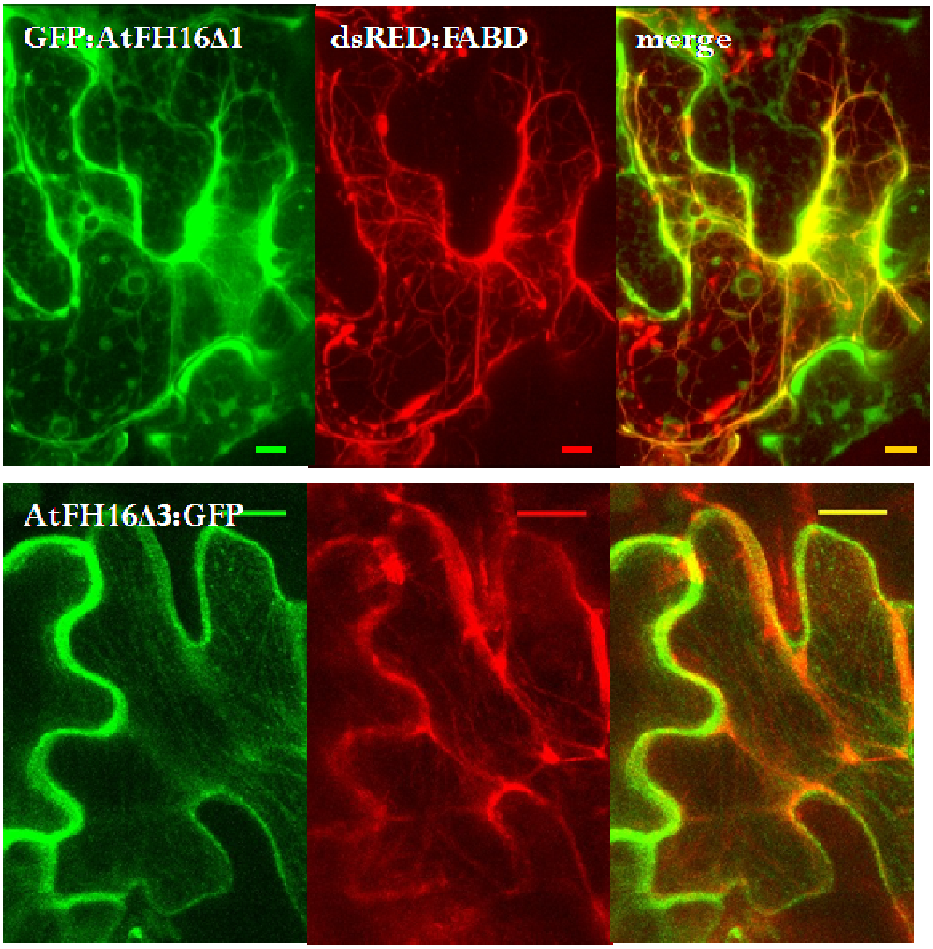

Fig 5.20 Co-localization expriment of selected AtFH16 subfragments with actin. *N.bentamiana* leaves were co-infiltrated with the actin marker dsRED:FABD together with GFP:AtFH16Δ1 (upper row of pictures) or AtFH16Δ3:GFP (lower picture line) subfragment. GFP:AtFH16Δ1 partially co-localizes with the actin signal, whereas filamentous structures labeled by AtFH16Δ3:GFP are distinct from the actin system. Scale bars represent 10 μm.

Concerning the origin of spots or dot-like structures, some of them appeared only in very strongly expressing cells as disorderly moving particles, which I consider to be inclusion bodies, while other, mostly steady dots were arranged on the microtubular strands like the beads on a string. Even the isolated dots that were not connected with any apparent filamentous system copied the trail of microtubules. Bottom line of figure 5.22 shows the co-expression of RFP:AtFH16Δ3 with AtFH4Δ5:GFP (Deeks, Fendrych et al., 2010), the part of Class I formin AtFH4 containing the GOE microtubule-binding domain.

In case of RFP:AtFH16Δ3, the signal is mostly cytosolic and perinuclear with a few spots within, all of them arranged on the apparent strands and fully co-localizing with the similar structures labeled by the AtFH4 subfragment. Analogous to the previous co-expression experiment, no differences of RFP:AtFH16Δ3 distribution were noted compared to its individual expression pattern. The shortest subfragment of AtFH16 exhibiting the localization to the assumed microtubular structures, GFP:AtFH16Δ2 was also co-expressed together with KMD:RFP, and as expected, both fibrous and dot-like structures decorated by GFP:AtFH16Δ2 co-localized with the red-labeled microtubules (Fig 5.22, middle line).

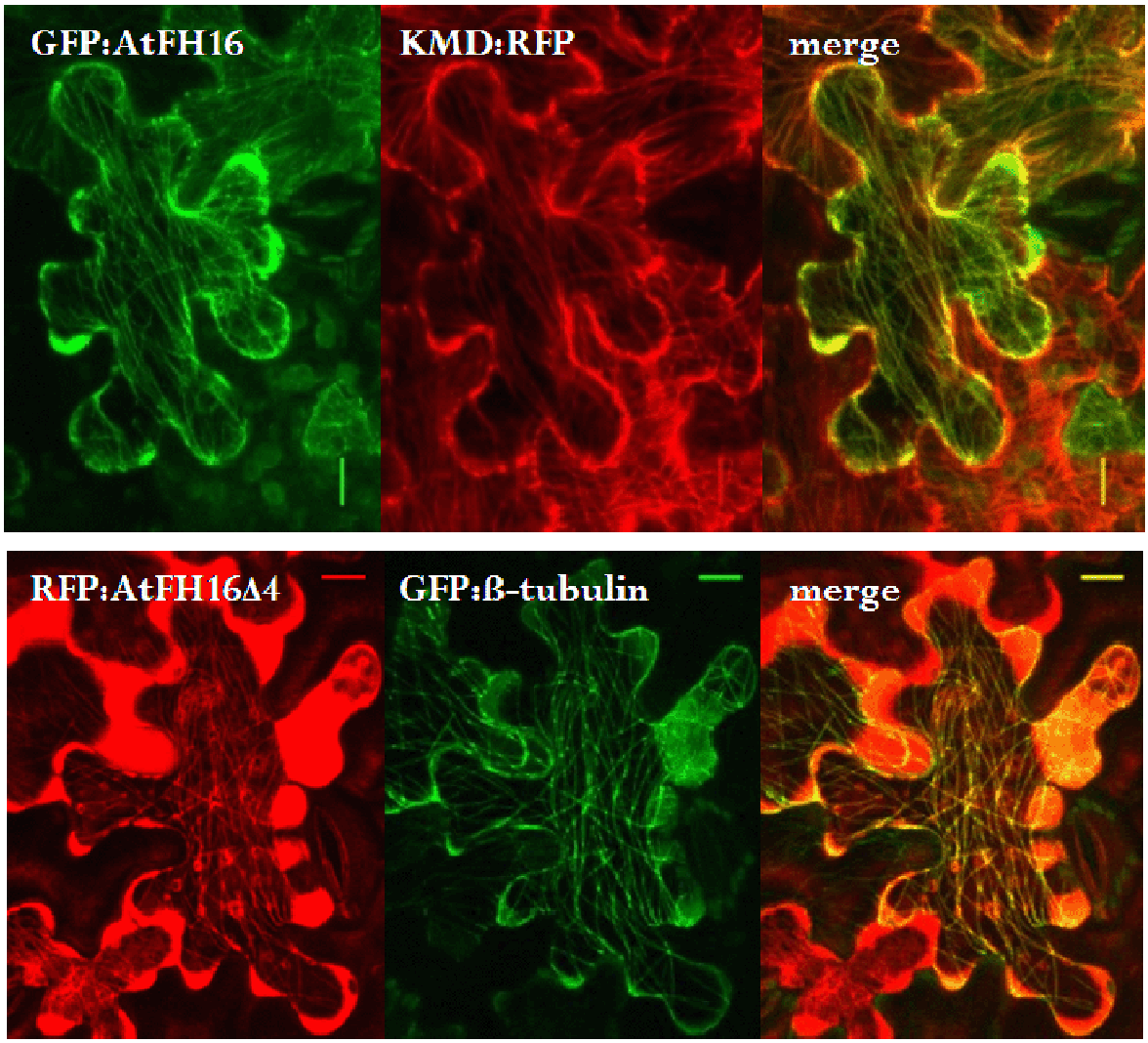

Fig 5.21 AtFH16 decorates microtubular system. *N.bentamiana* leaves were co-infiltrated with the microtubular marker KMD:RFP together with GFP:AtFH16 (upper row of pictures); additionaly, GFP:ß-tubulin (GFP:TUB6) was co-infiltrated with RFP:AtFH16Δ4 (bottom line). All filamentous structures decorated by AtFH16 variants co-localize with labeled microtubules. Scale bars represent 10 μm.

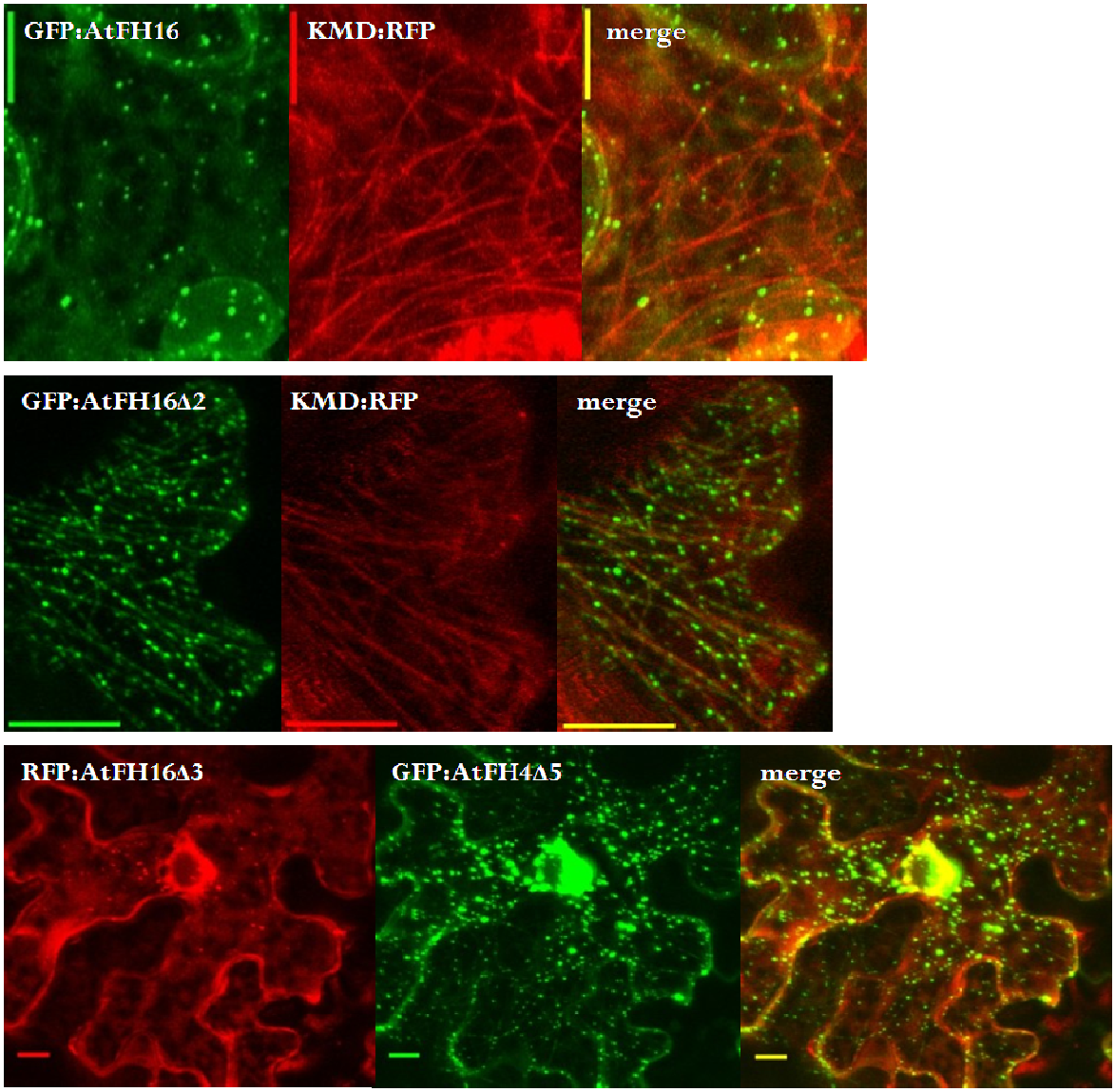

Fig 5.22 Steady punctae labeled by AtFH16 subfragments mostly co-localize with microtubules. A major portion of randomly distributed GFP:AtFH16 punctae resides on the microtubules labeled by KMD:RFP (upper line). Spots labeled by GFP:AtFH16Δ2 subfragment are arranged on tracs that fully co-localize with KMD:RFP (middle line). Emerging punctae of RFP:AtFH16Δ3 were shown to co-localize with similar structures labeled by GOE domain of AtFH4 (GFP:AtFH4Δ5) on pre-existing microtubules (bottom line). Scale bars represent 10 μm.

Taking these data together, AtFH16 and its different truncated variants are able to decorate cytoskeletar filaments *in vivo*. Formin localization on microtubules is mediated by the FH2 domain, whereas the localization on actin seems to be dependent on the N-terminal part of AtFH16 protein and does not require the presence of the conserved FH2 domain. However, this localization might be notably influenced by the presence of dsRED:FABD, as no actin-like structures were observed in the absence of this marker. Probably due to the tetramerization of the dsRED fluorophore (Baird et al., 2000; Heikal et al., 2000), actin filaments form thick bundles upon dsRED:FABD expression and AtFH16 may bind either directly or via other unknown proteins to such stabilized actin structures.

The stabilization effect of dsRED fluorophore was proved by infiltration of 10 μM LatB that induces actin depolymerization into *N. bentamiana* leaves expressing either dsRED:FABD or GFP:FABD (Sheanan et al., 2004), i.e. the same actin-binding domain fused to the different fluorescent markers. While depolymerization of the green-labeled actin filaments was clearly visible after 1 hour of the treatment, almost no fragmentation of the red-labeled actin was apparent after the same period of time and even after the overnight treatment, when some portion of the cells already underwent plasmolysis (not shown). Figure 5.23 shows the effect of LatB treatment on the cells co-expressing both dsRED:FABD and AtFH16:GFP, where the red actin fibres remain almost intact and still enable the binding of AtFH16:GFP, though the formin is also diffusely distributed throughout the cytoplasm.

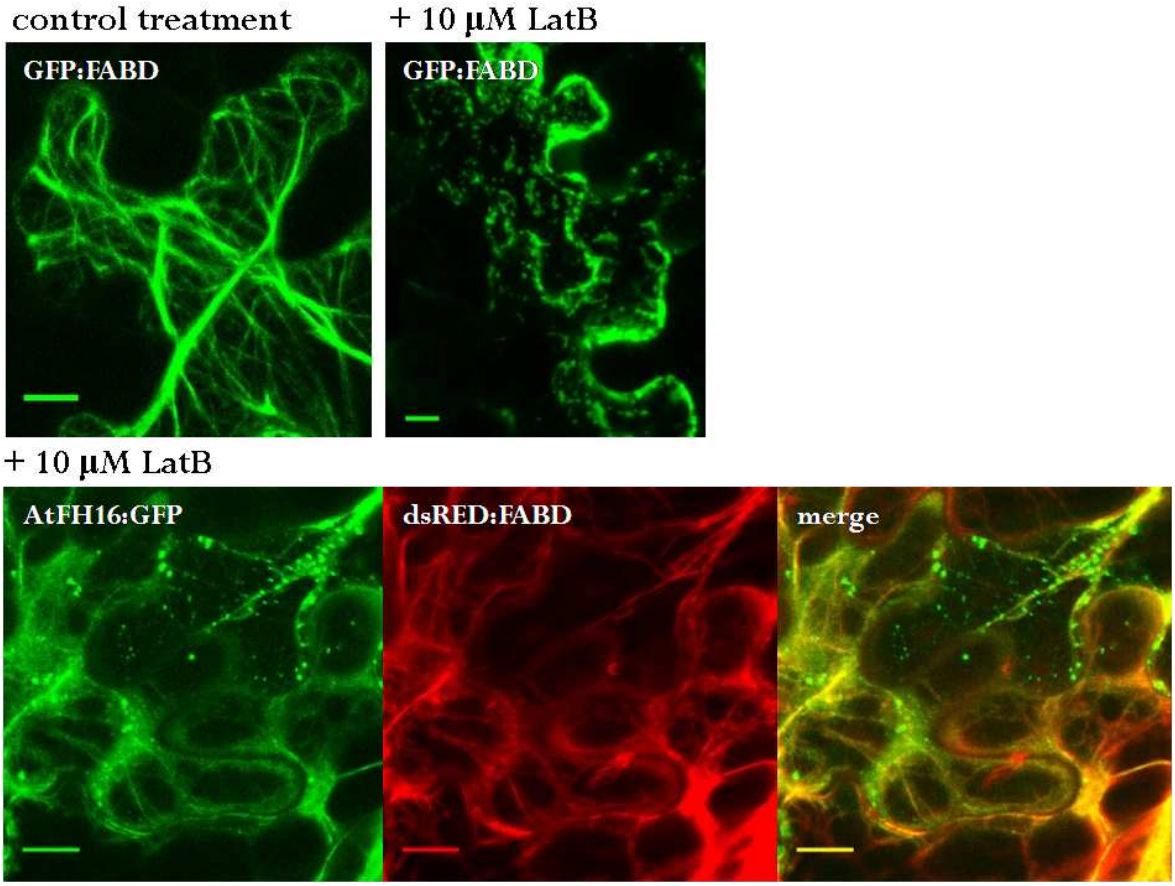

Fig 5.23 dsRED:FABD stabilizes actin network. *N. bentamiana* leaves expressing either GFP:FABD or dsRED:FABD together with AtFH16:GFP were subjected to 10 μM LatB treatment for 2 hours. Actin filaments labeled by GFP:FABD are disruptured compared to the control treatment (upper line), whereas actin system decorated by dsRED:FABD remains nearly unaffected after the same period of time (bottom line). Note the upper-cell lobe, where the AtFH16:GFP-labeled microtubule filaments distinct from actin meshwork and resistant to LatB treatment are formed. Scale bars represent 10 μm.

Moreover, the localization of AtFH16 on microtubules during transient expression in the leaf epidermal cells was commonly observed in case of all AtFH16-derived fusion proteins containing the conserved FH2 domain, except of AtFH16Δ2:GFP that did not

form any filamentous strucutres and was even excluded from the network of cytoplasmic strands. As its N-terminally fused analog labeled both cytoplasm, the ER-like network and microtubules, deletion of the N-terminus of AtFH16 combined with removal of the non-conserved proline-rich region behind the FH2 domain could have unmasked some sequence recognized as the nuclear localization signal.

On the whole, the Class II formin AtFH16 is able to localize to the various cellular structures *in vivo* including the cytoskeletar network. The decoration of actin system by AtFH16 is not commonly observed and when so, it does not require the FH2 domain, whereas microtubules represent the predominant cytoskeletar structures labeled by AtFH16. From the localization experiments with AtFH16-derived subfragments, the minimal region of AtFH16 required for microtubule binding was identified as the FH2 domain itself.

Chapter 6

DISCUSSION

6.1. Discussion of Experimental part I

6.1.1. Low antigenic peptides coupled to KLH produce a lot of KRAP in rat system

Specific antibodies, either polyclonal or monoclonal, are essential tools of modern biology. Besides recombinant proteins or their fragments, synthetic peptides are often used as antigens, taking advantage of almost unlimited quantity of pure and stable peptides, independence of previous cloning of a cDNA or gene encoding the antigen, as well as high specificity of resulting antibodies, which can be used even in cases where the studied organism possesses several mutually similar proteins that would be all recognized by a polyclonal antibody against the whole molecule. Anti-peptide antibodies can also be produced based on predicted protein sequence only, without the need for cDNA cloning. However, anti-peptide antibodies may not recognize the native protein, as the peptide conformation in conjugates used for immunisation may differ from that in native proteins (see e.g. van Regenmortel, 2001).

Choice of the immunogenic peptide is guided by several criteria, e.g. peptide length in the range of at least 7 but preferentially 10-20 amino acids (Welling and Fries, 1985), accessibility on the surface of the molecule (especially if the antisera are to be used for *in situ* immunolocalization) and good solubility, which often represents the limiting factor. However, even insoluble peptides can be coupled to a suitable carrier protein (Lateef et al., 2007). In principle, almost any peptide longer than 7 residues (Welling, 1985) coupled with a suitable carrier or modified by the MAP method (Tam, 1988) can be used for immunization.

To study a role of formins involved in pollen development and pollen tube growth, we attempted to produce antibodies against two KLH-conjugated peptides derived from the sequence of the *Arabidopsis* formin AtFH3. Since the main concerns were to avoid cross-reactivity towards other closely related proteins such as AtFH5, as well as to generate antibodies suitable for immunolocalization, the peptide design was based mainly on the sequence specificity and localization on the surface of the folded protein, using antigenicity only as a secondary criterion. However, a rabbit polyclonal antibody against a peptide of similarly low antigenicity was successfully used by others for detection of a related protein, AtFH1, on western blots (Banno and Chua, 2000). To avoid high non-specific background usually recognized in plant materials by rabbit antibodies that could interfere with the specific signal in immunolocalization studies, rats were chosen as the host animals for antibody protduction. The resulting antisera recognized a protein of the expected size on Western blots, which prompted us to attempt production of antibodies against several other antigens by a similar method. In the meantime, we proceeded to characterize the antigen recognized by the first antiserum.

Surprisingly, the antigen (KRAP75) did not exhibit membrane localization expected for a member of the Class I *Arabidopsis* formin family (Cvrčková et al., 2004) and experimentally documented for several plant Class I formins (Banno and Chua, 2000; Cheung and Wu, 2004; Van Damme et al., 2004; Favery et al., 2004; Deeks et al., 2005; Yi et al., 2005; Ingouff et al., 2005). Instead, antibodies against the GRS peptide recognized an antigen localized in discrete structures within the cytoplasm of tobacco pollen tubes. Identity of these structures, which morphologically resemble elements of the endomembrane system, has not been established but they may deserve further attention. In cell suspensions, the majority of KRAP75 is cytosolic, however we cannot exclude the presence of a minority membrane fraction. Since additional rat polyclonal antibodies against different KLH-peptide conjugates recognized KRAP75 on Western blots, and this signal was removed by depletion of antibodies reacting with KLH, I can conclude that KRAP75 corresponds to an endogenous plant protein cross-reacting with the KLH carrier.

Höglund et al. (2002) described a similar observation, since they found an identical pattern of immunocytochemical staining in *Zinnia* mesophyll cultures with several rabbit antisera against mutually unrelated peptides coupled to KLH. Their KLH-related antigens were present in xylem and vascular cambium, and antibodies against them were efficiently removed by affinity purification on columns with immobilized KLH. However, they provide neither sequences of the peptides used for immunization, nor data on the number and size of cross-reacting antigens that would allow direct comparison with KRAP75 or KRAP90 described in this study. Based on limited sequence similarity with KLH, they suggest that these endogenous antigens may be members of plant tyrosinase or catechol oxidase families. However, *Arabidopsis* has no significant relatives of the tomato tyrosinase (Uniprot: Q08307) suggested (Höglund et al., 2002) as a candidate for the KLH cross-reacting antigen; BLAST (McGinnis and Madden, 2004) E-value is higher than 1 for the best match, a zinc finger-containing protein. Moreover, the predicted tyrosinase size (66 kDa) does not fit our observations. Thus, other epitopes on the KLH molecule are apparently responsible for the cross-reactivity. These may include also carbohydrate determinants that are essential for the immunostimulatory function of KLH; some of them are also known to cross-react with glycoproteins of *Schistosoma mansoni*, a feature utilized successfully in the diagnostics of schistosomiasis (Grzych et al., 1987; Kurokawa et al., 2002; Geyer et al., 2004).

Nevertheless, successful use of polyclonal antisera against KLH-conjugated peptides in plant biology has been reported. In most cases, the antibodies were raised in rabbits and usually affinity purified before use (e.g. Grebe et al., 2000; Griesen et al., 2000; Harris et al., 1999; Qi et al., 2000). However, all but two of the rat antisera against peptide-KLH conjugates detected only KRAP, while no immunity response seemed to be induced by the peptides. Although different criteria have been used when designing the antigenic peptides (selection of soluble and exposed sequences on the surface of a 3D protein model *versus* comprehensive exploration of the whole protein sequence aiming for maximum antigenicity), no major differences in antigen parameters such as solubility, probability of surface exposure, secondary structure or antigenicity determined by a semi-empirical method (Kolaskar and Tongaonkar, 1990) were observed between the failed attempts and the successful ones. The only parameter that differed substantially was, surprisingly, antigenicity predicted according to the older method of Welling et al., (1985). Remarkably, the two discordant methods of antigenicity determination apparently differed by the initial selection of known antigen/antibody pairs used to derive the determining characteristics of good epitopes. Although it was not possible to recover complete information on animal species used for immunization in either case, a species bias cannot be excluded (human,

goat, rabbit, mouse and chicken data were used in the Kolaskar and Tongaokar study). Although antigenicity of particular epitopes is long believed to be species-independent, as far as we was able to establish, no rat immunization studies have been included in the classical papers on this topic (see Atassi, 1984 and references therein), and results of this study indeed suggest that rats might behave differently in this respect than the more conventional hosts for immunization.

Since a systematic failure to produce specific antibodies against a peptide antigen is costly both in terms of money and time, we believe that even negative results such as these should be reported if they could provide insight into possible causes of the failure, as well as hints for others who are considering similar immunizations in the future. Taken together, we do not recommend immunizing rats with KLH-coupled peptides for the purposes of plant experimental biologists; if such an immunization strategy is to be used at all, care should be taken to use a suitable method for selection of highly immunogenic peptides even at the expense of other factors such as position on the molecule.

6.2. Discussion of Experimental part II

6.2.1. The diversity of plant formins

This study provides a closer look on extensive family of *Arabidopsis* formins. Loss of function and overexpression effects of selected family members were examined. In particular, localization of AtFH16, a representative of the not yet experimentally studied Class II formin of type B (lacking PTEN domain), was closely characterized.

Formins, characterized by the presence of the conserved FH2 domain, have been extensively studied mainly in yeast and mammals and their role in the cytoskeleton regulation is now relatively well defined, especially that of actin nucleation and elongation. Recently, many studies have reported detailed evidence suggesting involvement of some formins also in regulation of microtubule dynamics and in actin-microtubule crosstalk in metazoans (e.g. Bartolini et al., 2008; Goulimari et al., 2008) and also in plants (Deeks and Fendrych et al., 2010). Such a connection could have been long expected, as some previous studies indicated such a possibility (Emmons et al., 1995; Lee et al., 1999; Palazzo et al., 2001).

Plant formins became a focus of attention later compared to yeast and animal ones, though the first reference showing the presence of FH2-containing proteins in plants was brought by Castrillon and Wasserman, who revealed the presence of FH2 domain in a rice EST already in 1994. Cloning of the first plant formin, AFH1 (now AtFH1) and discovery that plant formins form a large family followed several years later (Banno and Chua 2000, Cvrčková 2000; Deeks et al., 2002). All but one experimental studies dedicated to plant formins refer to *Arabidopsis* Class I members and describe primarily their function in actin nucleation and organization (Cheung and Wu, 2004; Favery et al., 2004; Deeks and Cvrčková et al., 2005; Ingouff et al., 2005; Michelot et al., 2005; Yi et al., 2005; Michelot et al., 2006; Ye and Zheng et al., 2009); the only exception is focused on a comparison of members of Class I, Class II and Class III formin families in the moss *Physcomitrella* (Vidali et al., 2009).

Similarly, non-plant formins were originally studied mostly on the model of diaphanous-related formins (DRFs), which resulted in a kind of „cramped“ view on the function and regulation generalized for the whole formin family. It took several years to not only appreciate the rich diversity of domain organization encountered among formins (e.g. Higgs and Peterson, 2005; Rivero et al., 2005; Grunt et al., 2008), but also to accept the relevance and importance of formin groups other than DRFs (e.g. compare the reviews by Good and Eck, 2007 and Chesarone et al., 2010; especially the chapters about regulation of formin function). Our laboratory has significantly contributed to the description of the evolutionary diversity of formins, especially plant ones, including original description of the transmembrane segment as a common feature of plant Class I formins (Cvrčková 2000), as well as the discovery of the PTEN-like domain in Class II formins (Cvrčková et al., 2004; Appendix 1) and the RhoGAP-like domain characteristic of Class III formins, which are absent in angiosperms (Grunt et al., 2008).

6.2.2. Functional redundancy among *Arabidopsis* formins

According to publicly available data, *Arabidopsis* formins differ greatly in their expression pattern, ranging from overally highly expressed genes (*AtFH1*), through specifically expressed members (*AtFH3* expressed specifically in pollen, *AtFH12* upregulated predominantly under salt stress). To study loss of function effects, we applied a reverse genetic approach, using mutants available from public collections (Sessions et al., 2002; Alonso et al., 2003).

As a whole, we collected 22 insertional mutants in 18 formin genes (mutants were not available in loci *AtFH9* and *AtFH21*), from which we selected and characterized following 17 homozygotes: *atfh1, atfh2, atfh3, atfh3-2, atfh4, atfh5, atfh5-2, atfh6, atfh7, atfh8, atfh10, atfh12, atfh13, atfh14, atfh15b, atfh16, atfh16-2* and *atfh18*. Plants homozygous in *atfh17* are going to be selected, heterozygous mutants are available now. Mutants *atfh11, atfh15a* and *atfh20* were not successfully verified by genotyping, so they were omitted from further studies. The absence of PCR product in the selection-resistant plants could raised either from rearrangements of T-DNA flanking sequences that occur with quite a high frequency (Tax and Vernon, 2001) and abolish annealing of the genotyping primers or from incorrect material sent by Garlic, as the propagation of seeds from the SAIL library (Sessions et al., 2002) was maintained by the database users and no additional control of seeds identity or quality was implemented.

Under standard laboratory conditions, all but one single mutant (*atfh16*, discussed below) did not phenotypically differ from WT plants. So far, only one plant study has reported about loss of function phenotype in case of single formin mutant. Impairment of *AtFH5* from *Arabidopsis* leads to discrepancy of endosperm cellularization, however, these are just temporary and during the later phases of embryo development, *atfh5* mutants resemble WT and complete seed maturation successfully; the phenotype was only discovered based on a detailed screen for endosperm formation impaired mutants (Ingouff et al., 2005). Although we have not tested any additional stress conditions that might reveal otherwise concealed mutant phenotypes in case of specifically expressed formins, the lack of any obvious mutant phenotype especially in case of highly expressed genes indicates the redundancy and functional overlap of *Arabidopsis* formins.

6.2.3. Pollen-specific Class I formins are not necessary for pollen tube growth

At the beginning, we focused on the role of plant formins in one of the most promising fields, the polarized cell growth. In this process, a dynamic turnover of actin filaments occurs and several yeast and animal formins were shown to play a crucial role in polarity estabilishment (e.g. Feierbach and Chang, 2001; Sagot and Klee et al., 2002). As a suitable plant model system, apically growing cells such as pollen tubes or root hairs are commonly used for the polarity studies. The *Arabidopsis* expression data available at Genevestigator (https://www.genevestigator.ethz.ch/; Zimmerman et al., 2004; Hruz et al., 2008) indicate that mRNAs of only two Class I formins, *AtFH3* and *AtFH5*, are strongly accumulated in mature pollen and during pollen tube growth (Honys and Twell, 2003; Pina et al., 2005), whereas a more uniform expression pattern can be observed in case of root hairs. For this reason, and also because of the haploid character of the male gametophyte, we gave priority to a pollen tube model. We selected homozygous insertional mutants in both predominantly expressed Class I genes (*AtFH3* and *AtFH5*, 2 independent lines for each of them), however, neither *atfh3* nor *atfh5* homozygotes exhibited any discrepancies in the pollen tube growth process. (Aberrations of microspore development observed on the background of mutation in *AtFH3* turned out not to correlate with the presence of mutated allele; thus, and after the brief characterization reported in chapter 4, it was not further studied with respect to formins).

To overcome a possible functional overlap, a double mutant *atfh3atfh5* was created. Even in this case, no abnormalities of pollen tube growth rate or architecture were detected. *AtFH7* is the last Class I formin with a significant expression in mature pollen and though its mRNA levels are much lower than that of *AtFH3* or *AtFH5*, its function can be still sufficient for proper progression of pollen tube growth. Therefore, selection of a triple mutant *atfh3atfh5atfh7* is now in progress. Interestingly, promoter of *AtFH1* can also function in germinating pollen, as proved by transformation of tobacco pollen (Cheung and Wu, 2004) and despite the fact that *AtFH1* transcript is not present in mature *Arabidopsis* pollen (only in bicellular microspores according to Honys et al., 2003), its involvement during germination processes cannot be excluded. Since some activity of the remaining Class I formins after the *AtFH3* and *AtFH5* knock-out can be expected, the second approach, a directed inhibition of the whole Class I group mediated by antisense oligopeptides (Moutinho et al., 2001) was tested in tobacco pollen. Three oligopeptide pairs derived from conserved regions of *AtFH3*, *AtFH5* and theirs *Solanaceae* homologues were delivered during *in vitro* germination into tobacco pollen and similarly to the observations from *Arabidopsis* mutants, no differences between antisense and control treatments with respect to pollen tube lenght and polarity were detected.

These results were quite unexpected, as the dynamics of both longitudinal actin cables and short filaments in apical growth in plants are believed to be regulated by formins (reviewed e.g. by Cheung and Wu, 2008). Overexpression of Class I formins that causes severing of actin system in tip growing cells accompanied by growth arrest, tip swelling or membrane deformations were repeatedly documented (Cheung and Wu, 2004; Deeks and Cvrčková et al., 2005; Yi et al., 2005; Ye and Zheng et al., 2009), whereas downregulation effects have not been reported until quite recently. Silencing of all formins was tested in the moss *Physcomitrella patens*, which contains only 9 formin genes classified into three classes. Plants lacking Class II members had affected polarized growth and failed to elongate their cells, however, the phenotype was not lethal. Surprisingly,

silencing of all formin genes belonging to the remaining groups, Class I and Class III, resulted only in mild phenotypical changes; smaller plants with no disruption of pollarized cell growth (Vidali et al., 2009).

On the contrary, Ye with Zheng and colleagues (2009) very recentrly reported effects of specific silencing of *AtFH3* by RNAi in *Arabidopsis* plants and observed a loss of actin cables in the shank of pollen tubes grown *in vitro*, together with a significant inhibition of pollen tube growth and increase of tube width, even though low levels of *AtFH3* transcript were still present in the RNAi lines. They also proved that no additional formins, such as *AtFH1*, *AtFH5* (Class I formins) or *AtFH13* (a Class II member) were targeted by their RNAi. It is somewhat curious that the same phenotype (shorter and broader tubes) was also induced by transient overexpression of two truncated versions of AtFH3, which otherwise enhanced the formation of actin cables that reached to the very tip as showed by co-transformation with the actin marker GFP-fABD2. However, the marker itself could have been a contributing factor, as expression of fimbrin-based actin markers is not free of phenotypic consequences (Hofmann et al., 2009). Both the AtFH3 fragments tested contained an incomplete FH2 domain and even though high levels of such protein can somehow interfere with the growth process - a similar truncated version of AtFH8 was shown to cause growth arrest of root hairs under ectopic expression (Deeks and Cvrčková et al., 2005), I would be cautious to interpret the extensive changes of actin cytoskeleton as the direct consequence of a FH2 domain-truncated formin.

Although we observed occassional pollen tubes with affected polarization resembling those from *AtFH3* RNAi plants in our insertional mutants containing disrupted *AtFH3*, the majority of *in vitro* germinated pollen grew normally. Since we examined our pollen tubes 5h after the germination onset or later, compared to 3h in case of the RNAi plants reported by Ye et al., it is possible that we had missed some critical period of the elongation process when the effect of *AtFH3* loss is apparent, though it does not seem very likely. Furthermore, we did not evaluate the mRNA content of either *AtFH3* nor *AtFH5* in the pollen of our mutants, so that the knock-out of both formins is only presumptive, yet not confirmed. Nevertheless, the data presented by Ye, Zheng and colleagues (2009) are at least partially in contradiction with our observation, as well as with the study by Vidali et al., (2009), while the moss example is consistent with our data and supports the hypothesis that the action of Class I formins may not be essential for apical growth of pollen tubes. In any case, our results confirm that plant formins are highly redundant in their function, as expected for such a large gene family.

6.2.4. Class II formin AtFH16 may be involved in some aspects of cell expansion in *Arabidopsis* seedlings

The large number of *Arabidopsis* formin genes together with a lack of any dramatic single mutation phenotype suggests that particular formins might either control discrete developmental stages or they can function in specific stress responses. Besides the pollen expressed genes, we also focused on a Class II formin *AtFH16*, which has quite an unusual structure compared to other subgroup members (Cvrčková et al., 2004). Under standard conditions, *AtFH16* expression based on microarray data is rather low and can be detected in both aboveground organs and roots. Higher expression occurs in adult leaves and in roots, where in the later case, *AtFH16* is predominantly expressed in elongation zone and in root hairs (the strongest expression among Class II formins). Furthermore, *AtFH16*

upregulation was detected during induced programme cell death (PCD) in cell suspension (prevailing Class II formin) and its additional involvement in senescence- and defense-related processes is also indicated by the consistently increased expression on the mutant backgrounds that exhibit accelerated senescence and/or constitutive defense response. During the microarray database search, we found only one situation, in which *AtFH16* expression considerably prevails among all other Class II formins, namely the rapid elongation phase of dark-grown (etiolated) hypocotyls. Interestingly, the most abundant transcript levels during this process belong to *AtFH7*, the only *Arabidopsis* formin sharing the similar domain architecture with *AtFH16*. Furthermore, *AtFH7* is strongly expressed during induced PCD as well, similarly as *AtFH16*.

With respect to the senescence, natural developmental course including cotyledon and leaf senescence was monitored in *atfh16* mutants grown under standard conditions. Neither the onset nor the progression of senescence in *atfh16* differed from the control plants. Such a finding was not surprising, as many formins, especially from the Class I group, are upregulated during natural senescence and *AtFH16* loss might be compensated by action of other formin genes such as *AtFH7* or *AtFH20*.

In agreement with the expression analysis, homozygous seedlings of the knock-out mutant *atfh16* have slightly affected growth of primary roots, which are less skewed, though no differences were surprisingly detected in case of root hairs. Moreover, shortening and waving of hypocotyls was detected in dark-grown mutants, indicating that at least some phases of growth, especially the rapid elongation of etiolated hypocotyls, are AtFH16-dependent.

Several hormones are known to influence skotomorphogenesis of *Arabidopsis* dark-grown seedlings, and some of them are responsible for hypocotyl growth reduction. Thus, a possible connection between AtFH16 function and selected hormone pathways, especially with those regulating also senescence, stress and defense-related processes was tested. A well-known effect of ethylene or its precursor 1-aminocyclopropane-1-carboxylate (ACC) on dark-grown plants is the so-called "triple response" characterized by the inhibition of hypocotyl and root cell elongation, radial swelling of the hypocotyl, and exaggerated curvature of the apical hook (Guzman and Ecker, 1990; Guo and Ecker, 2004; Lin et al., 2009). Dark-grown hypocotyl elongation was shown to be affected by a reduction of gibberellic acid (GA) levels (Cowling and Harberd, 1999) and GA also modulates ethylene response and its absence, impairs formation of the apical hook (Vriezen et al., 2004). ABA is a plant growth inhibitor and its supression effect on light-grown hypocotyls is well described (Ray et al., 1980; Chen et al., 2008; Miura et al., 2010), while less is known about ABA action during dark growth. A partially de-etiolated phenotype with reduced hypocotyl growth and emergence of true leaves can be observed in abscisic acid (ABA)-deficient mutants, though aplication of exogenous ABA cannot restore WT phenotype. Impairment of carotenoid biosynthesis is probably responsible for the observed skotomorphogenic deffects (Barrero and Rodríguez et al., 2008).

ACC treatment of *atfh16* and WT dark-grown seedlings reduced the overall growth especially of roots, as expected, while ABA caused major increase in variability in the elongation of hypocotyls, where the lengths were ranging from normally elongated to absolutely supressed ones. Similar effect as ACC was caused by methyl jasmonate (MeJA), a functional analogue of jasmonic acid (JA), while the aplication of salicylic acid (SA) resulted in root shortening accompanied by enhancement of hypocotyl elongation. In summary, neither of the hormones supplemented in the growing medium enhanced any differences between *atfh16* and WT plants already observed on the control medium,

although the treatments notably affected growth of all etiolated seedlings. Nevertheless, to decide wheather *AtFH16* impairment interferes with some hormonal signaling in skotomorphogenesis, effects of additional hormones involved in etiolated hypocotyl elongation, such as auxin, GA and brassinosteroids (Vandenbussche et al., 2005) should be tested.

All the hormones used in the etiolation study were also tested on primary root growth of the light-grown seedlings and similar effects were observed, which means that the treatments caused expectable changes in the root morphology, but the differences between *atfh16* and WT plants remained comparable to the control medium. In particular, ACC and MeJA had an obvious growth inhibitory effect, while ABA aplication slightly enhanced root elongation, a known ABA effect in water deficit conditions (Pilet, 1998). SA treated roots reached the lenght of untreated ones, while their skewing was slightly shifted rightwards. It would be interesting to test the further effect of lower ACC concentrations, as the dose used in this study turned out to suppress root elongation quite markedly and possible modulations of root waving intensity caused by ethylene (Buer et al., 2003) could not be examined. Also additional treatment with low concentration of auxin might be useful.

Despite *AtFH16* being upregulated in root hairs and its mutational loss might thus be expected to produce observable phenotypic effects, no abnormalities in root hair growth occur in *atfh16* mutant under standard conditions. Ethylene is known to accelerate elongation of root hairs and its signaling is modulated by sucrose (Gazzarrini and McCourt, 2001; Gibson, 2004). Higher sucrose levels prevent the formation of root hairs in *exo70A1,* a polarity and tip growth defective mutant with impaired function of the Exocyst complex subunit, while ACC rescues sucrose-induced phenotype (Synek et al., 2006). Neither the addition of ACC, nor elevated sucrose levels influenced polarized growth of root hairs in *atfh16*, showing that polarity of this specialized cell type might be maintained by other formins. Several Class I formins are expressed in root hairs including *AtFH8*, which is known to influence position and phenotype of root hairs when overexpressed (Yi et al., 2005; Deeks and Cvrčková et al., 2005). However, the knock-out of dominant Class I formins do not lead to polarity changes of the similar cell type, the tip-growing pollen tubes, as discussed above. Also polarity of moss cells is not affected by the loss of all Class I members, while function of Class II formins with PTEN-domain is essential for polarity establishment (Vidali et al., 2009). Indeed, besides *AtFH16*, two PTEN-containing formins *AtFH13* and *AtFH14* are strongly expressed in root hairs, suggesting that Class II formins with PTEN-domain might be important for the cell polarity regulation also in *Arabidopsis*.

Apart from hormonal signaling, elongation of plant organs is dependent on the cytoskeleton system. Rapidly expanding cells in the roots and the etiolated hypocotyls possess arrays of cortical microtubules that are arranged largely perpendicular to the cell's long axis (Sugimoto et al., 2000). In mutants with disrupted microtubule organization, elongating cells skew consistently either to the right or to the left resulting in a helical growth of plant organs (Thitamadee et al., 2002; Ishida et al., 2007). The only significant difference observed in *atfh16* light-grown seedlings was the angle, i.e. skewing (bending) of primary roots, a very mild phenotype compared to microtubule-affecting mutants. Pronounced skewing angles of roots can be also evoked by microtubule-affecting compounds (Oliva and Dunand, 2007). Roots of *atfh16* turned out to have increased sensitivity to low doses of microtubule drugs; microtubule-stabilizing taxol emphasized the differences in skewing and moreover, it induced increased root waving intensity. Consistently, more intensive waving of mutant roots was also detected on hard agar-containing half-MS plates angled at 45°, which was reported to highlight differences in

root growth of microtubule-associated mutants (Ishida et al., 2007; Sedbrook and Kaloriti, 2008). APM, a microtubule-depolymerizing drug, influenced mainly root lenght and waving parameters. At higher concentration, WT plants partially mimicked the *atfh16* phenotype. *Arabidopsis lefty* mutants containing dominant negative mutations of α-tubulins are more sensitive to propyzamide, which has similar effect as APM and causes shortening of primary roots in mutants (Thitamadee et al., 2002) and *spiral2* mutants lacking a microtubule-associated protein exhibit increased sensitivity to taxol, which is manifested as enhanced left-handed bending and reduced root growth (Furutani et al., 2000). On the contrary, *mpk18* seedlings, which have moderately stabilized microtubules, respond more sensitively in the root skewing to microtubule-destabilizing drugs, whereas they are more resistant to taxol (Walia et al., 2009).

Growth of *atfh16* etiolated hypocotyls turned out to be modified by taxol and APM analogously to the light-grown roots, i.e. mutant plants showed enhanced hypocotyl waving and shortening after the taxol treatment in a concentration dependent manner, while APM disguised the differences between *atfh16* and WT, partially because WT hypocotyls became shorter and wavier just like the mutant ones. Similarly, taxol pronounced shortening of etiolated hypocotyls in *lefty* mutants (Thitamadee et al., 2002). Generally, growth of *atfh16* seedlings is affected only in the organs with accelerated elongation and the experiments with microtubule-affecting drugs further suggest that microtubule system can be slightly destabilized in these parts as a result of *AtFH16* mutation. As discussed below, also localization experiments indicate a possible involvement of AtFH16 in regulation of microtubule dynamics, as AtFH16 is able to bind microtubules *in vivo*.

To test consequences of AtFH16 loss on actin cytoskeleton, both light- and dark-grown seedlings were treated by latrunculin B (LatB), which effectively depolymerizes actin filaments. F-actin is essential for the plant directed cell expansion and thus for organ elongation (Baluška et al., 2001) and FH2 proteins are proposed to be activly involved in elongation processes primarily through nucleation and elongation of actin filaments (Hussey et al., 2006). Indeed, the elongation of both light-grown roots and etiolated hypocotyls in *atfh16* mutants turned out to be hypersensitive to LatB treatment. Even the low concentration of LatB caused dramatic changes in the overall phenotype of dark-grown seedlings with the oustanding inhibition of hypocotyl elongation, as well as the root growth of the light-grown mutants was strongly affected. Besides experiments with cytoskeleton-disrupting drugs, genetic studies in *Arabidopsis* support a role for microfilaments in controlled cell expansion as well. The *act2-2D* mutant has shorter microfilament bundles in root epidermal cells and shows reduced cell elongation and defects in the radial expansion of trichoblasts (Nishimura et al., 2003). Reduced root growth accompanied by increased root twisting occurs in plants having mutation in *ACT7* gene (Gilliland et al., 2003). Etiolated seedlings underexpressing the actin-binding protein profilin display an overall dwarf phenotype with short, though not wavy, hypocotyls (Ramachandran et al., 2000), while formation of short and wavy etiolated hypocotyls together with reduced growth of light-grown seedlings can be induced by overexpression of the actin-depolymerizing factor *ADF* (Dong et al., 2001), which severs actin filaments and increases the depolymerization from the pointed ends (Carlier et al., 1997).

Aplication of cytoskeletal drugs thus indicates that AtFH16 could be implicated in the cross-talk between microfilaments and microtubules during elongation phases of growth. Interestingly, phenotypic variations analogous to *atfh16* were detected using actin-affecting drugs in case of a termosensitive mutant *mor1*, which has swollen organs, disrupted cortical microtubules (Whittington et al., 2001) and phragmoplast (Eleftheriou et

al., 2005) due to loss of an evolutionarily conserved microtubule-associated protein (MAP125). Root expansion of *mor1* is hypersensitive to the microfilament-disrupting drugs including LatB and moreover, even low doses of LatB exacerbate disruption of cortical microtubules. Similar effect can be induced by LatB also in *spiral1* mutants. Though organ elongation is not primarily altered in these mutants, LatB aplication generally enhances their microtubule-associated phenotypes (Collings et al., 2006).

Function of AtFH16 in the control of anisotropic cell expansion in rapidly elongating organs such as roots and etiolated hypocotyls could be complementary to Arp2/3 complex action. *Arabidopsis* mutants in Arp2/3 complex, the only plant actin nucleation factor known so far besides formins, show mainly defects in growth and differentiation of trichomes and leaf pavement cells, and sometimes of root hair growth under certain conditions, but the essential processes needed for the successful completion of life cycle and reproduction remain unaffected. Thus, unlike in other eukaryotes, the *Arabidopsis* Arp2/3 complex is not essential for life (reviewed in e.g. Mathur, 2005; Hussey et al., 2006). With respect to rapid organ elongation, slightly moderated parameters were detected in light-grown hypocotyls of *arp2* and *arp3* (Le et al., 2003). Impairment of the *Arabidopsis* Arp2/3 regulator NAP125 encoded by *GNARLED* (El-Assal Sel et al., 2004) causes the same phenotype as observed in *arp2/3* mutants and the examination of etiolated hypocotyls revealed a presence of epidermal cells with aberrant shape, but no reduction of hypocotyl elongation (Zimmermann et al., 2004b). Recently, a thorough analysis of Arp2/3-related mutants revealed growth reduction of primary roots, which is comparable to *atfh16* mutants grown in the presence of LatB (Dyachok et al., 2008). As the disruption of trichome actin system in Arp2/3-related mutants is accompanied by aberrant organization of cortical microtubules (Schwab et al., 2003; Zhang et al., 2005), analogous situation may be expected in roots, where AtFH16 implication in microtubule regulation is also suggested.

Nevertheless, observations on *atfh16* mutant yet need to be verified by additional independent experiments. Though the phenotype described above is bound exclusively to the disruption of the *AtFH16* locus, another allele *atfh16-2* does not seem to have similar phenoytpic alterations (tested on half-MS and 0.1 μM LatB). *atfh16-2* contains T-DNA insertion closer to the C-terminus compared to *atfh16* and the presence of mRNA has not been tested yet. The most convenient verification of the connection between a mutant phenotype and a disrupted locus can be made by complementation of the mutant. Unfortunately, AtFH16 GFP-fusion variants expressed under the 35S promoter are strongly silenced in *Arabidopsis* aboveground organs including etiolated hypocotyls. In roots, GFP-fusion proteins show only mosaic expression, where they localize into ER and cytoplasm-like structures and undergo early degradation. Thus, such plants are not suitable for complementation assay and at least expression of *AtFH16* regulated by its native promoter shall be further tested.

6.2.5. AtFH16 binds microtubules through its FH2 domain *in vivo*

In vivo subcellular localization of plant formins has been examined mostly on Class I *Arabidopsis* proteins, which were found to associate with membraneous structures, predominantly with the plasmatic membrane of various cell types (Cheung and Wu, 2004; Favery and Chelysheva et al., 2004; Van Damme et al., 2004; Deeks and Cvrčková et al., 2005) or with the cell plate in dividing root cells (Ingouff and Gerald et al., 2005).

Recently, transiently expressed AtFH4 was shown to associate simultaneously with both ER and microtubular systems (Deeks and Fendrych et al., 2010) and PTEN-containing Class II moss formins are localized into the apical membrane of growing cells (Vidali et al., 2009). Unlike those, AtFH16 lacks any known elements that could possibly mediate the association with membranes, so that its subcellular localization was predicted as cytoplasmic (Cvrčková et al., 2004). Indeed, GFP:AtFH16 or AtFH16:GFP transiently expressed in *N. bentamiana* leaves reside mostly in the cell cytoplasm, but moreover, AtFH16 often labels also two populations of spots (unidirectionally moving ones, probably inclusion bodies vs. nearly immobile dots), as well as cytoskeletal structures, which were identified in co-localization experiments predominantly as microtubules, rarely as actin filaments and cables.

Localization of yeast and animal formins into puctate structures *in vivo* is dependent on the FH2 domain and coheres with the processive capping of actin filaments. Continuous movement of formin speckles is usually directed towards the cell periphery and copies the elongating barbed ends of actin filaments (e.g. Higashida et al., 2004; Martin and Chang, 2006; Buttery et al., 2007; Bartolini et al., 2008). To test a contribution of particular regions to the subcellular localization, AtFH16 was subcloned into six additional fragments. Though the formation of AtFH16 dots occurred only in case of FH2-containing subfragments, no directional movement was detected and instead, persistent association of a portion of dots with microtubules was observed. When AtFH16Δ3 was co-expressed with the isolated microtubule-binding GOE region of AtFH4 (Deeks and Fendrych et al., 2010), even the randomly distributed dots turned out to completely co-localize on microtubular tracks with the similar strucures labeled by GOE. This suggests that the dots probably result from hyperaccumulation of the overexpressed proteins rather than from FH2-mediated formin activity, though a preferential recruitment of formins into microtubular regions via some specific activity cannot be excluded.

In vivo association of animal formins with filamentous actin strucures has been also reported. Diaphanous-related formin FHOD1 associates with bundled actin stress fibers and what's more, it co-alignes them with microtubules. Parallel organization of both cytoskeletal structures was shown to influence cell elongation without affecting cytokinesis (Gasteier et al., 2005). *Arabidopsis* AtFH1 decorates actin filaments *in vitro* as a result of its non-processive capping activity, when after the elongation step, AtFH1 slides at the side of the elongating filament and remains associated with it through the FH2 domain. Bound at the side, AtFH1 can further organize actin filaments into bundles (Michelot and Guérin and Huang et al., 2005; Michelot et al., 2006). We showed that AtFH16 binds only actin bundles stabilized by dsRED:FABD and upon co-expressuion of AtFH16-labeled actin together with microtubule markers within one cell, no significant co-alignment of both structures was observed. This could suggest that AtFH16 might preferentially associate with stabilized actin bundles through FH2 domain-mediated binding and/or dimerization with AtFH1-like endogenous formin(s). However, the localization of AtFH16 subfragments revealed that not the FH2 domain, but the N-terminal region of the protein including the FH1 domain is responsible for actin filament binding. Interestingly, ForC from *Dictyostelium discoideum,* which lacks the FH1 domain, specifically localizes at the crowns (macropinocytotic structures rich in filamentous actin) and this localization depends on the N-terminally located FH3 region, not the FH2 domain (Kitayama and Uyeda, 2003). Thus, it is possible that even the very N-terminus of AtFH16 without the FH1 domain might mediate association with bundled actin and it would be useful to examine such additional N-terminal subfragments.

As mentioned above, the majority of filamentous structures or immobile dots labeled by AtFH16 co-localized with microtubules. Four animal formins and one plant formin have been reported so far to decorate microtubular tracks. Overexpressed mDia1 and mDia2 can associate with microtubules *in vitro* (Palazzo et al., 2001) and mDia2 generates and associates with stabilized microtubules also *in vivo*, where the binding is mediated by the FH2 domain independently of its actin nucleation activity (Bartolini et al., 2008). Similarly, *Drosophila* formin Cappuccino interacts with microtubules through FH2 domain and is capable of microtubule-actin cross-linking (Rosales-Nieves et al., 2006). On the contrary, Fmn1 localization on cortical microtubules is mediated by N-terminally located peptide sequence encoded by exon-2 (Zhou et al., 2006) and the analogously located, though sequentially different fragment GOE provides formin-microtubule association of AtFH4 (Deeks and Fendrych et al., 2010). Human inverted formin INF1 induces formation of bundled, acetylated microtubules and binds them through the unique C-terminal region, within which two microtubule-binding sites were identified (Young et al., 2008). The three last formins mentioned above show microtubule-binding as a predominant *in vivo* localization pattern. All of them can also conventionally nucleate actin filaments via FH2 domains, which suggests a potential to cross-link both cytoskeletal systems in case of even such structurally and evolutionary different formins. With respect to microtubule-binding region, AtFH16 resembles mDia proteins and Cappuccino, as the binding activity was shown to be provided by FH2 domain present in AtFH16Δ2 subfragment.

Nevertheless, it remains unclear whether the AtFH16 association with microtubules is direct or indirect, and additional experiments are needed to be done. Unlike AtFH4 variants expressed in parallel during the same localization experiments, AtFH16 does not always decorate microtubular system. Instead, the localization seems to depend on some inner response of the transformed cells, as the microtubule decoration can be even absent. However, when it starts to occur (usually in a form of isolated dots), the majority of the AtFH16-expressing cells subsequently contains labeled microtubular structures. Such behaviour may suggest that AtFH16 could bind microtubules directly, but only some specific sub-population, e.g. stabilized microtubule bundles. As another possibility, an activation of AtFH16 from its potentially inhibited state (maintained either by autoinhibition or by an interactor) might promote the microtubule binding. Preliminary experiments (done by Tamara Pečenková, personal communication) with AtFH16 C-terminally tagged to split-YFP, a fluorescent tag used for *in vivo* detection of protein-protein interactions (Walter et al., 2004) surprisingly repeatedly revealed no interaction between AtFH16 molecules. Though these results need further elaboration, they suggest that C-terminus of AtFH16 protein may be important for the putative dimerization event. As AtFH16 fused C-terminally to GFP labels microtubules the same way as the N-terminally fused one, it is possible that molecule dimerization is not necessarily needed for AtFH16-microtubule association. This finding also makes less probable the possibility that AtFH16 dimerization with an AtFH4-like endogenous formin might recruit AtFH16 to microtubules. Analogously, a dimerization-impaired mutant of mDia2 still binds and stabilizes microtubules *in vivo* (Bartolini et al., 2008).

Furthermore AtFH16 localization to microtubules could be mediated by some additional endogenous interacting partners other than formins. For example, fission yeast formin for3p directly interacts with a microtubule-associated polarity factor tea4p (Martin et al., 2005) or with a microtubule plus-end-binding protein EB1 and its interactor (Minc and Bratman et al., 2009). Similarly, mDia1 localization during phagocytosis is controled by the microtubule-associated CLIP-170, a homologue of fission yeast tip1p (Lewkowicz

et al., 2008) and mDia proteins further associate with EB1 at stable microtubule ends (Wen et al., 2004). Interestingly, transiently expressed *Arabidopsis* EB1 protein decorates the very similar cortical microtubule structures as AtFH16; it labels microtubules evenly and also linear fragments together with dots can be observed. The dots associate with both microtubule growing plus ends and with minus ends, where the later ones were identified as microtubule nucleation sites and appear as slowly moving or steady foci connencted with filaments (Chan et al., 2003). Furthermore, overexpressed EB1 localizes also into ER (Mathur et al., 2003), much like AtFH4 (Deeks and Fendrych et al., 2010), which co-localizes in case of dot-like structures with AtFH16. In the same study by Mathur et al. (2003), EB1 associated with already stabilized regions on a microtubule, rather than having stabilizing activity. Like that, AtFH16 newly appearing dots were shown to co-localize with already formed microtubular structures. It may be not improbable that AtFH16 could be preferentially recruited via interacting proteins into discrete microtubular regions, e.g. at the nucleation sites, from which it could further catalyze directional assembly of actin filaments. Also another scenario, i.e. actin-dependent positioning of AtFH16 and its mediating of stabilization or other regulation of microtubule dynamics cannot be excluded.

On the whole, analysis of *atfh16* mutant together with *in vivo* localization of AtFH16 protein suggest that this Class II *Arabidopsis* formin may facilitate actin-microtubule cross-talk, especially during directional cell elongation processes.

Chapter 7

CONCLUSIONS

I. Expression analysis revealed that all *Arabidopsis* formins are expressed; some genes exhibit tissue specific expression (e.g. *AtFH3*) and some are preferentially expressed under specific conditions (e.g. *AtFH12*). Expression of Class I members is generally stronger and more ubiquitous compared to Class II formins. (Cvrčková et al., 2004; Appendix 1)

II. Insertional mutants in a majority of formin genes were collected, out of which homozygots in 14 family members were successfully selected. Furthermore, a double mutant *atfh3atfh5* impairing both dominant pollen formins was prepared, however, no abberations in microspore development or pollen tube growth were observed. Similarly, downregulation of Class I formins by antisense oligonucleotides (ODNs) did not alter germination and growth of tobacco pollen tubes, indicating that function of *AtFH3*, *AtFH5* or their tobacco homologues is not crucial for polarity control in pollen.

III. Preparation of specific polyclonal antibodies in rats immunized with KLH-conjugated oligopeptides was attempted; immunity response of rats against the oligopeptides was inefficient, while antibodies recognizing a KLH-related plant antigen (KRAP) have been detected in most antisera. In *Arabidopsis* and tobacco, KRAP is ubiquitously present in suspension cultures, light-grown plants and pollen. In *Arabidopsis* suspension, predominant KRAP of 75 kDa was detected in soluble protein fraction, where it occurred in a complex of ~ 440 kDa. In tobacco pollen tubes, *in situ* immunolabeling of KRAP revealed its localization on endomembrane-like system. A direct connection between the oligopeptide antigenicity determined according to Welling et al. (1985) and systematic failure of immunizations was identified (Oulehlová et al., 2009; Appendix 2).

IV. A detailed characterization of *atfh16* mutant seedlings revealed a presence of mild phenotypic changes in primary roots and etiolated hypocotyls. The mutants turned out to be hypersensitive to treatments with cytoskeletal drugs, especially latrunculin B, indicating a role of *AtFH16* in cytoskeleton-related processes.

V. AtFH16 localizes to various cellular structures *in vivo*. Besides cytoplasm, AtFH16 labels stabilized actin bundles through its N-terminus. Furthermore, AtFH16 co-localizes with microtubules in a form of both continous strands and isolated punctae. For the localization on microtubules, a presence of the FH2 domain turned out to be essential.

List of Figures

List of Tables

References

Ahuja R, Pinyol R, Reichenbach N, Custer L, Klingensmith J, Kessels MM, Qualmann B (2007) Cordon-bleu is an actin nucleation factor and controls neuronal morphology. Cell **131:** 337-350

Alberts AS (2001) Identification of a carboxyl-terminal diaphanous-related formin homology protein autoregulatory domain. J Biol Chem **276:** 2824-2830

Alonso JM, Stepanova AN, Leisse TJ, Kim CJ, Chen H, Shinn P, Stevenson DK, Zimmerman J, Barajas P, Cheuk R, Gadrinab C, Heller C, Jeske A, Koesema E, Meyers CC, Parker H, Prednis L, Ansari Y, Choy N, Deen H, Geralt M, Hazari N, Hom E, Karnes M, Mulholland C, Ndubaku R, Schmidt I, Guzman P, Aguilar-Henonin L, Schmid M, Weigel D, Carter DE, Marchand T, Risseeuw E, Brogden D, Zeko A, Crosby WL, Berry CC, Ecker JR (2003) Genome-wide insertional mutagenesis of Arabidopsis thaliana. Science **301:** 653-657

Amin NM, Hu K, Pruyne D, Terzic D, Bretscher A, Liu J (2007) A Zn-finger/FH2-domain containing protein, FOZI-1, acts redundantly with CeMyoD to specify striated body wall muscle fates in the Caenorhabditis elegans postembryonic mesoderm. Development **134:** 19-29

Aspenstrom P, Richnau N, Johansson AS (2006) The diaphanous-related formin DAAM1 collaborates with the Rho GTPases RhoA and Cdc42, CIP4 and Src in regulating cell morphogenesis and actin dynamics. Exp Cell Res **312:** 2180-2194

Baird GS, Zacharias DA, Tsien RY (2000) Biochemistry, mutagenesis, and oligomerization of DsRed, a red fluorescent protein from coral. Proc Natl Acad Sci U S A **97:** 11984-11989

Baluška F, Salaj J, Mathur J, Braun M, Jasper F, Šamaj J, Chua NH, Barlow PW, Volkmann D (2000) Root hair formation: F-actin-dependent tip growth is initiated by local assembly of profilin-supported F-actin meshworks accumulated within expansin-enriched bulges. Dev Biol **227:** 618-632

Baluška F, Jasik J, Edelmann HG, Salajová T, Volkmann D (2001) Latrunculin B-induced plant dwarfism: Plant cell elongation is F-actin-dependent. Dev Biol **231:** 113-124

Banno H, Chua NH (2000) Characterization of the arabidopsis formin-like protein AFH1 and its interacting protein. Plant Cell Physiol **41:** 617-626

Barrero JM, Rodriguez PL, Quesada V, Alabadi D, Blazquez MA, Boutin JP, Marion-Poll A, Ponce MR, Micol JL (2008) The ABA1 gene and carotenoid biosynthesis are required for late skotomorphogenic growth in Arabidopsis thaliana. Plant Cell Environ **31:** 227-234

Bartolini F, Moseley JB, Schmoranzer J, Cassimeris L, Goode BL, Gundersen GG (2008) The formin mDia2 stabilizes microtubules independently of its actin nucleation activity. J Cell Biol **181:** 523-536

Barzik M, Kotova TI, Higgs HN, Hazelwood L, Hanein D, Gertler FB, Schafer DA (2005) Ena/VASP proteins enhance actin polymerization in the presence of barbed end capping proteins. J Biol Chem **280:** 28653-28662

Basu R, Chang F (2007) Shaping the actin cytoskeleton using microtubule tips. Curr Opin Cell Biol **19:** 88-94

Bear JE, Svitkina TM, Krause M, Schafer DA, Loureiro JJ, Strasser GA, Maly IV, Chaga OY, Cooper JA, Borisy GG, Gertler FB (2002) Antagonism between Ena/VASP proteins and actin filament capping regulates fibroblast motility. Cell **109:** 509-521

Beli P, Mascheroni D, Xu D, Innocenti M (2008) WAVE and Arp2/3 jointly inhibit filopodium formation by entering into a complex with mDia2. Nat Cell Biol **10:** 849-857

Bensenor LB, Kan HM, Wang N, Wallrabe H, Davidson LA, Cai Y, Schafer DA, Bloom GS (2007) IQGAP1 regulates cell motility by linking growth factor signaling to actin assembly. J Cell Sci **120:** 658-669

Benz PM, Blume C, Seifert S, Wilhelm S, Waschke J, Schuh K, Gertler F, Munzel T, Renne T (2009) Differential VASP phosphorylation controls remodeling of the actin cytoskeleton. J Cell Sci **122:** 3954-3965

Bione S, Sala C, Manzini C, Arrigo G, Zuffardi O, Banfi S, Borsani G, Jonveaux P, Philippe C, Zuccotti M, Ballabio A, Toniolo D (1998) A human homologue of the Drosophila melanogaster diaphanous gene is disrupted in a patient with premature ovarian failure: evidence for conserved function in oogenesis and implications for human sterility. Am J Hum Genet **62:** 533-541

Bosch M, Le KH, Bugyi B, Correia JJ, Renault L, Carlier MF (2007) Analysis of the function of Spire in actin assembly and its synergy with formin and profilin. Mol Cell **28:** 555-568

Brandt DT, Grosse R (2007) Get to grips: steering local actin dynamics with IQGAPs. EMBO Rep **8:** 1019-1023

Brandt DT, Marion S, Griffiths G, Watanabe T, Kaibuchi K, Grosse R (2007) Dia1 and IQGAP1 interact in cell migration and phagocytic cup formation. J Cell Biol **178:** 193-200

Brill S, Li S, Lyman CW, Church DM, Wasmuth JJ, Weissbach L, Bernards A, Snijders AJ (1996) The Ras GTPase-activating-protein-related human protein IQGAP2 harbors a potential actin binding domain and interacts with calmodulin and Rho family GTPases. Mol Cell Biol **16:** 4869-4878

Butler B, Cooper JA (2009) Distinct roles for the actin nucleators Arp2/3 and hDia1 during NK-mediated cytotoxicity. Curr Biol **19:** 1886-1896

Buttery SM, Yoshida S, Pellman D (2007) Yeast formins Bni1 and Bnr1 utilize different modes of cortical interaction during the assembly of actin cables. Mol Biol Cell **18:** 1826-1838

Carlier MF, Laurent V, Santolini J, Melki R, Didry D, Xia GX, Hong Y, Chua NH, Pantaloni D (1997) Actin depolymerizing factor (ADF/cofilin) enhances the rate of filament turnover: implication in actin-based motility. J Cell Biol **136:** 1307-1322

Carramusa L, Ballestrem C, Zilberman Y, Bershadsky AD (2007) Mammalian diaphanous-related formin Dia1 controls the organization of E-cadherin-mediated cell-cell junctions. J Cell Sci **120:** 3870-3882

Castrillon DH, Wasserman SA (1994) Diaphanous is required for cytokinesis in Drosophila and shares domains of similarity with the products of the limb deformity gene. Development **120:** 3367-3377

Cole RA, Fowler JE (2006) Polarized growth: maintaining focus on the tip. Curr Opin Plant Biol **9:** 579-588

Collings DA, Lill AW, Himmelspach R, Wasteneys GO (2006) Hypersensitivity to cytoskeletal antagonists demonstrates microtubule-microfilament cross-talk in the control of root elongation in Arabidopsis thaliana. New Phytol **170:** 275-290

Cowling RJ, Harberd, N.P. (1999) Gibberellins control *Arabidopsis* hypocotyl growth via regulation of cellular elongation. J Exp Botany **50:** 1351-1357

Cramer LP, Siebert M, Mitchison TJ (1997) Identification of novel graded polarity actin filament bundles in locomoting heart fibroblasts: implications for the generation of motile force. J Cell Biol **136:** 1287-1305

Cvrčková F (2000) Are plant formins integral membrane proteins? Genome Biol **1:** RESEARCH001

Cvrčková F, Novotný M, Pícková D, Žárský V (2004) Formin homology 2 domains occur in multiple

contexts in angiosperms. BMC Genomics **5:** 44

Cvrčková F, Rivero F, Bavlnka B (2004b) Evolutionarily conserved modules in actin nucleation: lessons from Dictyostelium discoideum and plants. Review article. Protoplasma **224:** 15-31

Deeks MJ, Hussey PJ, Davies B (2002) Formins: intermediates in signal-transduction cascades that affect cytoskeletal reorganization. Trends Plant Sci **7:** 492-498

Deeks MJ, Cvrčková F, Machesky LM, Mikitová V, Ketelaar T, Žárský V, Davies B, Hussey PJ (2005) Arabidopsis group Ie formins localize to specific cell membrane domains, interact with actin-binding proteins and cause defects in cell expansion upon aberrant expression. New Phytol **168:** 529-540

Deeks MJ, Fendrych M, Smertenko A, Bell KS, Oparka K, Cvrčková F, Žárský V, Hussey PJ (2010) The plant formin AtFH4 interacts with both actin and microtubules, and contains a newly identified microtubule-binding domain. J Cell Sci **123:** 1209-1215

Delgehyr N, Lopes CS, Moir CA, Huisman SM, Segal M (2008) Dissecting the involvement of formins in Bud6p-mediated cortical capture of microtubules in S. cerevisiae. J Cell Sci **121:** 3803-3814

Destaing O, Saltel F, Gilquin B, Chabadel A, Khochbin S, Ory S, Jurdic P (2005) A novel Rho-mDia2-HDAC6 pathway controls podosome patterning through microtubule acetylation in osteoclasts. J Cell Sci **118:** 2901-2911

DeWard AD, Alberts AS (2009) Ubiquitin-mediated degradation of the formin mDia2 upon completion of cell division. J Biol Chem **284:** 20061-20069

Dong CH, Xia GX, Hong Y, Ramachandran S, Kost B, Chua NH (2001) ADF proteins are involved in the control of flowering and regulate F-actin organization, cell expansion, and organ growth in Arabidopsis. Plant Cell **13:** 1333-1346

Dong Y, Pruyne D, Bretscher A (2003) Formin-dependent actin assembly is regulated by distinct modes of Rho signaling in yeast. J Cell Biol **161:** 1081-1092

Dumont J, Million K, Sunderland K, Rassinier P, Lim H, Leader B, Verlhac MH (2007) Formin-2 is required for spindle migration and for the late steps of cytokinesis in mouse oocytes. Dev Biol **301:** 254-265

Dyachok J, Shao MR, Vaughn K, Bowling A, Facette M, Djakovic S, Clark L, Smith L (2008) Plasma membrane-associated SCAR complex subunits promote cortical F-actin accumulation and normal growth characteristics in Arabidopsis roots. Mol Plant **1:** 990-1006

Eisenmann KM, Harris ES, Kitchen SM, Holman HA, Higgs HN, Alberts AS (2007) Dia-interacting protein modulates formin-mediated actin assembly at the cell cortex. Curr Biol **17:** 579-591

El-Assal Sel D, Le J, Basu D, Mallery EL, Szymanski DB (2004) Arabidopsis GNARLED encodes a NAP125 homolog that positively regulates ARP2/3. Curr Biol **14:** 1405-1409

Eleftheriou EP, Baskin TI, Hepler PK (2005) Aberrant cell plate formation in the Arabidopsis thaliana microtubule organization 1 mutant. Plant Cell Physiol **46:** 671-675

Emmons S, Phan H, Calley J, Chen W, James B, Manseau L (1995) Cappuccino, a Drosophila maternal effect gene required for polarity of the egg and embryo, is related to the vertebrate limb deformity locus. Genes Dev **9:** 2482-2494

Evangelista M, Blundell K, Longtine MS, Chow CJ, Adames N, Pringle JR, Peter M, Boone C (1997) Bni1p, a yeast formin linking cdc42p and the actin cytoskeleton during polarized morphogenesis. Science **276:** 118-122

Evangelista M, Pruyne D, Amberg DC, Boone C, Bretscher A (2002) Formins direct Arp2/3-independent

actin filament assembly to polarize cell growth in yeast. Nat Cell Biol **4:** 260-269

Faix J, Grosse R (2006) Staying in shape with formins. Dev Cell **10:** 693-706

Favery B, Chelysheva LA, Lebris M, Jammes F, Marmagne A, De Almeida-Engler J, Lecomte P, Vaury C, Arkowitz RA, Abad P (2004) Arabidopsis formin AtFH6 is a plasma membrane-associated protein upregulated in giant cells induced by parasitic nematodes. Plant Cell **16:** 2529-2540

Feierbach B, Chang F (2001) Roles of the fission yeast formin for3p in cell polarity, actin cable formation and symmetric cell division. Curr Biol **11:** 1656-1665

Feierbach B, Verde F, Chang F (2004) Regulation of a formin complex by the microtubule plus end protein tea1p. J Cell Biol **165:** 697-707

Fernandez-Borja M, Janssen L, Verwoerd D, Hordijk P, Neefjes J (2005) RhoB regulates endosome transport by promoting actin assembly on endosomal membranes through Dia1. J Cell Sci **118:** 2661-2670

Ferron F, Rebowski G, Lee SH, Dominguez R (2007) Structural basis for the recruitment of profilin-actin complexes during filament elongation by Ena/VASP. EMBO J **26:** 4597-4606

Field C, Li R, Oegema K (1999) Cytokinesis in eukaryotes: a mechanistic comparison. Curr Opin Cell Biol **11:** 68-80

Fitz Gerald JN, Hui PS, Berger F (2009) Polycomb group-dependent imprinting of the actin regulator AtFH5 regulates morphogenesis in Arabidopsis thaliana. Development **136:** 3399-3404

Fujiwara T, Tanaka K, Mino A, Kikyo M, Takahashi K, Shimizu K, Takai Y (1998) Rho1p-Bni1p-Spa2p interactions: implication in localization of Bni1p at the bud site and regulation of the actin cytoskeleton in Saccharomyces cerevisiae. Mol Biol Cell **9:** 1221-1233

Fujiwara T, Tanaka K, Inoue E, Kikyo M, Takai Y (1999) Bni1p regulates microtubule-dependent nuclear migration through the actin cytoskeleton in Saccharomyces cerevisiae. Mol Cell Biol **19:** 8016-8027

Fujiwara T, Mammoto A, Kim Y, Takai Y (2000) Rho small G-protein-dependent binding of mDia to an Src homology 3 domain-containing IRSp53/BAIAP2. Biochem Biophys Res Commun **271:** 626-629

Fukata M, Watanabe T, Noritake J, Nakagawa M, Yamaga M, Kuroda S, Matsuura Y, Iwamatsu A, Perez F, Kaibuchi K (2002) Rac1 and Cdc42 capture microtubules through IQGAP1 and CLIP-170. Cell **109:** 873-885

Fukuoka M, Suetsugu S, Miki H, Fukami K, Endo T, Takenawa T (2001) A novel neural Wiskott-Aldrich syndrome protein (N-WASP) binding protein, WISH, induces Arp2/3 complex activation independent of Cdc42. J Cell Biol **152:** 471-482

Furutani I, Watanabe Y, Prieto R, Masukawa M, Suzuki K, Naoi K, Thitamadee S, Shikanai T, Hashimoto T (2000) The SPIRAL genes are required for directional control of cell elongation in Aarabidopsis thaliana. Development **127:** 4443-4453

Gasman S, Kalaidzidis Y, Zerial M (2003) RhoD regulates endosome dynamics through Diaphanous-related Formin and Src tyrosine kinase. Nat Cell Biol **5:** 195-204

Gasteier JE, Schroeder S, Muranyi W, Madrid R, Benichou S, Fackler OT (2005) FHOD1 coordinates actin filament and microtubule alignment to mediate cell elongation. Exp Cell Res **306:** 192-202

Gazzarrini S, McCourt P (2001) Genetic interactions between ABA, ethylene and sugar signaling pathways. Curr Opin Plant Biol **4:** 387-391

Geitmann A, Emons AM (2000) The cytoskeleton in plant and fungal cell tip growth. J Microsc **198:** 218-245

Geyer H, Wuhrer M, Kurokawa T, Geyer R (2004) Characterization of keyhole limpet hemocyanin (KLH) glycans sharing a carbohydrate epitope with Schistosoma mansoni glycoconjugates. Micron **35:** 105-106

Gibson SI (2004) Sugar and phytohormone response pathways: navigating a signalling network. J Exp Bot **55:** 253-264

Gilliland LU, Pawloski LC, Kandasamy MK, Meagher RB (2003) Arabidopsis actin gene ACT7 plays an essential role in germination and root growth. Plant J **33:** 319-328

Goode BL, Eck MJ (2007) Mechanism and function of formins in the control of actin assembly. Annu Rev Biochem **76:** 593-627

Goulimari P, Knieling H, Engel U, Grosse R (2008) LARG and mDia1 link Galpha12/13 to cell polarity and microtubule dynamics. Mol Biol Cell **19:** 30-40

Grunt M, Žárský V, Cvrčková F (2008) Roots of angiosperm formins: the evolutionary history of plant FH2 domain-containing proteins. BMC Evol Biol **8:** 115

Grzych JM, Dissous C, Capron M, Torres S, Lambert PH, Capron A (1987) Schistosoma mansoni shares a protective carbohydrate epitope with keyhole limpet hemocyanin. J Exp Med **165:** 865-878

Guitton AE, Page DR, Chambrier P, Lionnet C, Faure JE, Grossniklaus U, Berger F (2004) Identification of new members of Fertilisation Independent Seed Polycomb Group pathway involved in the control of seed development in Arabidopsis thaliana. Development **131:** 2971-2981

Guo H, Ecker JR (2004) The ethylene signaling pathway: new insights. Curr Opin Plant Biol **7:** 40-49

Guzman P, Ecker JR (1990) Exploiting the triple response of Arabidopsis to identify ethylene-related mutants. Plant Cell **2:** 513-523

Habas R, Kato Y, He X (2001) Wnt/Frizzled activation of Rho regulates vertebrate gastrulation and requires a novel Formin homology protein Daam1. Cell **107:** 843-854

Haffner C, Jarchau T, Reinhard M, Hoppe J, Lohmann SM, Walter U (1995) Molecular cloning, structural analysis and functional expression of the proline-rich focal adhesion and microfilament-associated protein VASP. EMBO J **14:** 19-27

Han Y, Eppinger E, Schuster IG, Weigand LU, Liang X, Kremmer E, Peschel C, Krackhardt AM (2009) Formin-like 1 (FMNL1) is regulated by N-terminal myristoylation and induces polarized membrane blebbing. J Biol Chem **284:** 33409-33417

Hannemann S, Madrid R, Stastna J, Kitzing T, Gasteier J, Schonichen A, Bouchet J, Jimenez A, Geyer M, Grosse R, Benichou S, Fackler OT (2008) The Diaphanous-related Formin FHOD1 associates with ROCK1 and promotes Src-dependent plasma membrane blebbing. J Biol Chem **283:** 27891-27903

Harris ES, Li F, Higgs HN (2004) The mouse formin, FRLalpha, slows actin filament barbed end elongation, competes with capping protein, accelerates polymerization from monomers, and severs filaments. J Biol Chem **279:** 20076-20087

Harris ES, Rouiller I, Hanein D, Higgs HN (2006) Mechanistic differences in actin bundling activity of two mammalian formins, FRL1 and mDia2. J Biol Chem **281:** 14383-14392

Hart MJ, Callow MG, Souza B, Polakis P (1996) IQGAP1, a calmodulin-binding protein with a rasGAP-related domain, is a potential effector for cdc42Hs. EMBO J **15:** 2997-3005

Haseloff J, Siemering KR, Prasher DC, Hodge S (1997) Removal of a cryptic intron and subcellular localization of green fluorescent protein are required to mark transgenic Arabidopsis plants brightly. Proc Natl Acad Sci U S A **94:** 2122-2127

Heikal AA, Hess ST, Baird GS, Tsien RY, Webb WW (2000) Molecular spectroscopy and dynamics of intrinsically fluorescent proteins: coral red (dsRed) and yellow (Citrine). Proc Natl Acad Sci U S A **97:** 11996-12001

Hepler PK, Vidali L, Cheung AY (2001) Polarized cell growth in higher plants. Annu Rev Cell Dev Biol **17:** 159-187

Higashida C, Miyoshi T, Fujita A, Oceguera-Yanez F, Monypenny J, Andou Y, Narumiya S, Watanabe N (2004) Actin polymerization-driven molecular movement of mDia1 in living cells. Science **303:** 2007-2010

Hofmann C, Niehl A, Sambade A, Steinmetz A, Heinlein M (2009) Inhibition of tobacco mosaic virus movement by expression of an actin-binding protein. Plant Physiol **149:** 1810-1823

Honys D, Twell D (2003) Comparative analysis of the Arabidopsis pollen transcriptome. Plant Physiol **132:** 640-652

Hotulainen P, Lappalainen P (2006) Stress fibers are generated by two distinct actin assembly mechanisms in motile cells. J Cell Biol **173:** 383-394

Hruz T, Laule O, Szabo G, Wessendorp F, Bleuler S, Oertle L, Widmayer P, Gruissem W, Zimmermann P (2008) Genevestigator v3: a reference expression database for the meta-analysis of transcriptomes. Adv Bioinformatics **2008:** 420747

Hussey PJ, Ketelaar T, Deeks MJ (2006) Control of the actin cytoskeleton in plant cell growth. Annu Rev Plant Biol **57:** 109-125

Chalkia D, Nikolaidis N, Makalowski W, Klein J, Nei M (2008) Origins and evolution of the formin multigene family that is involved in the formation of actin filaments. Mol Biol Evol **25:** 2717-2733

Chan J, Calder GM, Doonan JH, Lloyd CW (2003) EB1 reveals mobile microtubule nucleation sites in Arabidopsis. Nat Cell Biol **5:** 967-971

Chen H, Zhang J, Neff MM, Hong SW, Zhang H, Deng XW, Xiong L (2008) Integration of light and abscisic acid signaling during seed germination and early seedling development. Proc Natl Acad Sci U S A **105:** 4495-4500

Chereau D, Boczkowska M, Skwarek-Maruszewska A, Fujiwara I, Hayes DB, Rebowski G, Lappalainen P, Pollard TD, Dominguez R (2008) Leiomodin is an actin filament nucleator in muscle cells. Science **320:** 239-243

Chesarone MA, Goode BL (2009) Actin nucleation and elongation factors: mechanisms and interplay. Curr Opin Cell Biol **21:** 28-37

Chesarone M, Gould CJ, Moseley JB, Goode BL (2009) Displacement of formins from growing barbed ends by bud14 is critical for actin cable architecture and function. Dev Cell **16:** 292-302

Chesarone MA, DuPage AG, Goode BL (2010) Unleashing formins to remodel the actin and microtubule cytoskeletons. Nat Rev Mol Cell Biol **11:** 62-74

Cheung AY, Wu HM (2004) Overexpression of an Arabidopsis formin stimulates supernumerary actin cable formation from pollen tube cell membrane. Plant Cell **16:** 257-269

Cheung AY, Wu HM (2008) Structural and signaling networks for the polar cell growth machinery in pollen tubes. Annu Rev Plant Biol **59:** 547-572

Chhabra ES, Higgs HN (2006) INF2 Is a WASP homology 2 motif-containing formin that severs actin filaments and accelerates both polymerization and depolymerization. J Biol Chem **281:** 26754-26767

Chhabra ES, Ramabhadran V, Gerber SA, Higgs HN (2009) INF2 is an endoplasmic reticulum-associated formin protein. J Cell Sci **122:** 1430-1440

Imamura H, Tanaka K, Hihara T, Umikawa M, Kamei T, Takahashi K, Sasaki T, Takai Y (1997) Bni1p and Bnr1p: downstream targets of the Rho family small G-proteins which interact with profilin and regulate actin cytoskeleton in Saccharomyces cerevisiae. EMBO J **16:** 2745-2755

Ingouff M, Fitz Gerald JN, Guerin C, Robert H, Sorensen MB, Van Damme D, Geelen D, Blanchoin L, Berger F (2005) Plant formin AtFH5 is an evolutionarily conserved actin nucleator involved in cytokinesis. Nat Cell Biol **7:** 374-380

Ishida T, Kaneko Y, Iwano M, Hashimoto T (2007) Helical microtubule arrays in a collection of twisting tubulin mutants of Arabidopsis thaliana. Proc Natl Acad Sci U S A **104:** 8544-8549

Ishizaki T, Morishima Y, Okamoto M, Furuyashiki T, Kato T, Narumiya S (2001) Coordination of microtubules and the actin cytoskeleton by the Rho effector mDia1. Nat Cell Biol **3:** 8-14

Jing HC, Anderson L, Sturre MJ, Hille J, Dijkwel PP (2007) Arabidopsis CPR5 is a senescence-regulatory gene with pleiotropic functions as predicted by the evolutionary theory of senescence. J Exp Bot **58:** 3885-3894

Johnston RJ, Jr., Copeland JW, Fasnacht M, Etchberger JF, Liu J, Honig B, Hobert O (2006) An unusual Zn-finger/FH2 domain protein controls a left/right asymmetric neuronal fate decision in C. elegans. Development **133:** 3317-3328

Kato T, Watanabe N, Morishima Y, Fujita A, Ishizaki T, Narumiya S (2001) Localization of a mammalian homolog of diaphanous, mDia1, to the mitotic spindle in HeLa cells. J Cell Sci **114:** 775-784

Kieber JJ, Rothenberg M, Roman G, Feldmann KA, Ecker JR (1993) CTR1, a negative regulator of the ethylene response pathway in Arabidopsis, encodes a member of the raf family of protein kinases. Cell **72:** 427-441

Kiselar JG, Mahaffy R, Pollard TD, Almo SC, Chance MR (2007) Visualizing Arp2/3 complex activation mediated by binding of ATP and WASp using structural mass spectrometry. Proc Natl Acad Sci U S A **104:** 1552-1557

Kitayama C, Uyeda TQ (2003) ForC, a novel type of formin family protein lacking an FH1 domain, is involved in multicellular development in Dictyostelium discoideum. J Cell Sci **116:** 711-723

Kitzing TM, Sahadevan AS, Brandt DT, Knieling H, Hannemann S, Fackler OT, Grosshans J, Grosse R (2007) Positive feedback between Dia1, LARG, and RhoA regulates cell morphology and invasion. Genes Dev **21:** 1478-1483

Klimyuk VI, Carroll BJ, Thomas CM, Jones JD (1993) Alkali treatment for rapid preparation of plant material for reliable PCR analysis. Plant J **3:** 493-494

Kobielak A, Pasolli HA, Fuchs E (2004) Mammalian formin-1 participates in adherens junctions and polymerization of linear actin cables. Nat Cell Biol **6:** 21-30

Kohno H, Tanaka K, Mino A, Umikawa M, Imamura H, Fujiwara T, Fujita Y, Hotta K, Qadota H, Watanabe T, Ohya Y, Takai Y (1996) Bni1p implicated in cytoskeletal control is a putative target of Rho1p small GTP binding protein in Saccharomyces cerevisiae. EMBO J **15:** 6060-6068

Kolaskar AS, Tongaonkar PC (1990) A semi-empirical method for prediction of antigenic determinants on

protein antigens. FEBS Lett **276:** 172-174

Kost B, Spielhofer P, Chua NH (1998) A GFP-mouse talin fusion protein labels plant actin filaments in vivo and visualizes the actin cytoskeleton in growing pollen tubes. Plant J **16:** 393-401

Kovar DR, Kuhn JR, Tichy AL, Pollard TD (2003) The fission yeast cytokinesis formin Cdc12p is a barbed end actin filament capping protein gated by profilin. J Cell Biol **161:** 875-887

Kovar DR, Pollard TD (2004) Insertional assembly of actin filament barbed ends in association with formins produces piconewton forces. Proc Natl Acad Sci U S A **101:** 14725-14730

Kovar DR, Harris ES, Mahaffy R, Higgs HN, Pollard TD (2006) Control of the assembly of ATP- and ADP-actin by formins and profilin. Cell **124:** 423-435

Kozlov MM, Bershadsky AD (2004) Processive capping by formin suggests a force-driven mechanism of actin polymerization. J Cell Biol **167:** 1011-1017

Kurokawa T, Wuhrer M, Lochnit G, Geyer H, Markl J, Geyer R (2002) Hemocyanin from the keyhole limpet Megathura crenulata (KLH) carries a novel type of N-glycans with Gal(beta1-6)Man-motifs. Eur J Biochem **269:** 5459-5473

Kyte J, Doolittle RF (1982) A simple method for displaying the hydropathic character of a protein. J Mol Biol **157:** 105-132

Lai SL, Chan TH, Lin MJ, Huang WP, Lou SW, Lee SJ (2008) Diaphanous-related formin 2 and profilin I are required for gastrulation cell movements. PLoS One **3:** e3439

Lammers M, Rose R, Scrima A, Wittinghofer A (2005) The regulation of mDia1 by autoinhibition and its release by Rho*GTP. EMBO J **24:** 4176-4187

Lammers M, Meyer S, Kuhlmann D, Wittinghofer A (2008) Specificity of interactions between mDia isoforms and Rho proteins. J Biol Chem **283:** 35236-35246

Lateef SS, Gupta S, Jayathilaka LP, Krishnanchettiar S, Huang JS, Lee BS (2007) An improved protocol for coupling synthetic peptides to carrier proteins for antibody production using DMF to solubilize peptides. J Biomol Tech **18:** 173-176

Le J, El-Assal Sel D, Basu D, Saad ME, Szymanski DB (2003) Requirements for Arabidopsis ATARP2 and ATARP3 during epidermal development. Curr Biol **13:** 1341-1347

Leader B, Lim H, Carabatsos MJ, Harrington A, Ecsedy J, Pellman D, Maas R, Leder P (2002) Formin-2, polyploidy, hypofertility and positioning of the meiotic spindle in mouse oocytes. Nat Cell Biol **4:** 921-928

Lee L, Klee SK, Evangelista M, Boone C, Pellman D (1999) Control of mitotic spindle position by the Saccharomyces cerevisiae formin Bni1p. J Cell Biol **144:** 947-961

Lewkowicz E, Herit F, Le Clainche C, Bourdoncle P, Perez F, Niedergang F (2008) The microtubule-binding protein CLIP-170 coordinates mDia1 and actin reorganization during CR3-mediated phagocytosis. J Cell Biol **183:** 1287-1298

Li F, Higgs HN (2003) The mouse Formin mDia1 is a potent actin nucleation factor regulated by autoinhibition. Curr Biol **13:** 1335-1340

Li Z, Dong X, Wang Z, Liu W, Deng N, Ding Y, Tang L, Hla T, Zeng R, Li L, Wu D (2005) Regulation of PTEN by Rho small GTPases. Nat Cell Biol **7:** 399-404

Lin Z, Zhong S, Grierson D (2009) Recent advances in ethylene research. J Exp Bot **60:** 3311-3336

Liu R, Abreu-Blanco MT, Barry KC, Linardopoulou EV, Osborn GE, Parkhurst SM (2009) Wash functions downstream of Rho and links linear and branched actin nucleation factors. Development

136: 2849-2860

Liu W, Sato A, Khadka D, Bharti R, Diaz H, Runnels LW, Habas R (2008) Mechanism of activation of the Formin protein Daam1. Proc Natl Acad Sci U S A **105:** 210-215

Lu J, Meng W, Poy F, Maiti S, Goode BL, Eck MJ (2007) Structure of the FH2 domain of Daam1: implications for formin regulation of actin assembly. J Mol Biol **369:** 1258-1269

Luo M, Bilodeau P, Koltunow A, Dennis ES, Peacock WJ, Chaudhury AM (1999) Genes controlling fertilization-independent seed development in Arabidopsis thaliana. Proc Natl Acad Sci U S A **96:** 296-301

Marc J, Granger CL, Brincat J, Fisher DD, Kao T, McCubbin AG, Cyr RJ (1998) A GFP-MAP4 reporter gene for visualizing cortical microtubule rearrangements in living epidermal cells. Plant Cell **10:** 1927-1940

Martin SG, McDonald WH, Yates JR, 3rd, Chang F (2005) Tea4p links microtubule plus ends with the formin for3p in the establishment of cell polarity. Dev Cell **8:** 479-491

Martin SG, Chang F (2006) Dynamics of the formin for3p in actin cable assembly. Curr Biol **16:** 1161-1170

Martin SG, Rincon SA, Basu R, Perez P, Chang F (2007) Regulation of the formin for3p by cdc42p and bud6p. Mol Biol Cell **18:** 4155-4167

Mass RL, Zeller R, Woychik RP, Vogt TF, Leder P (1990) Disruption of formin-encoding transcripts in two mutant limb deformity alleles. Nature **346:** 853-855

Mateer SC, McDaniel AE, Nicolas V, Habermacher GM, Lin MJ, Cromer DA, King ME, Bloom GS (2002) The mechanism for regulation of the F-actin binding activity of IQGAP1 by calcium/calmodulin. J Biol Chem **277:** 12324-12333

Mateer SC, Morris LE, Cromer DA, Bensenor LB, Bloom GS (2004) Actin filament binding by a monomeric IQGAP1 fragment with a single calponin homology domain. Cell Motil Cytoskeleton **58:** 231-241

Matheos D, Metodiev M, Muller E, Stone D, Rose MD (2004) Pheromone-induced polarization is dependent on the Fus3p MAPK acting through the formin Bni1p. J Cell Biol **165:** 99-109

Mathur J (2005) The ARP2/3 complex: giving plant cells a leading edge. Bioessays **27:** 377-387

Matsuda K, Matsuda S, Gladding CM, Yuzaki M (2006) Characterization of the delta2 glutamate receptor-binding protein delphilin: Splicing variants with differential palmitoylation and an additional PDZ domain. J Biol Chem **281:** 25577-25587

Maupin P, Pollard TD (1986) Arrangement of actin filaments and myosin-like filaments in the contractile ring and of actin-like filaments in the mitotic spindle of dividing HeLa cells. J Ultrastruct Mol Struct Res **94:** 92-103

McCallum SJ, Wu WJ, Cerione RA (1996) Identification of a putative effector for Cdc42Hs with high sequence similarity to the RasGAP-related protein IQGAP1 and a Cdc42Hs binding partner with similarity to IQGAP2. J Biol Chem **271:** 21732-21737

Mellor H (2010) The role of formins in filopodia formation. Biochim Biophys Acta **1803:** 191-200

Michelot A, Guerin C, Huang S, Ingouff M, Richard S, Rodiuc N, Staiger CJ, Blanchoin L (2005) The formin homology 1 domain modulates the actin nucleation and bundling activity of Arabidopsis FORMIN1. Plant Cell **17:** 2296-2313

Michelot A, Derivery E, Paterski-Boujemaa R, Guerin C, Huang S, Parcy F, Staiger CJ, Blanchoin L

(2006) A novel mechanism for the formation of actin-filament bundles by a nonprocessive formin. Curr Biol **16:** 1924-1930

Minc N, Bratman SV, Basu R, Chang F (2009) Establishing new sites of polarization by microtubules. Curr Biol **19:** 83-94

Minin AA, Kulik AV, Gyoeva FK, Li Y, Goshima G, Gelfand VI (2006) Regulation of mitochondria distribution by RhoA and formins. J Cell Sci **119:** 659-670

Mironova E, Millette CF (2008) Expression of the diaphanous-related formin proteins mDia1 and mDia2 in the rat testis. Dev Dyn **237:** 2170-2176

Miura K, Lee J, Miura T, Hasegawa PM (2010) SIZ1 controls cell growth and plant development in Arabidopsis through salicylic acid. Plant Cell Physiol **51:** 103-113

Miyagi Y, Yamashita T, Fukaya M, Sonoda T, Okuno T, Yamada K, Watanabe M, Nagashima Y, Aoki I, Okuda K, Mishina M, Kawamoto S (2002) Delphilin: a novel PDZ and formin homology domain-containing protein that synaptically colocalizes and interacts with glutamate receptor delta 2 subunit. J Neurosci **22:** 803-814

Moseley JB, Sagot I, Manning AL, Xu Y, Eck MJ, Pellman D, Goode BL (2004) A conserved mechanism for Bni1- and mDia1-induced actin assembly and dual regulation of Bni1 by Bud6 and profilin. Mol Biol Cell **15:** 896-907

Moseley JB, Goode BL (2005) Differential activities and regulation of Saccharomyces cerevisiae formin proteins Bni1 and Bnr1 by Bud6. J Biol Chem **280:** 28023-28033

Moseley JB, Maiti S, Goode BL (2006) Formin proteins: purification and measurement of effects on actin assembly. Methods Enzymol **406:** 215-234

Moutinho A, Camacho, L., Haley, A., Pais, M., Trewavas, A. and Malho, R. (2001) Antisense perturbation of protein function in living pollen tubes. Sex Plant Reprod **14:** 101–104

Mullins RD, Stafford WF, Pollard TD (1997) Structure, subunit topology, and actin-binding activity of the Arp2/3 complex from Acanthamoeba. J Cell Biol **136:** 331-343

Nakano K, Imai J, Arai R, Toh EA, Matsui Y, Mabuchi I (2002) The small GTPase Rho3 and the diaphanous/formin For3 function in polarized cell growth in fission yeast. J Cell Sci **115:** 4629-4639

Neidt EM, Scott BJ, Kovar DR (2009) Formin differentially utilizes profilin isoforms to rapidly assemble actin filaments. J Biol Chem **284:** 673-684

Nezami AG, Poy F, Eck MJ (2006) Structure of the autoinhibitory switch in formin mDia1. Structure **14:** 257-263

Nishimura T, Yokota E, Wada T, Shimmen T, Okada K (2003) An Arabidopsis ACT2 dominant-negative mutation, which disturbs F-actin polymerization, reveals its distinctive function in root development. Plant Cell Physiol **44:** 1131-1140

Noritake J, Fukata M, Sato K, Nakagawa M, Watanabe T, Izumi N, Wang S, Fukata Y, Kaibuchi K (2004) Positive role of IQGAP1, an effector of Rac1, in actin-meshwork formation at sites of cell-cell contact. Mol Biol Cell **15:** 1065-1076

Oliva M, Dunand C (2007) Waving and skewing: how gravity and the surface of growth media affect root development in Arabidopsis. New Phytol **176:** 37-43

Otomo T, Tomchick DR, Otomo C, Panchal SC, Machius M, Rosen MK (2005) Structural basis of actin filament nucleation and processive capping by a formin homology 2 domain. Nature **433:** 488-494

Oulehlová D, Hála M, Potocký M, Žárský V, Cvrčková F (2009) Plant antigens cross-react with rat

polyclonal antibodies against KLH-conjugated peptides. Cell Biol Int **33:** 113-118

Palazzo AF, Cook TA, Alberts AS, Gundersen GG (2001) mDia mediates Rho-regulated formation and orientation of stable microtubules. Nat Cell Biol **3:** 723-729

Paul AS, Pollard TD (2009a) Review of the mechanism of processive actin filament elongation by formins. Cell Motil Cytoskeleton **66:** 606-617

Paul AS, Pollard TD (2009b) Energetic requirements for processive elongation of actin filaments by FH1FH2-formins. J Biol Chem **284:** 12533-12540

Pawson C, Eaton BA, Davis GW (2008) Formin-dependent synaptic growth: evidence that Dlar signals via Diaphanous to modulate synaptic actin and dynamic pioneer microtubules. J Neurosci **28:** 11111-11123

Pechlivanis M, Samol A, Kerkhoff E (2009) Identification of a short Spir interaction sequence at the C-terminal end of formin subgroup proteins. J Biol Chem **284:** 25324-25333

Pelham RJ, Chang F (2002) Actin dynamics in the contractile ring during cytokinesis in fission yeast. Nature **419:** 82-86

Pellegrin S, Mellor H (2005) The Rho family GTPase Rif induces filopodia through mDia2. Curr Biol **15:** 129-133

Petersen J, Nielsen O, Egel R, Hagan IM (1998) FH3, a domain found in formins, targets the fission yeast formin Fus1 to the projection tip during conjugation. J Cell Biol **141:** 1217-1228

Petrášek J, Schwarzerová K (2009) Actin and microtubule cytoskeleton interactions. Curr Opin Plant Biol **12:** 728-734

Pilet PE (1998) Some cellular and molecular properties of abscisic acid: its particular involvement in growing plant roots Cell Mol Life Sci **54:** 851-865

Pina C, Pinto F, Feijo JA, Becker JD (2005) Gene family analysis of the Arabidopsis pollen transcriptome reveals biological implications for cell growth, division control, and gene expression regulation. Plant Physiol **138:** 744-756

Pitts RJ, Cernac A, Estelle M (1998) Auxin and ethylene promote root hair elongation in Arabidopsis. Plant J **16:** 553-560

Pleskot R, Potocký M, Pejchar P, Linek J, Bezvoda R, Martinec J, Valentová O, Novotná Z, Žárský V (2010) Mutual regulation of plant phospholipase D and the actin cytoskeleton. Plant J

Pollard TD, Cooper JA (1984) Quantitative analysis of the effect of Acanthamoeba profilin on actin filament nucleation and elongation. Biochemistry **23:** 6631-6641

Pollard TD, Borisy GG (2003) Cellular motility driven by assembly and disassembly of actin filaments. Cell **112:** 453-465

Pollard TD (2007) Regulation of actin filament assembly by Arp2/3 complex and formins. Annu Rev Biophys Biomol Struct **36:** 451-477

Potocký M, Eliáš M, Profotová B, Novotná Z, Valentová O, Žárský V (2003) Phosphatidic acid produced by phospholipase D is required for tobacco pollen tube growth. Planta **217:** 122-130

Pring M, Evangelista M, Boone C, Yang C, Zigmond SH (2003) Mechanism of formin-induced nucleation of actin filaments. Biochemistry **42:** 486-496

Pruyne D, Evangelista M, Yang C, Bi E, Zigmond S, Bretscher A, Boone C (2002) Role of formins in actin assembly: nucleation and barbed-end association. Science **297:** 612-615

Pruyne D, Gao L, Bi E, Bretscher A (2004) Stable and dynamic axes of polarity use distinct formin isoforms in budding yeast. Mol Biol Cell **15:** 4971-4989

Qiu JL, Zhou L, Yun BW, Nielsen HB, Fiil BK, Petersen K, Mackinlay J, Loake GJ, Mundy J, Morris PC (2008) Arabidopsis mitogen-activated protein kinase kinases MKK1 and MKK2 have overlapping functions in defense signaling mediated by MEKK1, MPK4, and MKS1. Plant Physiol **148:** 212-222

Quack T, Knobloch J, Beckmann S, Vicogne J, Dissous C, Grevelding CG (2009) The formin-homology protein SmDia interacts with the Src kinase SmTK and the GTPase SmRho1 in the gonads of Schistosoma mansoni. PLoS One **4:** e6998

Quinlan ME, Heuser JE, Kerkhoff E, Mullins RD (2005) Drosophila Spire is an actin nucleation factor. Nature **433:** 382-388

Quinlan ME, Hilgert S, Bedrossian A, Mullins RD, Kerkhoff E (2007) Regulatory interactions between two actin nucleators, Spire and Cappuccino. J Cell Biol **179:** 117-128

Ramachandran S, Christensen HE, Ishimaru Y, Dong CH, Chao-Ming W, Cleary AL, Chua NH (2000) Profilin plays a role in cell elongation, cell shape maintenance, and flowering in Arabidopsis. Plant Physiol **124:** 1637-1647

Ray SD, Guruprasad, K.N., Laloraya, M.M. (1980) Antagonistic action of phenolic compounds on abscisic acid-induced inhibition of hypocotyl growth. J Exp Bot **31:** 1651-1656

Rhee SY, Somerville CR (1998) Tetrad pollen formation in quartet mutants of Arabidopsis thaliana is associated with persistence of pectic polysaccharides of the pollen mother cell wall. Plant J **15:** 79-88

Ridley AJ, Hall A (1992) The small GTP-binding protein rho regulates the assembly of focal adhesions and actin stress fibers in response to growth factors. Cell **70:** 389-399

Ridley AJ (2006) Rho GTPases and actin dynamics in membrane protrusions and vesicle trafficking. Trends Cell Biol **16:** 522-529

Rivero F, Muramoto T, Meyer AK, Urushihara H, Uyeda TQ, Kitayama C (2005) A comparative sequence analysis reveals a common GBD/FH3-FH1-FH2-DAD architecture in formins from Dictyostelium, fungi and metazoa. BMC Genomics **6:** 28

Robinson NG, Guo L, Imai J, Toh EA, Matsui Y, Tamanoi F (1999) Rho3 of Saccharomyces cerevisiae, which regulates the actin cytoskeleton and exocytosis, is a GTPase which interacts with Myo2 and Exo70. Mol Cell Biol **19:** 3580-3587

Rodriguez-Fernandez JL, Rozengurt E (1996) Bombesin, bradykinin, vasopressin, and phorbol esters rapidly and transiently activate Src family tyrosine kinases in Swiss 3T3 cells. Dissociation from tyrosine phosphorylation of p125 focal adhesion kinase. J Biol Chem **271:** 27895-27901

Romero S, Le Clainche C, Didry D, Egile C, Pantaloni D, Carlier MF (2004) Formin is a processive motor that requires profilin to accelerate actin assembly and associated ATP hydrolysis. Cell **119:** 419-429

Romero S, Didry D, Larquet E, Boisset N, Pantaloni D, Carlier MF (2007) How ATP hydrolysis controls filament assembly from profilin-actin: implication for formin processivity. J Biol Chem **282:** 8435-8445

Rosales-Nieves AE, Johndrow JE, Keller LC, Magie CR, Pinto-Santini DM, Parkhurst SM (2006) Coordination of microtubule and microfilament dynamics by Drosophila Rho1, Spire and Cappuccino. Nat Cell Biol **8:** 367-376

Rose R, Weyand M, Lammers M, Ishizaki T, Ahmadian MR, Wittinghofer A (2005) Structural and mechanistic insights into the interaction between Rho and mammalian Dia. Nature **435:** 513-518

Rundle DR, Gorbsky G, Tsiokas L (2004) PKD2 interacts and co-localizes with mDia1 to mitotic spindles of dividing cells: role of mDia1 IN PKD2 localization to mitotic spindles. J Biol Chem **279:** 29728-29739

Sagot I, Klee SK, Pellman D (2002) Yeast formins regulate cell polarity by controlling the assembly of actin cables. Nat Cell Biol **4:** 42-50

Sagot I, Rodal AA, Moseley J, Goode BL, Pellman D (2002) An actin nucleation mechanism mediated by Bni1 and profilin. Nat Cell Biol **4:** 626-631

Satoh S, Tominaga T (2001) mDia-interacting protein acts downstream of Rho-mDia and modifies Src activation and stress fiber formation. J Biol Chem **276:** 39290-39294

Sedbrook JC, Ehrhardt DW, Fisher SE, Scheible WR, Somerville CR (2004) The Arabidopsis sku6/spiral1 gene encodes a plus end-localized microtubule-interacting protein involved in directional cell expansion. Plant Cell **16:** 1506-1520

Sedbrook JC, Kaloriti D (2008) Microtubules, MAPs and plant directional cell expansion. Trends Plant Sci **13:** 303-310

Segal M, Bloom K (2001) Control of spindle polarity and orientation in Saccharomyces cerevisiae. Trends Cell Biol **11:** 160-166

Semenova I, Burakov A, Berardone N, Zaliapin I, Slepchenko B, Svitkina T, Kashina A, Rodionov V (2008) Actin dynamics is essential for myosin-based transport of membrane organelles. Curr Biol **18:** 1581-1586

Sessions A, Burke E, Presting G, Aux G, McElver J, Patton D, Dietrich B, Ho P, Bacwaden J, Ko C, Clarke JD, Cotton D, Bullis D, Snell J, Miguel T, Hutchison D, Kimmerly B, Mitzel T, Katagiri F, Glazebrook J, Law M, Goff SA (2002) A high-throughput Arabidopsis reverse genetics system. Plant Cell **14:** 2985-2994

Seth A, Otomo C, Rosen MK (2006) Autoinhibition regulates cellular localization and actin assembly activity of the diaphanous-related formins FRLalpha and mDia1. J Cell Biol **174:** 701-713

Severson AF, Baillie DL, Bowerman B (2002) A Formin Homology protein and a profilin are required for cytokinesis and Arp2/3-independent assembly of cortical microfilaments in C. elegans. Curr Biol **12:** 2066-2075

Sheahan MB, Rose RJ, McCurdy DW (2004a) Organelle inheritance in plant cell division: the actin cytoskeleton is required for unbiased inheritance of chloroplasts, mitochondria and endoplasmic reticulum in dividing protoplasts. Plant J **37:** 379-390

Sheahan MB, Staiger CJ, Rose RJ, McCurdy DW (2004b) A green fluorescent protein fusion to actin-binding domain 2 of Arabidopsis fimbrin highlights new features of a dynamic actin cytoskeleton in live plant cells. Plant Physiol **136:** 3968-3978

Shemesh T, Otomo T, Rosen MK, Bershadsky AD, Kozlov MM (2005) A novel mechanism of actin filament processive capping by formin: solution of the rotation paradox. J Cell Biol **170:** 889-893

Schirenbeck A, Bretschneider T, Arasada R, Schleicher M, Faix J (2005) The Diaphanous-related formin dDia2 is required for the formation and maintenance of filopodia. Nat Cell Biol **7:** 619-625

Schonichen A, Alexander M, Gasteier JE, Cuesta FE, Fackler OT, Geyer M (2006) Biochemical characterization of the diaphanous autoregulatory interaction in the formin homology protein FHOD1. J Biol Chem **281:** 5084-5093

Schulte A, Stolp B, Schonichen A, Pylypenko O, Rak A, Fackler OT, Geyer M (2008) The human formin FHOD1 contains a bipartite structure of FH3 and GTPase-binding domains required for activation. Structure **16:** 1313-1323

Schwab B, Mathur J, Saedler R, Schwarz H, Frey B, Scheidegger C, Hulskamp M (2003) Regulation of cell expansion by the DISTORTED genes in Arabidopsis thaliana: actin controls the spatial organization of microtubules. Mol Genet Genomics **269:** 350-360

Sugimoto K, Williamson RE, Wasteneys GO (2000) New techniques enable comparative analysis of microtubule orientation, wall texture, and growth rate in intact roots of Arabidopsis. Plant Physiol **124:** 1493-1506

Swan KA, Severson AF, Carter JC, Martin PR, Schnabel H, Schnabel R, Bowerman B (1998) cyk-1: a C. elegans FH gene required for a late step in embryonic cytokinesis. J Cell Sci **111 (Pt 14):** 2017-2027

Synek L, Schlager N, Eliáš M, Quentin M, Hauser MT, Žárský V (2006) AtEXO70A1, a member of a family of putative exocyst subunits specifically expanded in land plants, is important for polar growth and plant development. Plant J **48:** 54-72

Takeya R, Taniguchi K, Narumiya S, Sumimoto H (2008) The mammalian formin FHOD1 is activated through phosphorylation by ROCK and mediates thrombin-induced stress fibre formation in endothelial cells. EMBO J **27:** 618-628

Tam J (1988) Synthetic Peptide Vaccine Design: Synthesis and Properties of a High-Density Multiple Antigenic Peptide System. PNAS **85:** 5409-5413

Tax FE, Vernon DM (2001) T-DNA-associated duplication/translocations in Arabidopsis. Implications for mutant analysis and functional genomics. Plant Physiol **126:** 1527-1538

Thitamadee S, Tuchihara K, Hashimoto T (2002) Microtubule basis for left-handed helical growth in Arabidopsis. Nature **417:** 193-196

Thompson JD, Higgins DG, Gibson TJ (1994) CLUSTAL W: improving the sensitivity of progressive multiple sequence alignment through sequence weighting, position-specific gap penalties and weight matrix choice. Nucleic Acids Res **22:** 4673-4680

Tobacman LS, Brenner SL, Korn ED (1983) Effect of Acanthamoeba profilin on the pre-steady state kinetics of actin polymerization and on the concentration of F-actin at steady state. J Biol Chem **258:** 8806-8812

Tolliday N, VerPlank L, Li R (2002) Rho1 directs formin-mediated actin ring assembly during budding yeast cytokinesis. Curr Biol **12:** 1864-1870

Tominaga T, Sahai E, Chardin P, McCormick F, Courtneidge SA, Alberts AS (2000) Diaphanous-related formins bridge Rho GTPase and Src tyrosine kinase signaling. Mol Cell **5:** 13-25

Uetz P, Fumagalli S, James D, Zeller R (1996) Molecular interaction between limb deformity proteins (formins) and Src family kinases. J Biol Chem **271:** 33525-33530

Vaillant DC, Copeland SJ, Davis C, Thurston SF, Abdennur N, Copeland JW (2008) Interaction of the N- and C-terminal autoregulatory domains of FRL2 does not inhibit FRL2 activity. J Biol Chem **283:** 33750-33762

Valiente M, Andres-Pons A, Gomar B, Torres J, Gil A, Tapparel C, Antonarakis SE, Pulido R (2005) Binding of PTEN to specific PDZ domains contributes to PTEN protein stability and phosphorylation by microtubule-associated serine/threonine kinases. J Biol Chem **280:** 28936-28943

Van Damme D, Bouget FY, Van Poucke K, Inze D, Geelen D (2004) Molecular dissection of plant cytokinesis and phragmoplast structure: a survey of GFP-tagged proteins. Plant J **40:** 386-398

Vandenbussche F, Verbelen JP, Van Der Straeten D (2005) Of light and length: regulation of hypocotyl growth in Arabidopsis. Bioessays **27:** 275-284

Vavylonis D, Kovar DR, O'Shaughnessy B, Pollard TD (2006) Model of formin-associated actin filament elongation. Mol Cell **21:** 455-466

Vidali L, van Gisbergen PA, Guerin C, Franco P, Li M, Burkart GM, Augustine RC, Blanchoin L, Bezanilla M (2009) Rapid formin-mediated actin-filament elongation is essential for polarized plant cell growth. Proc Natl Acad Sci U S A **106:** 13341-13346

Voigt B, Timmers AC, Samaj J, Muller J, Baluska F, Menzel D (2005) GFP-FABD2 fusion construct allows in vivo visualization of the dynamic actin cytoskeleton in all cells of Arabidopsis seedlings. Eur J Cell Biol **84:** 595-608

Voinnet O, Rivas S, Mestre P, Baulcombe D (2003) An enhanced transient expression system in plants based on suppression of gene silencing by the p19 protein of tomato bushy stunt virus. Plant J **33:** 949-956

Vriend G (1990) WHAT IF: a molecular modeling and drug design program. J Mol Graph **8:** 52-56, 29

Vriezen WH, Achard P, Harberd NP, Van Der Straeten D (2004) Ethylene-mediated enhancement of apical hook formation in etiolated Arabidopsis thaliana seedlings is gibberellin dependent. Plant J **37:** 505-516

Walia A, Lee JS, Wasteneys G, Ellis B (2009) Arabidopsis mitogen-activated protein kinase MPK18 mediates cortical microtubule functions in plant cells. Plant J **59:** 565-575

Wallar BJ, Stropich BN, Schoenherr JA, Holman HA, Kitchen SM, Alberts AS (2006) The basic region of the diaphanous-autoregulatory domain (DAD) is required for autoregulatory interactions with the diaphanous-related formin inhibitory domain. J Biol Chem **281:** 4300-4307

Wallar BJ, Deward AD, Resau JH, Alberts AS (2007) RhoB and the mammalian Diaphanous-related formin mDia2 in endosome trafficking. Exp Cell Res **313:** 560-571

Walter M, Chaban C, Schutze K, Batistic O, Weckermann K, Nake C, Blazevic D, Grefen C, Schumacher K, Oecking C, Harter K, Kudla J (2004) Visualization of protein interactions in living plant cells using bimolecular fluorescence complementation. Plant J **40:** 428-438

Wang J, Neo SP, Cai M (2009) Regulation of the yeast formin Bni1p by the actin-regulating kinase Prk1p. Traffic

Watanabe N, Madaule P, Reid T, Ishizaki T, Watanabe G, Kakizuka A, Saito Y, Nakao K, Jockusch BM, Narumiya S (1997) p140mDia, a mammalian homolog of Drosophila diaphanous, is a target protein for Rho small GTPase and is a ligand for profilin. EMBO J **16:** 3044-3056

Watanabe N, Kato T, Fujita A, Ishizaki T, Narumiya S (1999) Cooperation between mDia1 and ROCK in Rho-induced actin reorganization. Nat Cell Biol **1:** 136-143

Watanabe S, Ando Y, Yasuda S, Hosoya H, Watanabe N, Ishizaki T, Narumiya S (2008) mDia2 induces the actin scaffold for the contractile ring and stabilizes its position during cytokinesis in NIH 3T3 cells. Mol Biol Cell **19:** 2328-2338

Wear MA, Cooper JA (2004) Capping protein: new insights into mechanism and regulation. Trends Biochem Sci **29:** 418-428

Weissbach L, Settleman J, Kalady MF, Snijders AJ, Murthy AE, Yan YX, Bernards A (1994) Identification of a human rasGAP-related protein containing calmodulin-binding motifs. J Biol Chem **269:** 20517-20521

Welch MD, Iwamatsu A, Mitchison TJ (1997) Actin polymerization is induced by Arp2/3 protein complex at the surface of Listeria monocytogenes. Nature **385:** 265-269

Welling GW, Fries H (1985) Choice of peptide and peptide length for the generation of antibodies reactive with the intact protein. FEBS Lett **182:** 81-84

Welling GW, Weijer WJ, van der Zee R, Welling-Wester S (1985) Prediction of sequential antigenic regions in proteins. FEBS Lett **188:** 215-218

Wen Y, Eng CH, Schmoranzer J, Cabrera-Poch N, Morris EJ, Chen M, Wallar BJ, Alberts AS, Gundersen GG (2004) EB1 and APC bind to mDia to stabilize microtubules downstream of Rho and promote cell migration. Nat Cell Biol **6:** 820-830

Whittington AT, Vugrek O, Wei KJ, Hasenbein NG, Sugimoto K, Rashbrooke MC, Wasteneys GO (2001) MOR1 is essential for organizing cortical microtubules in plants. Nature **411:** 610-613

Xu Y, Moseley JB, Sagot I, Poy F, Pellman D, Goode BL, Eck MJ (2004) Crystal structures of a Formin Homology-2 domain reveal a tethered dimer architecture. Cell **116:** 711-723

Yamana N, Arakawa Y, Nishino T, Kurokawa K, Tanji M, Itoh RE, Monypenny J, Ishizaki T, Bito H, Nozaki K, Hashimoto N, Matsuda M, Narumiya S (2006) The Rho-mDia1 pathway regulates cell polarity and focal adhesion turnover in migrating cells through mobilizing Apc and c-Src. Mol Cell Biol **26:** 6844-6858

Yamashita T, Miyagi Y, Ono M, Ito H, Watanabe K, Sonoda T, Tsuzuki K, Ozawa S, Aoki I, Okuda K, Mishina M, Kawamoto S (2005) Identification and characterization of a novel Delphilin variant with an alternative N-terminus. Brain Res Mol Brain Res **141:** 83-94

Yasuda S, Oceguera-Yanez F, Kato T, Okamoto M, Yonemura S, Terada Y, Ishizaki T, Narumiya S (2004) Cdc42 and mDia3 regulate microtubule attachment to kinetochores. Nature **428:** 767-771

Ye J, Zheng Y, Yan A, Chen N, Wang Z, Huang S, Yang Z (2009) Arabidopsis formin3 directs the formation of actin cables and polarized growth in pollen tubes. Plant Cell **21:** 3868-3884

Yi K, Guo C, Chen D, Zhao B, Yang B, Ren H (2005) Cloning and functional characterization of a formin-like protein (AtFH8) from Arabidopsis. Plant Physiol **138:** 1071-1082

Young KG, Thurston SF, Copeland S, Smallwood C, Copeland JW (2008) INF1 is a novel microtubule-associated formin. Mol Biol Cell **19:** 5168-5180

Zahner JE, Harkins HA, Pringle JR (1996) Genetic analysis of the bipolar pattern of bud site selection in the yeast Saccharomyces cerevisiae. Mol Cell Biol **16:** 1857-1870

Žárský V, Cvrčková F, Potocký M, Hála M (2009) Exocytosis and cell polarity in plants - exocyst and recycling domains. New Phytol **183:** 255-272

Zhang X, Dyachok J, Krishnakumar S, Smith LG, Oppenheimer DG (2005) IRREGULAR TRICHOME BRANCH1 in Arabidopsis encodes a plant homolog of the actin-related protein2/3 complex activator Scar/WAVE that regulates actin and microtubule organization. Plant Cell **17:** 2314-2326

Zhou F, Leder P, Martin SS (2006) Formin-1 protein associates with microtubules through a peptide domain encoded by exon-2. Exp Cell Res **312:** 1119-1126

Zigmond SH, Evangelista M, Boone C, Yang C, Dar AC, Sicheri F, Forkey J, Pring M (2003) Formin leaky cap allows elongation in the presence of tight capping proteins. Curr Biol **13:** 1820-1823

Zimmermann P, Hirsch-Hoffmann M, Hennig L, Gruissem W (2004) GENEVESTIGATOR. Arabidopsis microarray database and analysis toolbox. Plant Physiol **136:** 2621-2632

Zimmermann I, Saedler R, Mutondo M, Hulskamp M (2004b) The Arabidopsis GNARLED gene encodes the NAP125 homolog and controls several actin-based cell shape changes. Mol Genet Genomics **272:** 290-296

Zuchero JB, Coutts AS, Quinlan ME, Thangue NB, Mullins RD (2009) p53-cofactor JMY is a multifunctional actin nucleation factor. Nat Cell Biol **11:** 451-459

Zuniga A, Michos O, Spitz F, Haramis AP, Panman L, Galli A, Vintersten K, Klasen C, Mansfield W, Kuc S, Duboule D, Dono R, Zeller R (2004) Mouse limb deformity mutations disrupt a global control region within the large regulatory landscape required for Gremlin expression. Genes Dev **18:** 1553-1564

Abbreviations

ABA - abscisic acid
ACC -1-aminocyclopropane-1-carboxylic acid
APC - adenomatous polyposis coli protein
APM - amiprophos-methyl
BFA - brefeldin A
CC - coiled-coil region
DAD - diaphanous autoregulatory domain
DD - dimerization domain
DID - diaphanous-related formin inhibitory domain
DIP - Dia interacting protein
DRF - diaphanous-related formin
Ena/VASP - enabled/vasodilatator stimulated phosphoprotein
ER - endoplasmic reticulum
FABD - fimbrin actin-binding domain
FH - formin homology
GAP - GTPase activating protein
GBD - GTPase-binding domain
GEF - guanine nucleotide exchange factor
GFP - green fluorescent protein
KLH - keyhole limpet hemocyanin
KRAP - KLH-related plant antigen
LARG - leukemia-associated Rho-GEF (guanosine exchange factor)
LatB - latrunculin B
LB - left border
MAP - microtubule associated protein
MeJA - methyl jasmonate
NPF - nucleation promoting factor
ODNs - antisense oligodeoxynucleotides
PAGE - polyacrylamide gel electrophoresis
PPT - ammonium 2-amino-4-(hydroxymethylphosphinyle) butyrate
PTEN - phosphatase and tensin-related domain
RBD - Rho-binding domain
RT-PCR - reverse transcription - polymerase chain reaction
SA - salicylic acid
TM - transmembrane domain
WASP - Wiskott-Aldrich syndrome protein
WH2 - Wiskott-Aldrich syndrome protein homology domain
WT - wild type

List of Publications

Cvrčková F, Novotný M, Pícková D, Žárský V (2004) Formin homology 2 domains occur in multiple contexts in angiosperms. BMC Genomics **5:** 44

For this study, I collected available sequence data of formins from higher plants that shed light on transcriptional activity of particular genes and brought new information about non-*Arabidopsis* formins.

Oulehlová D, Hála M, Potocký M, Žárský V, Cvrčková F (2009) Plant antigens cross-react with rat polyclonal antibodies against KLH-conjugated peptides. Cell Biol Int **33:** 113-118

In this study, I did a majority of experimental work and together with Fatima Cvrčková, I wrote the manuscript.

Oulehlová D, Fendrych M, Grunt M, Žárský V, Cvrčková F *Arabidopsis* Class II formins associate with multiple cellular structures including microtubules. *In preparation*

The manuscript contains my experimental data about Class II formin AtFH16 presented in this thesis together with data about evolutionary dynamics of Class II group and another member AtFH12 done by the co-authors.

Supplemental data

Supplemental data 1: List of primers

Primer	Sequence
AtFH1	5´-CTG AGC CTT CTT CGG GTC CAG G-3´
AtFH1aA	5´-ACA TCT CCT AAG TTA TCT TCC CGG-3´
AtFH2	5´-TCG ACA CGC TCT TAA AAC TGG TAG-3´
AtFH2aA	5´-CAG ACC AAT TAG GAA ATG CGC GA-3´
AtFH3	5´-GGG AGA GTT CTC AGT AGA TCC TG-3´
FH3aA	5´-TGC ATG GCG GTT TGT CTC CGG C-3´
AtFH3-2	5´-AAG AAT TCG AAG GTG AAC TAT CCT C-3´
AtFH3-2aA	5´-CAG GTG GGA TCC AAG AAA CTT AGA A-3´
AtFH4	5´-GAG CCT CCA TTA GAT CGC CAT CG-3´
AtFH4aA	5´-CGA TTC GGC GGA AAC GTA AAG GG-3´
AtFH5	5´-CAT CAA CAG GGC AGG TCA ATG AAC-3´
AtFH5aA	5´-TTC CCT ACT ATC CTT TGA TCC TGG-3´
AtFH6	5´-TCG CCA TGA AAG CTC TTC AAT CC-3´
AtFH6aA	5´-GTT ATC AGA GGG TTG CGG GGG-3´
AtFH7	5´-CGA CCT GGT CAA CGC GTC GG-3´
AtFH7aA	5´-CAC TTG TAG CAT AGG AAG TTC GCG-3´
AtFH8	5´-CTT CCA CCT TCG TCA AAC CCA TC-3´
AtFH8aA	5´-GAA ACG TCT CCG CAT CAG CAA GC-3´
AtFH10	5´-TCT GCA ATG CGC ACT ATC TGA GG-3´
AtFH11	5´-TCT TTG CCT AAT GGT CTA CGC TC-3´
AtFH12	5´-ATG CAA ATG TTA CAG ATT TTC GGG G-3´
AtFH12aA	5´-GCA ACA CAC AAC ACA AGG CCC AC-3´
AtFH13	5´-AGG AGG GGG AGA AGA GGT ATG -3´
AtFH13aA	5´-CAA ATG CTG TCC AAG AAG GAC 3´
AtFH14	5´-ACG TCA CAT TCT GCC TGG AGC C-3´
AtFH14aA	5´-ACC AGA TGG ATT ACT TGA ATT TGC TG-3´
AtFH15a	5´-GGA CAG ATT AAG TGT TAA AAG GAT G-3´
AtFH15a-aA	5´-ACT GCA GTC CTG GCA ATG GAT GAG-3´
AtFH15b	5´-AAG CGA CAC ATG TGC ACC TAA CAG-3´
AtFH16	5´-GAC TTA AAC ACA CCT GCT CAG AC-3´
AtFH16aA	5´-TTG ATC TAT CAG AGA TAG AGG CCC-3´
AtFH16-2	5´-AAT CTT ATA CAA CTT TGC CCA ACA A-3´
AtFH17	5´-AGA ATG GTG AGG TTG TAG AAG AG-3´
AtFH17aA	5´-GCA CTA TTG AAA CTC TGT ATT GGT C-3´
AtFH18	5´-TCA TGG ACT ATC CTC GCC ATT ATG-3´
AtFH18aA	5´-AAC TCG AAG TCC ACG CGA TTC GT-3´
AtFH20	5´-GAT TGT GCA TCA GAT GAT TCA AAC C-3´
LBb1	5´-GCG TGG ACC GCT TGC TGC AAC-3´
LB3	5´-CAT CTG AAT TTC ATA ACC AAT CTC G-3´
AtFH3-ATG	5´-ATG GGG AGA TTG AGA TTA GCG T-3´
AtFH3-ATG-Pci	5´-CAA GTA CAT GTG GAG ATT GAG ATT AG-3´
AtFH3-re-Eco	5´-AAG AAT TCG AAG GTG AAC TAT CCT C-3´
AtFH3-2D-Bam	5´-TGG ATC CGA TTC TGA GAC TGG AGC T-3´
AtFH3-2D-ATG-Bam	5´-AAG AAT TCA AGA ATG GTT TGT GGT-3´
AtFH3-1+2-Pci	5´-GGC AGA CAT GTT TCC TCC GTT GAA GCT-3´
AtFH3-2D-Pci	5´-CTG ACA TGT ATT CTG AGA CTG GAG C-3´
AtFH3-re-Pci	5´-AAG ACA TGT AAG GTG AAC TAT CCT C-3´
AtFH3-1+2-Y2H-Eco	5´-CTG AAT TCC CTC CGT TGA AGC TTC-3´
AtFH3-2D-Y2H-Eco	5´-TGA ATT CGA TTC TGA GAC TGG AGC-3´
AtFH3-re-Y2H-Pst	5´-AAA GCT GCA GAA GGT GAA CTA TCC TC-3´
AtFH16-fb-Eco	5´-AAG AAT TCT CTG ATC CAA TGT TCC C-3´
AtFH16-re-Xho	5´-GGC TCG AGG AGC TGT TCT ACT GGT ACC-3´

AtFH16-Sal	5´-AAT CTG GAA GTC GAC GAG AAG CT-3´
AtFH16-Bgl	5´-AAG TCC AGT AGA TCT GCT GCC TTG G-3´
AtFH16-re-os-Xho	5´-GAG CTC GAG TAC TGG TAC CTT AAC-3´
AtFH16-2D-Eco	5´-GTG AAT TCC GAT GTC CAG TTA CA-3´
AtFH16-1+2-Eco	5´-CCG AAT TCC CAC TAC CAC CAC-3´
AtFH16-1+2-ATG-Eco	5´-CGC TGA ATT CAT GGT ACC ACT ACC ACC-3´
AtFH16-2D-re-Xho	5´-GAA CTC GAG GGT CTT ATT CTA GAA GG-3´
AtFH16-N-re-Xho	5´-TTC TCG AGT TAT TGG TTT TGC CCC AAC AGA G-3´
AtFH16-fb-Sma	5´-GTT CCC GGG CCA ATG TCC CCT GT-3´
AtFH16-2D-Sma	5´-GTT CCC GGG TTT CGA TGT CCA GT-3´
AtFH16-re-Sma	5´-GGA CCC GGG CTA CTG GTA CCT TAA C-3´
AtFH16-2D-re-Sma	5´-GGT ATC CCG GGC TAA GGT CTT ATT CTA GA-3´
ACT7-fb	5´-TGA TAG GAC TCT TAA GGC TGC T-3´
ACT7-re	5´-TGC ATC CTC TGG ACA TCC TCT-3´

Supplemental data 2: Experiments used in expression analysis.

AT-00009	AT-00112	AT-00161	AT-00221	AT-00316
AT-00010	AT-00116	AT-00163	AT-00226	AT-00317
AT-00013 - 15	AT-00117	AT-00164	AT-00229	AT-00319
AT-00019	AT-00121	AT-00166	AT-00231	AT-00321 - 323
AT-00022 - 26	AT-00123	AT-00168	AT-00232	AT-00327
AT-00029	AT-00124	AT-00172	AT-00234 - 239	
AT-00046	AT-00128	AT-00174	AT-00241	
AT-00055 - 58	AT-00133	AT-00178	AT-00243	
AT-00064	AT-00136	AT-00179 - 82	AT-00277	
AT-00066	AT-00138	AT-00184	AT-00280	
AT-00071	AT-00139	AT-00186	AT-00284	
AT-00072	AT-00141	AT-00188	AT-00286	
AT-00074	AT-00142	AT-00191	AT-00288 - 291	
AT-00075	AT-00144	AT-00192	AT-00294 - 296	
AT-00078 - 80	AT-00150	AT-00195	AT-00298	
AT-00082 - 83	AT-00152	AT-00196	AT-00305 - 307	
AT-00087 - 93	AT-00153	AT-00203 - 205	AT-00309	
AT-00096	AT-00156	AT-00210	AT-00310	
AT-00098	AT-00158	AT-00214	AT-00312	
AT-00099	AT-00160	AT-00218	AT-00314	

Supplemental data 3: Sequence of the cloned version of *AtFH3* and its translation in ORF 3.

```
ATGGGGAGATTGAGATTAGCGTTTTTGGCGATCTCTCTCGTTGTTTTCGTTTGTGTTTCC
GAGGAGATTTTCTCTCGAGGCGGTCTAAATCTCTTACGATTCTCTGTTTATGGCGAAGAT
GTGAGCAAACATGGATTCATCAAAATCCGAGAAGGAAGCTGATCAGTTATCCAAAAAAGT
TTAGTGTCTCTGCTCCAAATTTAGCTTTTGGTCCTGCACCGAGTTTCGCGCCAGGACCTG
GGCCAAGTTTTGCGCCAGGTCCTGCACCGAATCCTCGTAGTTATGATTGGTTAGCACCTG
CAAGTTCTCCAAATGAACCTCCAGCTGAGACACCGGATGAATCGAGTCCCAGCCCAAGTG
AGGAGACACCGAGTGTTGTTGCTCCTAGTCAAAGTGTTCCGGGTCCTCCTCGTCCTCCTC
CACAACGGGAGAAGAAGGATGATATCTTGATGAAACTTATCATCGCGGTTGCTTCTACCG
CTGTCTTAACGTTTGTTTTTGTTGCATTGATCTTGTGTTGCTTCAAACGCAATTGCAACA
ACGCGGTTGGTTCTAGAGATGGACCTAGAGATGAAGGACCACTTCTACGTTTATCAACTG
GATCTACTGAGAACTCTCCCACCGTCGCAAGCACGAGCCGGAAAATGTTTAGTGTTGCTA
GTTCGAAAAAGAGGTCGTTTCTTTCTAGAGTATCTTTAAAGAGAAATGGTCATGAGTTTT
CAACGGCTGAATCGTCATCGGCAGCTGGACTTCCTCCGTTGAAGCTTCCCCCGGGAAGAT
```

```
CAGCACCTCCTCCACCTCCTGCTGCTGCTCCACCTCCACAGCCACCACCTCCTCCTCCTC
CTAAACCACAACCTCCTCCACCGCCTAAAATTGCTCGTCCTCCACCTGCGCCACCTAAAG
GTGCGGCTCCAAAACGTCAAGGAAACACTTCCTCTGGAGATGCATCTGATGTTGATTCTG
AGACTGGAGCTCCAAAAACAAAACTAAAGCCTTTCTTTTGGGATAAAATGGCTAACCCTG
ATCAAAAAATGGTTTGGCATGAGATTAGCGCCGGTTCATTCCAGTTCAACGAAGAGGCGA
TGGAGTCGCTTTTCGGTTACAACGATGGGAACAAAAACAAGAATGGTCAGAAGAGTACTG
ATTCGTCGTTACGCGAATCTCCTCTACAATATATACAGATCATTGACACTAGGAAAGCTC
AAAACTTATCTATTCTTCTTCGAGCTCTGAATGTAACAACAGAGGAAGTCGTTGATGCCA
TCAAAGAAGGTAATGAGCTCCCAGTGGAGCTTCTACAAACATTGCTGAAGATGGCTCCAA
CTTCAGAAGAAGAACTCAAACTTAGACTATACTCGGGAGATCTTCACTTACTTGGCCCCG
CGGAGCGGTTCTTGAAAATTCTTGTTGATATACCTTTTGCATTTAAACGTATAGAGTCAC
TTCTATTTATGATCTCACTTCAAGAAGAAGTCTCTGGCCTCAAAGAAGCTCTCGGAACTC
TCGAGGTGGCTTGCAAGAAACTTAGAAACAGCAGACTGTTTTTAAAACTACTAGAGGCAG
TCCTCAAGACAGGGAATCGAATGAATGTTGGAACTTTCCGCGGTGATGCGCAGGCTTTCA
AGCTCGATACTCTTTTGAAGCTCTCTGACGTGAAAGGAACTGATGGCAAAACTACACTTT
TACATTTTGTTGTTCTTGAGATCATTCGTTCCGGAGGCGTTCGTGCTCTTCGCCTTCAGA
GCCGAAGCTTCTCAAGCGTTAAAACCGATGATTCAAACGCGGATTCTAGTCCACAATCTG
TGGAGCGTTACCGCAGCACGGGTCTTCAAGTGGTTACGGGGTTAACGACAGAGCTTGAAG
ATGTCAAGAGAGCAGCCATCATAGACGCTGATGGTTTGGCTGCAACATTGGCGAATATAA
GCGGTTCACTTACGAATGCGAGGGAGTTTTTGAAAACAATGGATGAAGAGAGCGATTTCG
AACGAGCATTAGCTGGATTTATAGAACGTGCAGATGCTGATATTAAATGGTTGAAGGAAG
AAGAAGAGAGAATCATGGTGTTGGTGAAAAGCTCTGCTGATTATTTCCATGGGAAGTCTG
CGAAAAACGAAGGATTACGTTTGTTCGCTATAGTGCGCGGTTTCTTGATAATGTTGGAGA
AAGTTTGCAGAGAAGTTAAGGAAACTACAAAGACGACGAACCATTCCGGTAAGAAGGAAA
GCGAAATGACAACTTCGGACAGTAATCAACCGTCTCCGGACTTCCGACAACGTTTGTTTC
CAGCGATTGCTGAACGAAGAATGGATAGTTCGGATGATTCAGACGATGAAGAGGATAGTT
CACCTTCGTAG
```

```
GEIEISVFGDLSRCFRLCFRGDFLSRRSKSLTILCLWRRCEQTWIHQNPRRKLISYPKKF
SVSAPNLAFGPAPSFAPGPGPSFAPGPAPNPRSYDWLAPASSPNEPPAETPDESSPSPSE
ETPSVVAPSQSVPGPPRPPPQREKKDDILMKLIIAVASTAVLTFVFVALILCCFKRNCNN
AVGSRDGPRDEGPLLRLSTGSTENSPTVASTSRKMFSVASSKKRSFLSRVSLKRNGHEFS
TAESSSAAGLPPLKLPPGRSAPPPPPAAAPPPQPPPPPPPKPQPPPPPKIARPPPAPPKG
AAPKRQGNTSSGDASDVDSETGAPKTKLKPFFWDKMANPDQKMVWHEISAGSFQFNEEAM
ESLFGYNDGNKNKNGQKSTDSSLRESPLQYIQIIDTRKAQNLSILLRALNVTTEEVVDAI
KEGNELPVELLQTLLKMAPTSEEELKLRLYSGDLHLLGPAERFLKILVDIPFAFKRIESL
LFMISLQEEVSGLKEALGTLEVACKKLRNSRLFLKLLEAVLKTGNRMNVGTFRGDAQAFK
LDTLLKLSDVKGTDGKTTLLHFVVLEIIRSGGVRALRLQSRSFSSVKTDDSNADSSPQSV
ERYRSTGLQVVTGLTTELEDVKRAAIIDADGLAATLANISGSLTNAREFLKTMDEESDFE
RALAGFIERADADIKWLKEEEERIMVLVKSSADYFHGKSAKNEGLRLFAIVRGFLIMLEK
VCREVKETTKTTNHSGKKESEMTTSDSNQPSPDFRQRLFPAIAERRMDSSDDSDDEEDSS
PS
```

Supplemental data 4: Sequence of the cloned version of *AtFH16* followed by its translation.

```
ATGTCCCCTGTCGAGATCACTGGCGCTGATGCCGTGGTGACGCCTCCTATGCGTGGAAGA
GTACCACTTCCACCACCGCCTCCTCCTCCTATGCGTAGAAGTGCACCATCACCTCCTCCT
ATGAGTGGAAGAGTACCACCACCACCACCTCCACCTCCGATGTTTGATCCCAAGGGTGCA
GGAAGAGTTATTTGTTGTCTACGTCCAGGTCAAAACAAGTCTTCTCTGAAGCGATTTCAA
TGTGGTAAACTAACAAATGCCTGGGAAGAGTTACAGAGACATGGAGAAGCACAAACTGCC
CCAGAATTTGATCTATCAGAGATAGAGGCCCTTTTCTCTGCTGCAGTACAAAACCAGGCT
GATAAATCTGGAAGTCGACGAGAAGCTTCTGAGGCAAACCCCGATAAACTTCAACCGTCG
CTTGTCGAGATCTCTGGCGCTGATGCCCTGGTACCACTACCACCACCTCCACCTCCTATG
CCTAGAAGATCACCTCCACCACCACCTCCGAGGTTTGATGCCTTTGATCATAAGGGCGCA
AGAATGGTTTGTGGTTTTCGATGTCCAGTTACAAAAAGGTCTTCCCTGAAGCCTTTACAT
TGGGTTAAAATAACAAGGGCTTTGCAGGGGAGCTTATGGGATGAGTTACAGATACAATAT
GGAGAATCACAAACTGCAATAGAACTTGATGTACCAGAAATAGAGACCCTTTTCTCTGTT
GGGGCAAAACCAAGACCAAAACCAAAACCTGAAAAAGTTCCACTGATTGACCTTAAGAGA
```

GCCAATAACACGATAGTTAACTTAAAGATATTAAAGATGCCGCTGCCTGATATGATGGCT
GCAGTCATGGCAATGGATGAGTCTGTACTAGATGTTGATCAAATAGAGAATCTTATACAA
CTTTGCCCAACAAAGGAGGAGATGGAGCTTCTTAAGAACTATACTGGTGACAAGGCAACC
TTGGGAAAGTCTGAGCAGTGCTTACTAGAGCTAATGAAGGTGCCACGATTTGAGGCAAAG
CTTAGAGTACTTTCCTTCAAGATTCCATTTGGCACTAAGATAACAAAATTCAGAAAAATG
TTAAATGTGGTCAATTCTGCGTGTGAGGAGGTACGTTCTTCACAAATGCTAAAAGAGATT
ATGAAAATTATTCTCTTCCTAGGGAACACACTGAACCAAGGAACTGCGAGGGGCAGTGCA
GTGGGATTCAGGTTGGATAGTTTATTGATATTAAGCGAGACACGTGCTGATAACAACAAG
ATGACTCTCATGCATTATCTTTGCAAGGTCCTTGCTTCCAAGGCAGCAGATCTACTGGAC
TTCCATAAGGATCTTCAAAGTCTTGAATCAACTTTAGAGATAAATTTGAAGTCTCTGGCT
GAGGAAATACATGCTATAACCAAAGGATTGGAAAAACTGAAGCAGGAGCTCACCGCATCC
GAAACTGATGGTCCTGTTTCTCAAGTTTTCCGTAAATTATTGAAGGACTTCATATCCAGT
GCTGAGACTCAAGTAGCAACTGTATCGACTCTTTACTCCTCGGCGAGAATAAATGCTGAT
GCACTTGCACACTATTTTGGCGAGGATCCTAACCATTATCCATTTGAAAAAGTTAGCGCG
GCACTCTTGAGTTTTATAAGGTTGTTTAAGAAAGCACACCAAGAGAATGTCAAGCAAGAG
GACTTGGAGAAGAAGAAAGCTGCAACGGATGATGTATTTGGTGGGCCTGACCACAACATA
GACTCAGATACTTCTTTAGATGATTCGGAGGCCAAATCGCCTTCTAGAATAAGACCTCCG
CCTTCTATACCAAGACCCCCTTCACGTCCAAGGTATGCATGCTGCCGAATACCTGCAGTT
AATCCGCCTCCTCGCTTGGTGTGTGGCCCATATCCGCTACCTCGCTTAGTGCGTGTAGGA
TCCCCATCACCACCACCTCCCTCGATGAGTGGAGGAGCTCCACCGCCACCACCTCCACCT
CCAATGCTTGTTGCCAGTAGAACAGCTCCACCTCCTCACTTGAGTCATGTACGTTCAATC
CCTTTCCAAACTCGCTTGGTGATGGGCACATCTCCGCTACCTCTTTTAGTGCGCGAAGGA
GCCCCACCACCAACACTTCCCTCGATGAGTGGAGGAGCTCCACCGCCACCACCTCCACTT
CCAATGTTAAGGTACCAGTAG

MSPVEITGADAVVTPPMRGRVPLPPPPPPPMRRSAPSPPPMSGRVPPPPPPPPMFDPKGA
GRVICCLRPGQNKSSLKRFQCGKLTNAWEELQRHGEAQTAPEFDLSEIEALFSAAVQNQA
DKSGSRREASEANPDKLQPSLVEISGADALVPLPPPPPPMPRRSPPPPPPRFDAFDHKGA
RMVCGFRCPVTKRSSLKPLHWVKITRALQGSLWDELQIQYGESQTAIELDVPEIETLFSV
GAKPRPKPKPEKVPLIDLKRANNTIVNLKILKMPLPDMMAAVMAMDESVLDVDQIENLIQ
LCPTKEEMELLKNYTGDKATLGKSEQCLLELMKVPRFEAKLRVLSFKIPFGTKITKFRKM
LNVVNSACEEVRSSQMLKEIMKIILFLGNTLNQGTARGSAVGFRLDSLLILSETRADNNK
MTLMHYLCKVLASKAADLLDFHKDLQSLESTLEINLKSLAEEIHAITKGLEKLKQELTAS
ETDGPVSQVFRKLLKDFISSAETQVATVSTLYSSARINADALAHYFGEDPNHYPFEKVSA
ALLSFIRLFKKAHQENVKQEDLEKKKAATDDVFGGPDHNIDSDTSLDDSEAKSPSRIRPP
PSIPRPPSRPRYACCRIPAVNPPPRLVCGPYPLPRLVRVGSPSPPPPSMSGGAPPPPPPP
PMLVASRTAPPPHLSHVRSIPFQTRLVMGTSPLPLLVREGAPPPTLPSMSGGAPPPPPPL
PMLRYQ